THE MASS SPECTRA AND IONIZATION EFFICIENCY CURVES OF CYCLOBUTANONE

by

CLAUDIO KONG NAM PUA
B.Sc., University of Adelaide, 1969

A THESIS SUBMITTED IN PARTIAL FULFILLMENT
OF THE REQUIREMENTS FOR THE DEGREE OF

MASTER OF SCIENCE
in the Department
of
Chemistry

We accept this thesis as conforming
to the required standard

[redacted]

UNIVERSITY OF VICTORIA
August 1972

ABSTRACT

Supervisor : Dr. G.R. Branton

A Hitachi Perkin-Elmer RMU-7 double focusing mass spectrometer was modified in order to determine ionization and appearance potentials by the Energy Distribution Difference (EDD) technique. The validity of the technique and the experimental system was established by a study of xenon and argon, for which the ionization efficiency curves have been reported in the literature. Cyclobutanone was studied in detail in this work.

Cyclobutanone was found to undergo two major fragmentation pathways in the mass spectrometer.

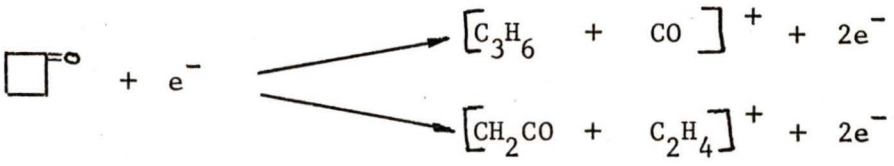

The ionization potential of cyclobutanone was found to be 9.58±0.1 V and appearance potentials of $C_3H_6^+$ and CH_2CO^+ ions were found to be 9.85±0.2 V and 10.53±0.2 V respectively. A good correlation exists between the mass spectral fragmentation pathways and the pyrolytic and photolytic decompositions of cyclobutanone. From energetic considerations, the mass spectral fragmentation processes probably proceed via a concerted mechanism. However, for the formation of CH_2CO^+ ions, a biradical mechanism cannot be completely ruled out.

Breaks were observed at the same electron energy in the ionization efficiency curve of the parent molecular ion as in the ionization efficiency curves of the fragment ions, $C_3H_6^+$ and CH_2CO^+. This suggested that autoionizing states could contribute to the fragmentation processes. It was found that the EDD technique can be used for the determinations of ionization and appearance potentials but for the observation of breaks in the ionization efficiency curves, reproducibility was poor.

[redacted] [redacted] [redacted]

Table of Contents

List of Tables

List of Figures

page

Acknowledgment

I wish to express my sincere appreciations to my supervisor, Dr. G.R. Branton for his constant guidance and advice. His interest in the project coupled with many discussions with him contribute to the success of this project. At the same time, I wish to thank Mr. J-C Regenass (Scientific Assistant) who taught me how to operate the mass spectrometer and made valuable suggestions from time to time. Finally, I would like to thank Departmental technical staff whose help in one way or another, is highly appreciated.

Chapter One
Introduction

In the last or twenty years, organic chemists have begun to use mass spectrometers as routine instruments in helping them to solve the problem of structural determinations of chemical compounds. As in the computing field, almost every university has at least one mass spectrometer. With the introduction of high resolution double focusing instruments, mass spectrometry has become a very powerful technique, which is now being applied more and more widely. The use of mass spectrometers, in conjunction with other instruments such as nuclear magnetic resonance (N.M.R.), infra-red (I.R.), and ultra-violet (U.V.) spectrometers, enables us to know more about the properties of chemical compounds.

1.1 Basic Principles of Mass Spectrometry

The basic units of a mass spectrometer are an ionization chamber, a mass analyser, and an ion detector. Samples (gases, liquids or solids) are introduced through an inlet system. Most general purpose commercial mass spectrometers employ an electron impact ion source. In an electron impact ion source, the sample is bombarded with electrons from a heated filament, thus causing ionization. Such ion sources require that the sample should have an appreciable vapour pressure (much greater than 10^{-6} torr). The required vapour pressure may be achieved, if necessary, by heating the sample. The ions formed are accelerated out of the ionization chamber. They pass through a mass analyser and ions of the same mass to charge (m/e) ratio are detected.

The energy of the bombarding electrons is normally sufficiently high (frequently around 70 eV) that the sample molecules are not only ionized but also decompose into fragment ions. The molecular ions and fragment ions are separated according to their mass to charge (m/e) ratios and detected. The record of these ions and their relative abundances is known as the mass spectrum of the molecule. It is known experimentally that every chemical compound has its own distinctive fragmentation pattern, which may be used as a "fingerprint"

for the molecule. This useful property is the basis for identifications and structural determinations of chemical compounds using mass spectrometry. Thus we see that mass spectrometry can provide both qualitative and quantitative information about a compound or a mixture of compounds; yet only a very small amount of sample (about a milligram) is needed.

1.2 Ionization Efficiency Curves

The variation of the ion current for a given m/e ratio as a function of the energy of bombarding electrons is known as the ionization efficiency curve. To a first approximation, the ion current increases linearly with the energy of the bombarding electrons in excess of a certain threshold energy. For parent molecular ions, this threshold energy corresponds to the ionization potential of the molecule; for fragment ions the minimum energy required to produce the ion is known as the appearance potential. The approximately linear nature of the ionization efficiency curve has been experimentally verified for atoms and some molecules (1). If monoenergetic electron beams are used, changes in slope (breaks) are usually observed in the ionization efficiency curve. These breaks can be assigned to autoionizing states, excited states of the ion and, if fragment ions are being studied, to different fragmentation processes for the molecular ion. The electron beam produced by most commercial mass spectrometer sources is not monoenergetic and the spread of energies blurs the fine structure of the ionization efficiency curves. Various experimental and mathematical techniques have been developed to overcome this problem (see section 2.10).

1.3 Aim of This Work

The aim of this work was to develop a technique for the detailed study of ionization efficiency curves of the parent molecular ion and of the fragment ions using a Hitachi Perkin-Elmer RMU-7 double focusing mass spectrometer. The technique was developed, tested and applied to the study of the ions produced by electron impact ionization of cyclobutanone. Due to the thermal energy spread of the bombarding electrons, the breaks (fine structure) in the ionization efficiency curves are difficult to observe. However, applying an analytical method,

the energy distribution difference (EDD) method, the fine structure can be observed.

The advantages of the EDD method using a commercial instrument relative to other methods available for the study of ionization efficiency curves (these other methods are outlined in Chapter Two) are as follows:

(1) Only slight modifications are needed to a commercial instrument,
(2) Gas, liquid and solid inlet systems are thus available,
(3) The energy of the electron beams can be varied easily,
(4) Intense electron beams can be produced,
(5) High mass range is available, and
(6) High resolving power of the commercial mass analyser may be used.

The EDD method was tested by measuring the ionization efficiency curves for Xe^+ and Ar^+ and comparing these with the literature. The ionization potential of cyclobutanone and appearance potentials of the fragment ions $C_3H_6^+$ and CH_2CO^+ were determined. The fine structure in the ionization efficiency curve for the parent molecular ion (m/e=70) was correlated with that in the fragment ions $C_3H_6^+$ and CH_2CO^+ (m/e=42). This information, together with a study of the mass spectrum as a function of the electron energy was used to discuss the fragmentation of cyclobutanone in a mass spectrometer.

Therefore, it was shown that with only slight modifications to a commercial instrument (Hitachi Perkin-Elmer RMU-7 double focusing mass spectrometer), the ionization potential of a molecule and appearance potentials of ions can be determined and the fine structure in the ionization efficiency curves can be observed.

Chapter Two
Basic Principles

2.1 Vacuum Requirements

The operating pressure of the analyser section of a mass spectrometer is normally maintained at about 10^{-6} torr. A pressure, no higher than this, is necessary in order that the mean free path of the ions will be greater than the distance they must travel from the ion source to the detector. At 10^{-6} torr, the mean free path is of the order of 50 meters and the ion path length in the mass spectrometer is usually less than 2 meters. Therefore, ion-molecule interactions are very rare. If the operating pressure is too high, the ion would collide with other gas molecules. This results in the ions being scattered and the detected ion peak being broadened.

2.2 Ion Sources

There are many methods available for ion production. The main ones are surface emission, hot spark, field ionization, photoionization and electron impact ion sources. The principles, advantages and limitations of these ion sources will be briefly described here.

(a) Surface Emission (Thermal Emission, Thermal Ionization) Ion Sources

The surface emission ion sources consist of a filament assembly and an ion beam accelerating and collimating slit system. The filament, in the form of a boat or a ribbon, is coated with the sample to be analysed. The whole filament assembly is inserted into the ion source of the mass spectrometer at a reduced pressure. The heating of the filament causes some of the sample to evaporate directly as ions. These ions are then accelerated and collimated into an ion beam. The main use of this ion source is in the analysis of selected elements, such as in the nuclear applications. This is because the amount of sample required is very small (in the order of microgram or less) and the sensitivity is extremely high. One advantage of this ion source is that it does not ionize background gases. However, the limitations are that the ion source can only be used for samples having low ionization potentials and there is no way to vary the ionization energies.

(b) Hot Spark Ion Sources

The construction of the hot spark ion source is similar to the surface emission ion source. The only difference is that, instead of the filament assembly, a primary electrode consisting of the sample to be analysed and a secondary electrode are introduced into the ion source of the mass spectrometer. A spark discharge is maintained between the two electrodes and this causes some of the sample to evaporate directly as ions. These ions are accelerated and collimated into an ion beam. This ion source has been mainly used for involatile materials such as metals and inorganic solids. However, the ion source is unstable and the kinetic energy spread of the ions is about 1000 eV.

(c) Field Ionization Ion Sources

Extremely high electric fields of the order of 10^8 V/cm, when acting on atoms or molecules, may cause ionization. The mass spectra obtained by this ion source are much simpler than those obtained by electron impact ion source. This is advantageous for the analysis of organic compounds. However, the ion source is difficult to operate and ion intensities are low.

(d) Photoionization Ion Sources

Photoionization ion sources are similar in principle to the electron impact ion sources. Instead of using electrons from a heated filament, ultraviolet light of sufficiently short wavelength is used to bombard the samples in gaseous or vapour state at a reduced pressure (about 10^{-6} torr).

$$AB + h\nu \longrightarrow AB^+ + e^-$$

Compared to the electron impact ion source, this ion source gives simpler mass spectra which can be used for analysis of organic compounds. However, ion intensities are generally low and the ionization energy available is only up to about 20 eV (limited by the availability of suitable light sources).

(e) Electron Impact Ion Sources

This is by far the most versatile and widely used ion source in mass spectrometry

In the present studies, an electron impact ion source is used and therefore the principle, construction and operation of this ion source will be described in some detail .

The basic principle is that electrons from a heated filament bombard the samples in the gaseous or vapour state. There is an exchange of energy between bombarding electrons and the neutral gas atoms or molecules. One or more electrons are removed from the neutral gas atoms or molecules, thus causing ionization. The energy of the bombarding electrons is usually about 70 eV (section 2.6). At this energy, most atoms and molecules can be ionized.

$$AB + e^- \longrightarrow AB^+ + 2e^-$$

The common materials for filaments are tungsten and rhenium. In the present studies, a rhenium filament is used. Compared to tungsten as a material for filament, the advantages are that rhenium does not form stable carbides, its oxides are unstable at operating temperatures and it does not become brittle at high temperatures.

A schematic diagram and operating conditions for the ion source of the Hitachi Perkin-Elmer RMU-7 double focusing mass spectrometer is shown in fig. 1. Electrons are emitted from the heated filament F. A grid G, at a slightly negative potential with respect to the filament is situated just behind the filament. The main function of the grid is to direct the electron beams toward the ionization chamber. The energy of the electrons is controlled by the potential difference between the filament and the chamber C. This electron energy can be varied by a potentiometer. A weak external magnetic field (not shown in the diagram), parallel to the electron beam , acts as a collimator and keeps the width of the electron beam small. The collimated electron beam bombards the sample atoms or molecules, thus causing ionization. Generally, fragmentation of molecules also occurs to yield various types of ions (a detailed description of the types of ions formed by an electron impact ion source is given in section 2.3). A target T, slightly positive with respect to the chamber, collects all the electrons. When ions are formed in the ionization chamber, they are repelled by the repellers R out of the chamber. These ions are then accelerated and slits and lens are used to collimate the ion beam . The accelerating voltage is normally about 3000 V and therefore all of the ions have acquired nearly the

Fig. 1. Diagram and operating conditions for the ion source of the Hitachi Perkin-Elmer RMU-7 double focusing mass spectrometer.

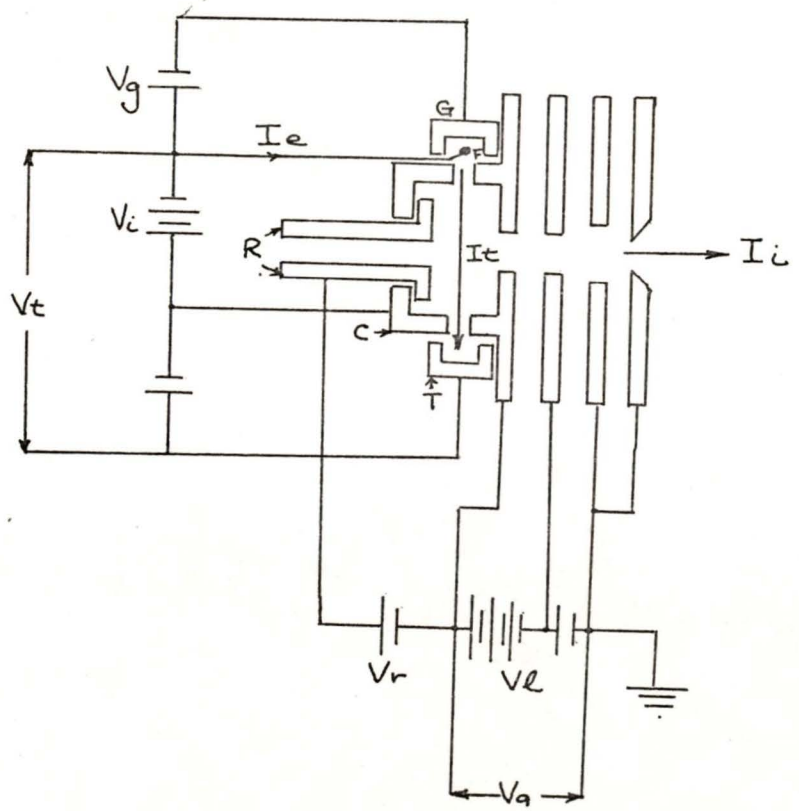

G : Grid
F : Filament
R : Repeller
C : Chamber
T : Target

Va	: Ion accel. voltage	3600V
Vl	: Lens voltage	3100V
Vr	: Repeller voltage	8V
Vt	: Target voltage	110V
Vi	: Chamber voltage	80V
Vg	: Grid voltage	-15V
Ie	: Total emission current	80μA
It	: Target current	70μA
Ii	: Ion current$\propto$Ii or It	

same kinetic energy before entering the analyser section, since the accelerating voltage is large compared to the variations of kinetic energies of the ions.

The advantages of electron impact ion sources are high yield, small kinetic energy spread in the ion beam, a very stable ion beam, convenient sample handling, easy operation and readily variable ionization energy.

Table 1 summarizes the salient features of the above mentioned five ion sources.

2.3 Types of Ions Produced by Electron Impact Ion Sources

The main types of ions formed by electron impact ion sources are molecular (parent molecular) ions, fragment ions, rearrangement ions and metastable ions. The formation and importance of these ions will be described here.

(a) Molecular Ions

A molecular ion is formed when one electron is removed from the neutral molecule by bombarding electrons. The molecular ion is the ion of highest mass which can be produced by simple ionization process.

$$AB + e^- \longrightarrow AB^+ + 2e^-$$

An accurate mass determination of the molecular ion of a compound will yield its molecular weight. However, due to the fragmentation processes occurring in the ionization chamber, the molecular ion peak is not necessarily the most intense peak.

(b) Fragment Ions

The mass spectrometer is normally operated at an electron energy of about 70 eV. At this electron energy, the molecular ions are formed with excess energy and they may decompose into fragment ions by bond cleavage.

$$AB^+ \longrightarrow A^+ + B \qquad \text{or}$$

$$AB^+ \longrightarrow A + B^+$$

Table 1.

Summary of Ion Sources

Type	Ion energy spread, eV	Analyser required	Sample type	Sensitivity	Current stability	Used for
Electron impact	0.1–5.0	Single	Gases, vapours of organic liquids, vapours of solids	High	Good	General purpose
Surface emission	0.2	Single	Inorganic solids, salts	Very high or very low	Fair	Isotope abundance, trace analysis
Hot spark	1000	Double	Inorganic solids, metals	Very high	Fair	Isotope abundance
Field ionization	0.5–5.0	Single	Organic vapours	Varies	Fair	Organic, no fragments; surfaces
Photoionization	0.05–0.2	Single	Gases, vapours	Medium	Good	Molecular spectroscopy

It should be noted here that fragmentation processes are very similar to ordinary chemical unimolecular decomposition reactions. The observed fragment ions in the mass spectra of molecules may often be correlated with functional groups of chemical compounds.

(c) Rearrangement Ions

Rearrangement ions are formed from the molecular ion by redistribution of atoms or groups of atoms at the moment of unimolecular decomposition of the molecular ion. Rearrangements involving hydrogen atoms are very common and the processes often involve the elimination from the ion of an even electron molecule such as CO, HCN, or C_2H_2. A general type of hydrogen rearrangement process is known as the "McLafferty rearrangement". This is shown by the following example.

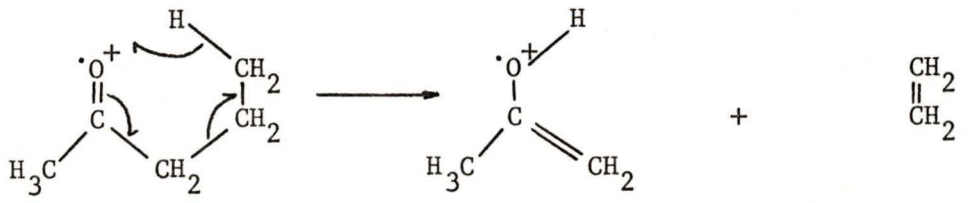

(d) Metastable Ions

Most ions such as molecular ions and fragment ions do not spend much time in the ionization chamber and they are stable enough that they do not decompose when they leave the ionization chamber (the time of flight from the ion source to the detector is approximately 10^{-6} sec.). However, there are some ions whose half-lives are of the order of 10^{-6} sec. These ions are sufficiently long-lived to be accelerated out of the ionization chamber but decompose in transit. These ions are known as metastable ions. In a metastable process, the metastable parent ion m_1^+ decomposes into a stable fragment ion m_2^+ and a neutral particle m_3.

$$m_1^+ \longrightarrow m_2^+ + m_3 \qquad (2.1)$$

The decomposition processes may take place anywhere between the ionization chamber and the detector. However, only those metastable peaks resulting from metastable parent ions which decompose in the vicinity of the magnetic analyser (after acceleration), are usually observed. Such an ion will have been accelerated

as the undecomposed ion which will then fragment in transit. The energy carried by the ion will be only a fraction of the original kinetic energy but this new ion will now be deflected by the magnetic field as an ion of mass to charge ratio equal to the fragment. It will thus appear on the display at an apparent "mass" m^*, which corresponds neither to that of the undecomposed ion (the "metastable" ion is deflected by the magnetic field with a different m/e) nor that of the fragment ion (since the "metastable" ion has a different kinetic energy to the main ion beam). It can be shown that (2):

$$m^* = m_2^2/m_1 \qquad (2.2)$$

where m^* (the apparent mass) is the position on the display of the metastable ion. Note: This only refers to ions which decompose after acceleration but prior to entering the magnetic field.

There are four apparent characteristics of metastable peaks. These are:

(1) They appear at both integral or non-integral masses,

(2) Their shapes are broad and diffuse,

(3) Their intensities are usually very low, and

(4) Their relative intensities with respect to those of the fragment ions can be varied by changing the slit width (change in resolution) or by altering the ion repeller voltage (change in the time spent in the ionization chamber).

The importance of observing metastable peaks is that a metastable transition is considered as evidence of a one step decomposition process. The detection of m_1^+, m_2^+, and m^* shows that the unimolecular decomposition reaction is occurring according to equation (2.1). Such observations serve as an aid to the study of reaction mechanisms.

2.4 Mass Analysers

(a) Single Focusing

After the ions are accelerated out of the ionization chamber, they pass

through a magnetic field which serves as a mass analyser. At the end of acceleration, the ions have gained the kinetic energy T.

i.e. $$T = mv^2/2 = eV \qquad (2.3)$$

where m: mass of the ion

v: velocity after acceleration

e: charge associated with the ion, usually one unit

V: the accelerating voltage

Note : the cgs system of units is used.

In the presence of a magnetic field, the ions experience a force F_H:

$$F_H = Hev \qquad (2.4)$$

where H is the magnetic field

At the same time, the centripetal force which would make the ion follow the same circular path is F_c where

$$F_c = mv^2/r \qquad (2.5)$$

Note: r is the radius of the path travelled by the ion.

Since the force due to the magnetic field F_H is equivalent to this centripetal force F_c,

$$F_H = F_c \qquad (2.6)$$

Therefore $$mv^2/r = Hev \qquad (2.7)$$

Rearranging equation (2.7),

$$v = Her/m \qquad (2.8)$$

Combining equations (2.3) and (2.8)

$$m/e = H^2r^2/2V \qquad (2.9)$$

Thus the principle involved in the operation of mass analysers is based on equation (2.9).

For practical considerations, r is always held constant. In order to scan the mass spectrum i.e. vary the m/e ratio, either the magnetic field strength or the accelerating voltage may be varied. Keeping the accelerating voltage constant, a magnetic scan is obtained by varying the magnetic field strength. Instrumentally, magnetic scan is easier than voltage scan. However, the m/e ratios obtained are not linear with respect to the magnetic field and thus the display is not linear. Also scanning time is longer. On the other hand, keeping magnetic field strength constant, a voltage scan is obtained by varying the accelerating voltage. The advantages of a voltage scan are that the scanning time is short and the m/e ratios are linear with respect to the voltage and also the display. However, instrumental problems arise since varying the accelerating voltage also affects the focusing properties of the ion lens. Consequently, a magnetic field scan is the most common.

(b) Double Focusing High Resolution Mass Spectrometers

When the ions are accelerated out of the ionization chamber but just before entering the magnetic field, they have gained almost the same kinetic energy. In this case, the kinetic energy T depends on the accelerating voltage V as given by equation (2.3).

$$T = mv^2/2 = eV \qquad (2.3)$$

If all the ions have the same kinetic energy before entering the accelerating field, they will have the same kinetic energy after leaving the accelerating field. Resolution is here defined as the ability of the mass spectrometer to separate ions of slightly different masses and the resolution of a magnetic analyser is largely dependent on the kinetic energy spread of the ion beam before it enters the analyser. Usually, there is a spread in the kinetic energy of the ions when they leave the

ionization chamber, and thus there is also a spread of kinetic energies when the ions leave the accelerating field and enter the magnetic field, thus limiting the resolution of the analyser. In order to have the same kinetic energy for all the ions before entering the magnetic field, and thus improve the resolution of the mass spectrometer, an electrostatic selector is incorporated to the mass spectrometer. This selector is situated before the magnetic analyser and it acts as an energy filter. The incorporation of an electrostatic selector is the basis of double focusing high resolution mass spectrometers. A schematic diagram of the ion optical system and the dimensions of the Hitachi Perkin-Elmer RMU-7 double focusing mass spectrometer is shown in fig. 2.

2.5 Accurate Mass Determination by Peak Matching Technique

Quite often, it is necessary and useful to know the value of the accurate mass of a molecular ion or a fragment ion. This can be determined by matching the peak of the unknown ion with those of the known (standard) ions. The peak matching system employed by the Hitachi MK-14 B Peak Matcher used in the present studies is described here. Two known peaks are required such that the unknown sample peak is somewhere in between. For high accuracy, the two known peaks should be as close as possible to each other.

From equation (2.9),

$$m/e = H^2r^2/2V \qquad (2.9)\ ;$$

$$\text{therefore} \quad m = K/V \qquad (2.10)$$

where K is a constant when r and H are held constant and the charge e is unity.

Using equation (2.9), the formula for finding the accurate mass of the unknown ion can be derived. First, let the two known peaks be $m_o=K/V_o$ and $m_1=K/V_1$ where $m_o > m_1$, and V_o and V_1 are their respective accelerating voltages. The unknown peak is $m=K/V$ where V is its accelerating voltage. The reading on the peak matcher is given by Δm where

Fig. 2. Diagram of the ion optical system and the dimensions of the Hitachi Perkin-Elmer RMU-7 double focusing mass spectrometer.

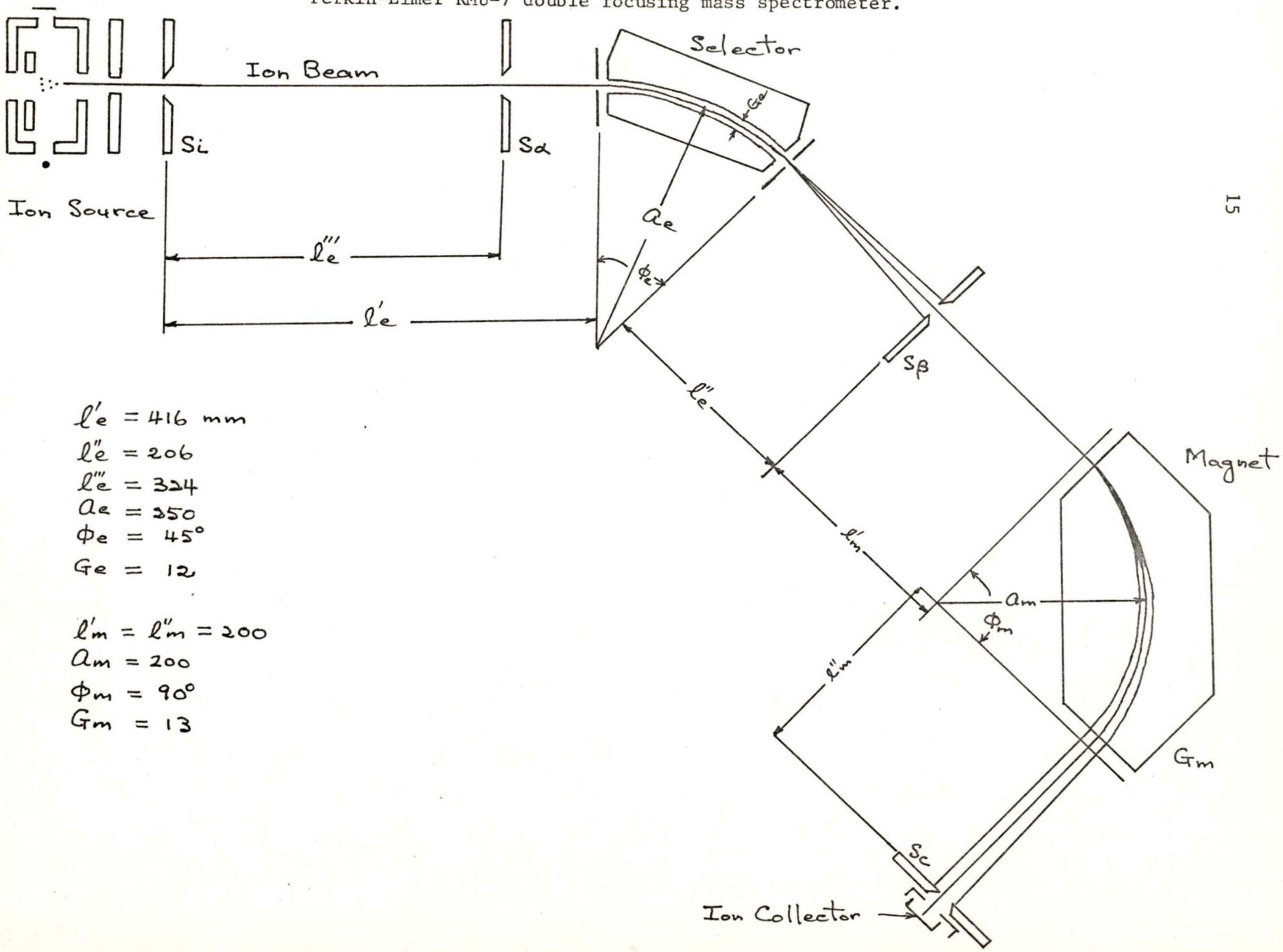

$l'_e = 416$ mm
$l''_e = 206$
$l'''_e = 324$
$a_e = 250$
$\phi_e = 45°$
$G_e = 12$

$l'_m = l''_m = 200$
$a_m = 200$
$\phi_m = 90°$
$G_m = 13$

$$\Delta m = \frac{V_o - V}{V_o - V_1} \qquad (2.11)$$

Thus, knowing m_o and m_1, and recording Δm, the accurate mass m of the unknown peak is given by:

$$m = \frac{m_o}{1 + \left[\frac{m_o}{m_1} - 1\right]\Delta m} \qquad (2.12)$$

2.6 Mass Spectra at Threshold, Medium and High Voltages

Mass spectra are normally obtained at an electron energy of 70 eV. This is because at this voltage, the ion currents for most substances reach a broad flat maximum in the ionization efficiency curve as shown in fig. 3. Thus, even with a small fluctuation in electron energy around 70 eV, the ion currents will be almost the same for a particular ion, and for most substances, the mass spectrum is more readily reproduced at this electron energy.

However, it is sometimes advantageous to obtain mass spectra at low voltages near to the threshold of ionization, where the mass spectra are usually much simpler. A lot of information about fragmentation processes can also be obtained. If the mass spectrometer system is stable, the simpler mass spectra at low voltages can be used for qualitative and quantitative analysis of mixtures of compounds. Limitations of this technique are that ion intensities are usually very low, and that the ion intensities are very sensitive to changes in the electron energy.

Apart from high and low voltage mass spectrometry, medium voltage i.e. around 20 eV, mass spectrometry can also provide useful information about chemical compounds. This is particularly so for isomeric compounds. Usually, the technique of medium voltage mass spectrometry is used to determine the group composition of various isomers more accurately than low voltage mass spectrometry. Such information is the basis of the use of mass spectrometry in structural determinations of organic compounds. Therefore, in order to gain more information about a chemical compound, mass spectra at low, medium and high voltages should be recorded.

Fig. 3. Ionization efficiency curve.

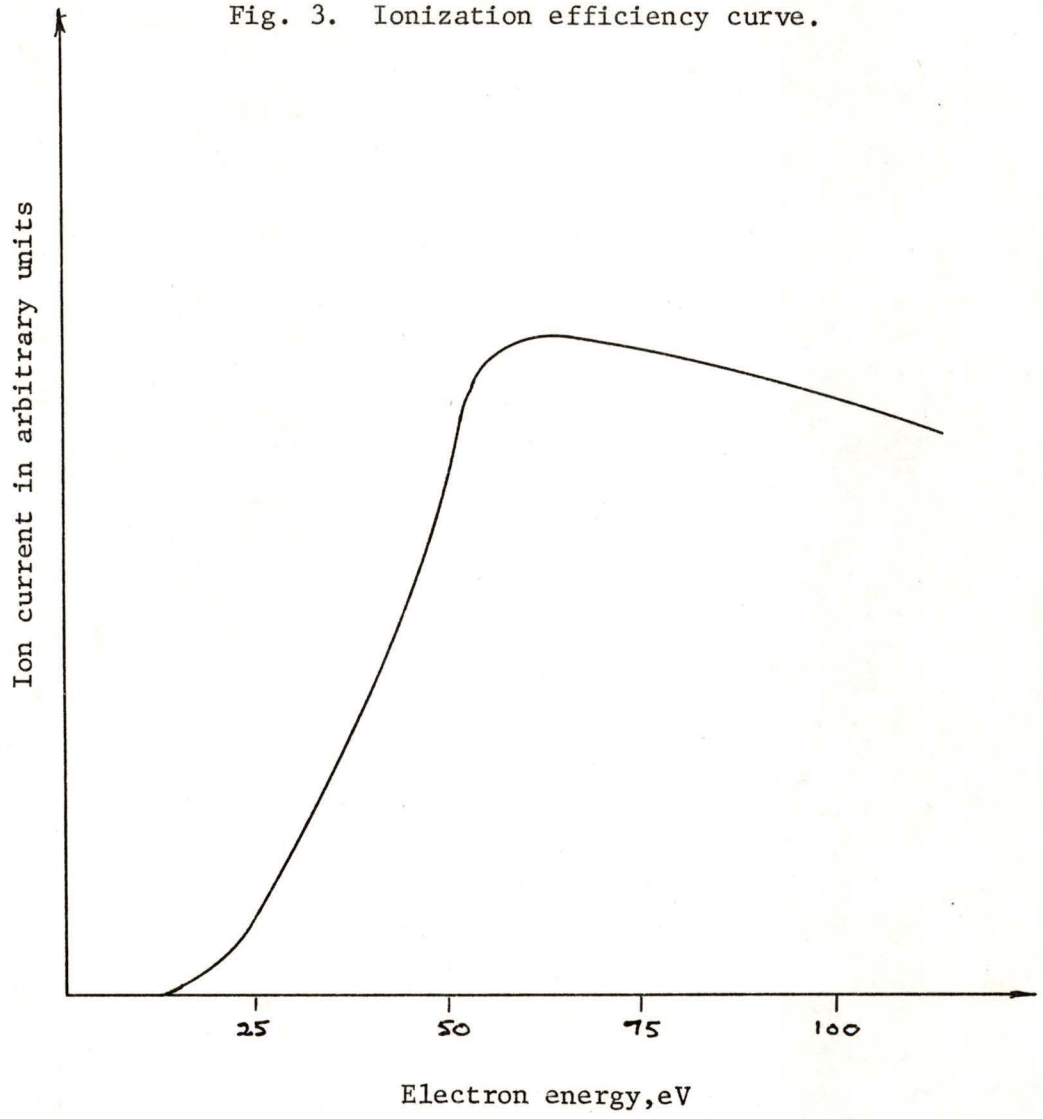

2.7 Quasi-Equilibrium Theory of Mass Spectra

There is considerable experimental evidence to show that every chemical compound has its own distinctive mass spectrum (fingerprint). At 70 eV, the mass spectra of chemical compounds are relatively easily reproduced. These conclusions from experimental evidence are the basis for qualitative and quantitative analyses of a compound or a mixture of compounds by mass spectrometry. At the same time, using peak matching technique, accurate mass of an unknown ion can be determined and an empirical formula can be assigned to the ion. However, until 1952, all of this information was purely empirical and no unifying theory explaining the fragmentation processes occurring in a mass spectrometer had been developed. Therefore, to add to the knowledge about physical and chemical processes involved, Rosenstock et al (3) in 1952 formulated the Quasi-Equilibrium Theory of Mass Spectra. The Theory tries to correlate the fragmentation processes with the physical and chemical properties of the molecule and also tries to explain the mechanism of ion formation.

The Quasi-Equilibrium Theory of Mass Spectra is based on the following assumptions.

(a) When the bombarding electron collides with the neutral molecule, there is a transfer of energy from the energetic electron to the neutral molecule, thus causing the formation of the molecular ion. Ionization is extremely fast and follows the Franck-Condon Principle. If the resulting molecular ion decomposes, then it is in an excited state.

(b) There is an intramolecular energy transfer among various bonds of the molecular ion, resulting finally in the breaking of certain bonds. This is known as the fragmentation process and there is a time delay between the formation of the molecular ion and the fragmentation process in which energy may be transferred between the various modes of the molecule. This explains why the cracking patterns are related to molecular structures and thus why the mass spectrum can serve as a fingerprint for a particular compound.

(c) Fragmentation processes are a series of competing and consecutive unimolecular reactions and the rate constants can be calculated by using the absolute reaction rate theory.

The essential point in the above assumptions is that fragmentation processes occurring in the mass spectrometer are unimolecular decomposition reactions. Therefore, the intensities of the molecular and fragment ions are related to the kinetics of the processes. If the rate constants for all the fragmentation processes can be calculated, the relative ion intensitites can also be calculated.

Using the theory that fragmentation processes occurring in the mass spectrometer are similar to the rate processes of conventional chemical kinetics, the rate constants can be calculated by using the absolute reaction rate theory. In this way, the following simple rate constant expression k was derived (3).

$$k = \left(\frac{E - \varepsilon_o}{E}\right)^{N-1} \frac{\prod_{j=1}^{N} \nu_j}{\prod_{i=1}^{N-1} \nu_i^{\ddagger}} \qquad (2.13)$$

where E: the excitation energy

ε_o: the activation energy

N: number of harmonic oscillators

ν_j: the frequencies of the harmonic oscillators

$\nu_i^{\ddagger}$: the frequencies of the harmonic oscillators of the activated complex

In order to compare the calculated mass spectrum with the experimental one, the first step is to work out all the possible fragmentation processes. Rate constants for these processes are then calculated by using equation (2.13). A typical example of the calculations is given by Kiser (2). From the rate constants, the calculated mass spectrum is obtained and this is compared with the experimental mass spectrum.

Since 1952, there have been many modifications and improvements (4) to the rate expression but the basic form remains the same. On the whole, the Quasi-Equilibrium Theory of Mass Spectra does offer us some explanations about fragmentation processes in the mass spectrometer. So far the calculated mass spectra are only qualitatively correct. Improvements are still needed to the rate expression and suitable means of finding the values of some parameters in the rate expression have to be worked out. Detailed studies, like those undertaken in the present work, are required to help to provide some of this information, and test the Theory.

2.8 Ionization Efficiency Curves

A plot of the ion currents versus the energy of the bombarding electrons is known as the ionization efficiency curve. It is experimentally confirmed for atoms and some molecules that the ion currents vary approximately linearly with the energy of the bombarding electrons in excess of the threshold energy for the production of the ion (1). This is known as the linear threshold law. If monoenergetic electron beams are used, the onset of ion production for atoms or molecules corresponds to the ionization potential of the atom or molecule (fig. 4). Thus, the ionization potential is the minimum amount of energy necessary to remove an electron from an atom or molecule.

$$A + e^- \longrightarrow A^+ + 2e^-$$

or

$$AB + e^- \longrightarrow AB^+ + 2e^-$$

The process of ionization is extremely fast i.e. of the order of 10^{-15} sec., compared to vibrational interval of the order of 10^{-12} sec. Thus, the Franck-Condon Principle will hold and during the ionization process there will be no change in the nuclear configurations for the neutral and ionized systems, i.e. the internuclear distances are the same for both states. The ionization process may be represented by a vertical transition between potential energy surfaces. An illustration of the potential energy surfaces for a diatomic molecule is shown in fig. 5. The ionization potential measured by the electron impact technique is known as the vertical ionization potential. This is in contrast to the adiabatic ionization potential which is the energy difference between the equilibrium minima of the potential energy curves of the neutral and the ionized states. The adiabatic ionization potentials can be determined by U.V. spectroscopy in certain cases.

In the fragmentation process dissociation follows immediately the process of ionization, and the minimum amount of energy required for the appearance of a particular fragment ion in its ground state from the molecule also in its ground state is called the appearance potential of that particular fragment ion.

$$AB + e^- \longrightarrow AB^+ + 2e^- \longrightarrow A^+ + B + 2e^-$$

or more directly

$$AB + e^- \longrightarrow A^+ + B + 2e^-$$

Fig. 4. Linear threshold law and ionization potential.

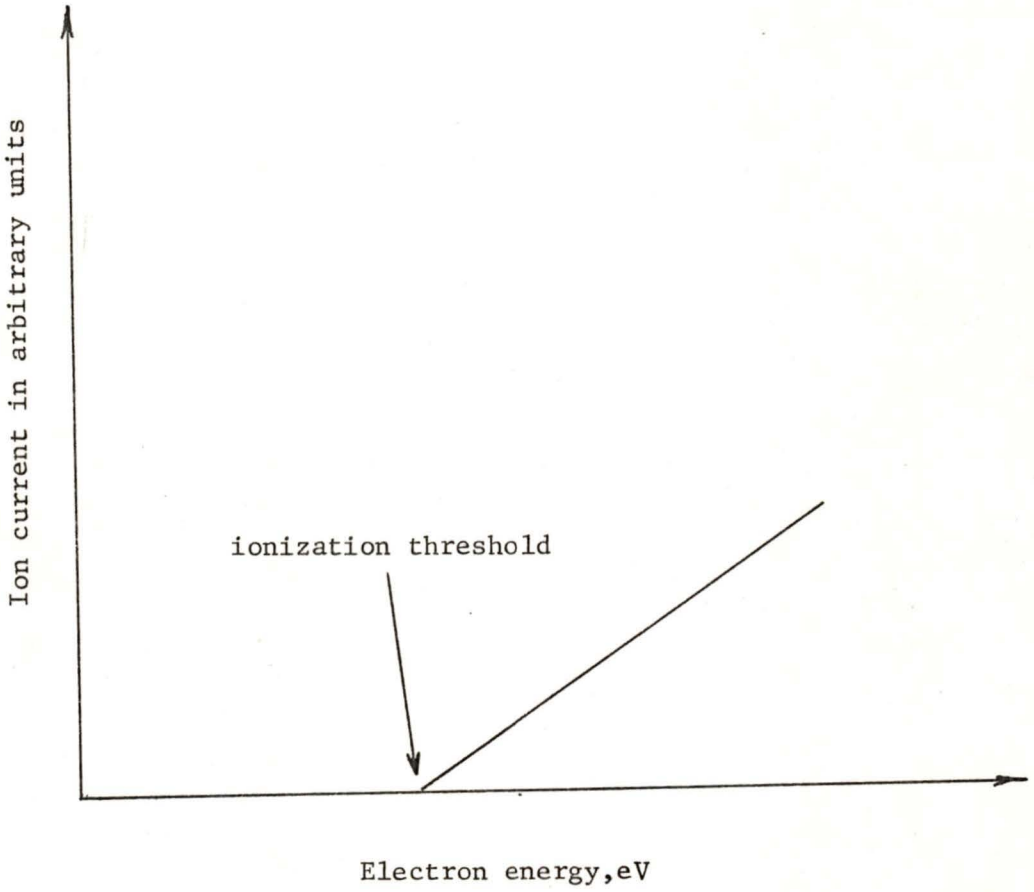

Fig. 5. Potential energy surfaces for a diatomic molecule.

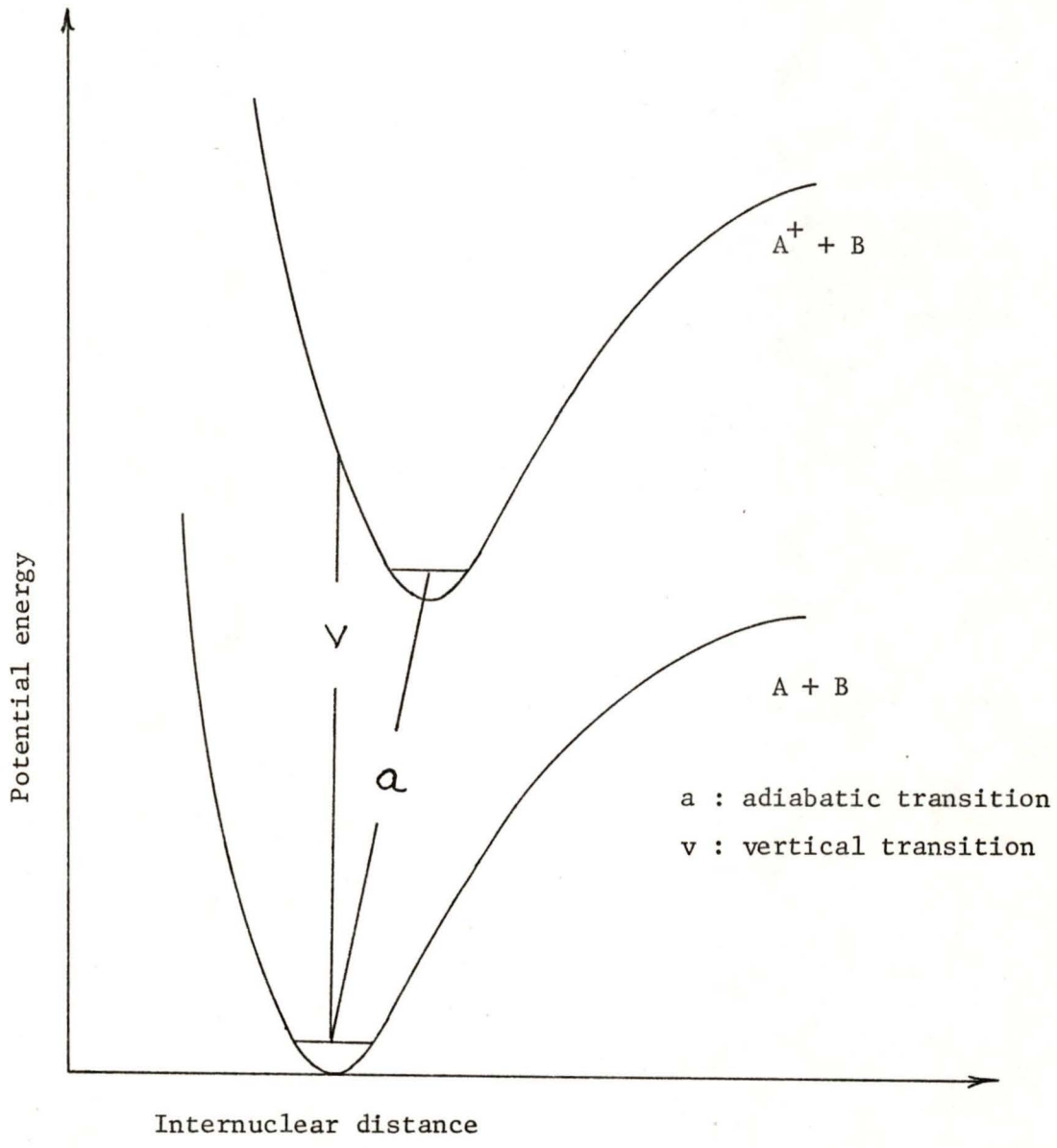

For the determination of ionization and appearance potentials by the electron impact technique, both the neutral and the ionized species are assumed to be in their ground states. This is because very little is known about their excited states. Therefore, the values determined are only approximate. These values are useful if the true values are not available. Quite often, these values can be compared with those obtained by other techniques.

2.9 Fine Structure in the Ionization Efficiency Curves

If monoenergetic electron beams are used (this is an ideal condition), changes in slope (breaks, fine structure) are observed in the ionization efficiency curve as the energy of the electrons is increased (fig. 6). These breaks can be correlated with excited electronic states of the ion, autoionization or different fragmentation processes for the molecule. Unless compared with results from other sources such as U.V. spectroscopy, there is no way of distinguishing these three possibilities.

For molecules, the onset of ionization corresponds to the removal of an electron from the outermost orbital of the ground state of the neutral molecule. This is known as the first ionization potential. The energy necessary to remove an electron from the inner orbital just below the outermost orbital is known as the second ionization potential. The molecular ion is still singly charged. Such "higher" ionization potentials show up as breaks in the ionization efficiency curve. The importance of these "inner orbital" or "higher" ionization potentials is that a better picture of the electronic structure of the molecule can be obtained. The experimental values can be compared with those obtained by theoretical calculations. This adds to our knowledge and understanding of molecules. The values determined by the electron impact method can also be compared with those obtained by other techniques such as ultraviolet and photoelectron spectroscopy. The principles involved in the determination of ionization potentials by ultraviolet and photoelectron spectroscopy will be briefly described here.

In ultraviolet spectroscopy, one electron in the ground state of the atom (or the molecule) may be excited into a higher orbital. The energy difference between the ground state and the higher orbital shows up as a line in the spectrum.

Fig. 6. Fine structure in the ionization efficiency curve.

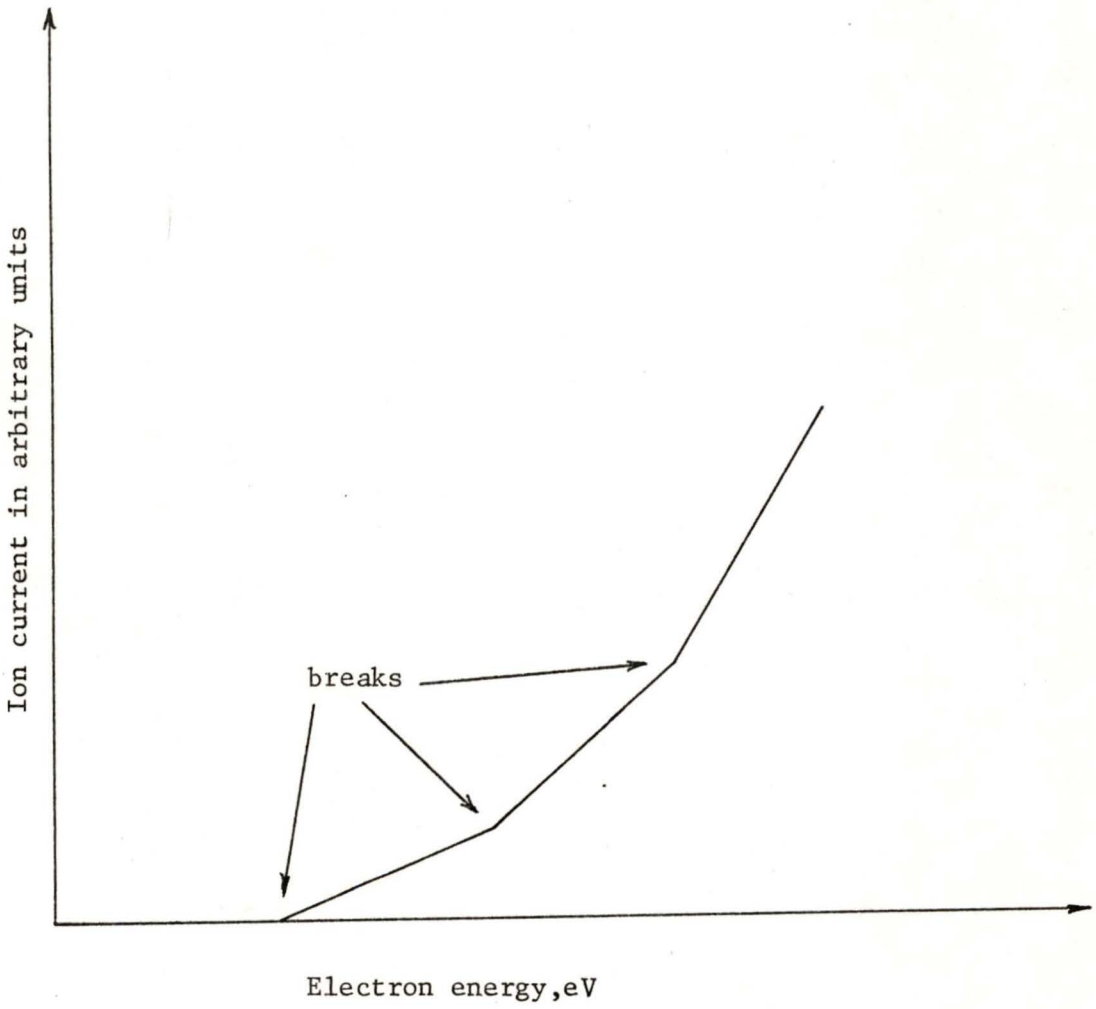

If sufficient energy is available, the observed spectrum will show many lines which finally converge to a series limit (a continuum). The continuum is a region where the electron is completely free from the influence of the nucleus and therefore a positive ion is formed. The energy difference between the series limit and the ground state of the atom (or the molecule) is the ionization potential.

In photoelectron spectroscopy, a photon of sufficient energy to cause ionization is used to bombard the molecule. Instead of examining the ions formed as in the case of photoionization processes, the kinetic energy spectrum of photoelectrons ejected from the molecule is examined. The energy of the photon, $h\nu$, should be greater than the first ionization potential of the molecule. Therefore, the kinetic energy E_k of the resulting photoelectron can be related to the ionization potentials of the molecule by the Einstein equation:

$$E_k = h\nu - I_i - E_{vib} - E_{rot} \qquad (2.14)$$

where I_i : one of the ionization potentials of the molecule
E_{vib}: vibrational energy
E_{rot}: rotational energy

Therefore, ionization potentials can be obtained by photoelectron spectroscopy. Table 2 shows the higher ionization potentials of oxygen determined by different techniques (5).

Table 2. Higher Ionization Potentials of O_2 (eV) (5)

Electronic state of the O_2^+ ion	Spectroscopic	Electron Impact		Photoelectron
		R.P.D.	Selector	spectroscopy
$^2\Pi_g$	12.16	12.21	12.20	12.07
$^4\Pi_u$	16.11	16.30	16.24	16.42
$^2\Pi_u$	16.97	17.18	17.12	
$^4\Sigma_g$	18.16	18.42	18.40	17.99
?	?	21.34	21.29	20.12

Note: R.P.D. denotes Retarding Potential Difference method.

Autoionizing states are usually observed in atoms and molecules. The process is readily explained for atoms and the concepts can be extended to molecules. The bombarding electrons can excite the atom to an excited neutral state, the energy of which is above the first ionization potential of the atom. This is achieved by exciting an electron from the inner orbital to a higher orbital. This higher orbital is known as the autoionizing state. Then the excited atom may undergo radiationless transition to yield the ground state of an ion with the ejection of an electron.

Excitation process $A + e^- \longrightarrow A^* + e^-$

Ionization process $A^* \longrightarrow A^+ + e^-$

where A^* is the excited atom.

Studies carried out by Nicholson (6) show that the threshold laws for direct ionization and autoionization are different. This is because the time for direct ionization is of the order of 10^{-15} sec. whereas that for autoionization is of the order of 10^{-12} sec. However, in certain cases, the lifetime of the excited state is very short. Therefore, an intermediate threshold law may hold for autoionization. For electron impact studies, this intermediate threshold law is

somewhere between the linear threshold law and the step function law. Theoretical curves for autoionization threshold laws are shown in fig. 7. Consequently, autoionization may show up as a hump in the ionization efficiency curves. Evidence of this phenomenom has been observed for atoms such as Zn^+, Cd^+, Hg^+ (7), Kr^+, Xe^+ (8) and for molecules such as CO^+ and $C_6H_6^+$ (9).

For molecules, sometimes the breaks in the ionization efficiency curve for the fragment ions can be assigned as the onset of a new process of ion formation from the parent ion. Such interpretaion was made by McDowell et al (10) in the case of ionization efficiency curve for CH_2^+ from CH_4. The appearance potential of CH_2^+ was found to be 15.6 eV. A break in the ionization efficiency curve was found at 20.1 eV. The difference in energy is 4.5 eV. This energy difference is equivalent to bond dissociation energy of H_2 molecule. The initial break was assigned to the following process.

$$CH_4 + e^- \longrightarrow CH_2^+ + H_2 + 2e^-$$

The break at 4.5 eV above the threshold ionization is the onset of the new process:

$$CH_4 + e^- \longrightarrow CH_2^+ + 2H + 2e^-$$

2.10 Electron Energy Spread

It is obvious from the above that the fine structure in the ionization efficiency curves provides us with considerable information about a particular atom or molecule. However, in order to observe the fine structure, the energy of electron beams causing ionization must be well defined. Unfortunately, in most commercial electron impact ion sources this is not the case. The electron energy spread arises from the fact that the bombarding electrons are obtained from a thermal emission process of a filament. Electrons obtained in this way possess considerable spread of kinetic energies. The electron energy spread is found experimentally to be similar to a Maxwellian distribution.

Fig. 7. Theoretical curves for autoionization threshold laws.

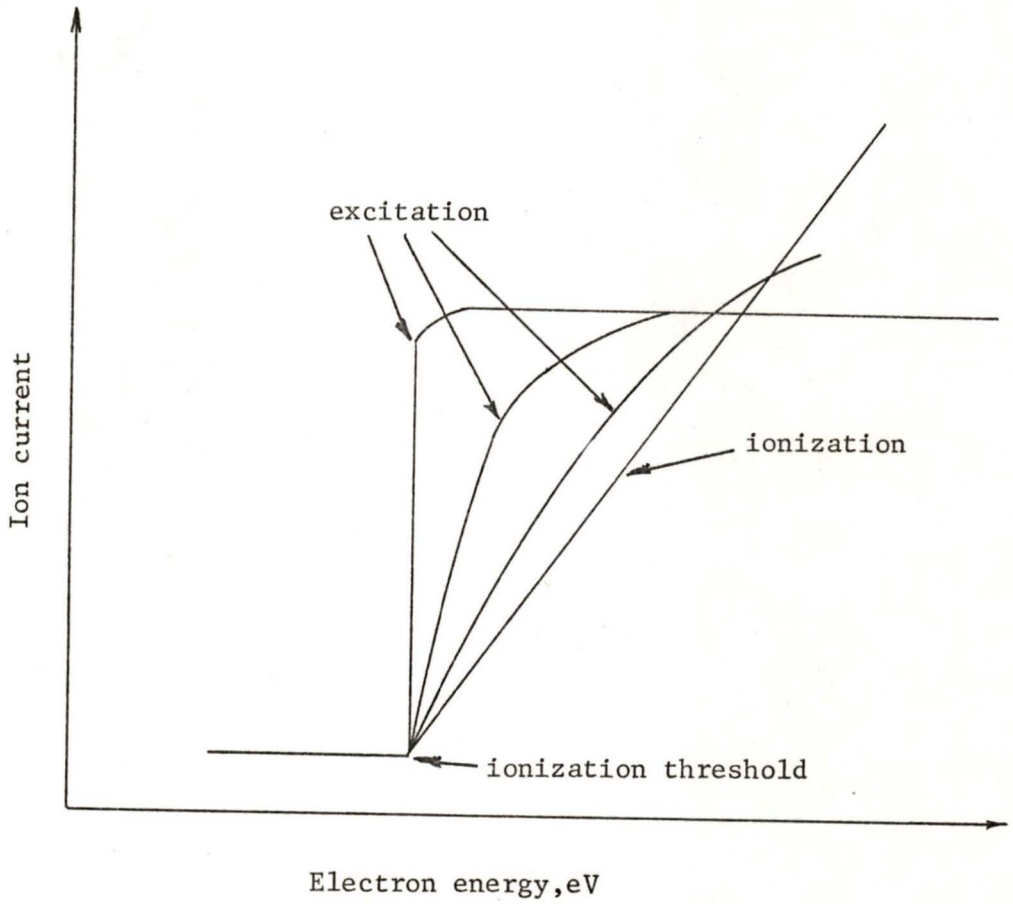

Thus $$dN(U) = (4\pi mA/h^3)\ U \exp\left[-(W+U)/kT\right] dU \qquad (2.15)$$

where dN: the number of electrons with energy U
m: mass of the electron
A: surface area of the filament
h: Planck's constant
k: Boltzmann's constant
W: work function of the filament
T: absolute temperature of the filament
U: kinetic energy of the electrons

For rhenium, the thermionic work function is 5.12 eV. If the rhenium filament is operating at 2000^{o}K, the half width of the electron energy spread is about 0.5 eV.

In order to observe the fine structure in the ionization efficiency curves, it is necessary to reduce this energy spread of the bombarding electrons. There are two principal experimental techniques for the production of essentially monoenergetic (very narrow energy spread) electron beams. These are the electrostatic energy selector and retarding potential difference (RPD) methods. Other methods, such as deflection by a magnetic field or combination of magnetic and electric fields have also been applied, but only the two most common methods will be brielfy described here.

(a) Electrostatic Energy Selector

The principle involved here is exactly the same as that for the electrostatic energy selector (fig. 8) used in the double focusing mass spectrometer. As the electrons pass through an electrostatic field, they feel an electrstatic force which may be equated with an equivalent centripetal force.

i.e. $$m_e v^2/r = eE$$

or $$m_e v^2/2 = reE/2 \qquad (2.16)$$

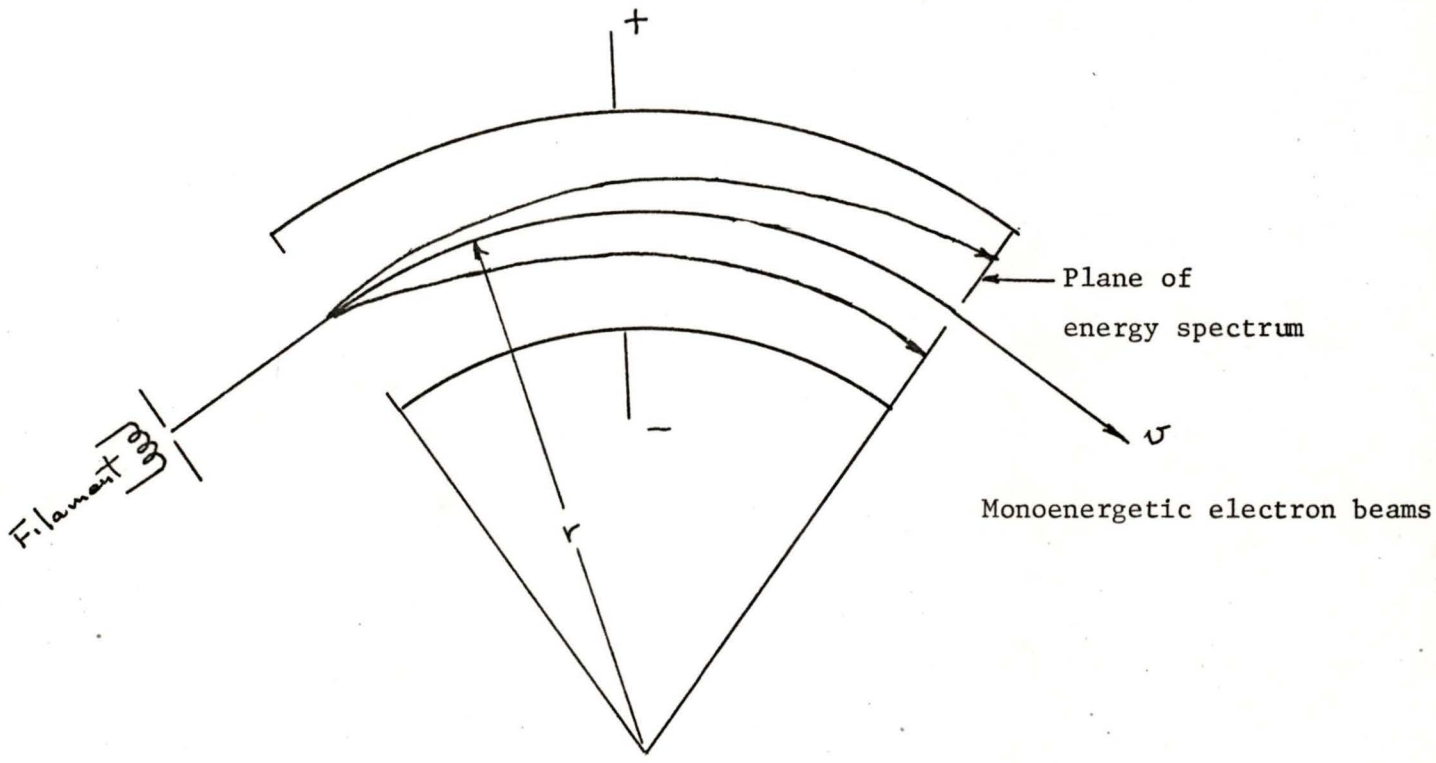

Fig. 8. Electrostatic energy selector.

where m_e : mass of the electron

v : velocity of the electron

r : radius of the electron orbit

e : charge associated with the electron

E : electrostatic field strength

The kinetic energy T acquired by the electron is:

$$T = 1/2\ m_e v^2 = eV \qquad (2.17)$$

where V is the accelerating voltage.

From equations (2.16) and (2.17)

$$r = 2V/E \qquad (2.18)$$

If E is held constant, r is related to the kinetic energy of the electrons and thus to the accelerating voltage and the initial energy. Slight variations in the initial kinetic energy will lead to slightly different values of r and with a very narrow exit slit for the electrostatic field, an essentially monoenergetic electron beam can be produced.

Using such an electrostatic selector, Marmet et al (11) obtained an electron beam with a half-width of 0.04 eV in the ion source of a mass spectrometer. Similar arrangements have also been used by other workers (12).

(b) Retarding Potential Difference (RPD) Method

In 1951, Fox et al (13) developed a method of producing monoenergetic electron beams known as the retarding potential difference method. In this method, a retarding electrode (fig. 9) is introduced between the filament and the ionization chamber. When no retarding potential is applied to this electrode, the normal potential for the electrons is V, and the electron beam reaching the ionization chamber will have the normal Maxwellian energy spread. A potential V_R, which is negative with respect to the filament (cathode), is applied to the retarding electrode. Any electrons which have potentials lower than this retarding potential, will not pass the retarding electrode. In this way, the low energy

Fig. 9. Retarding potential difference (RPD) method.

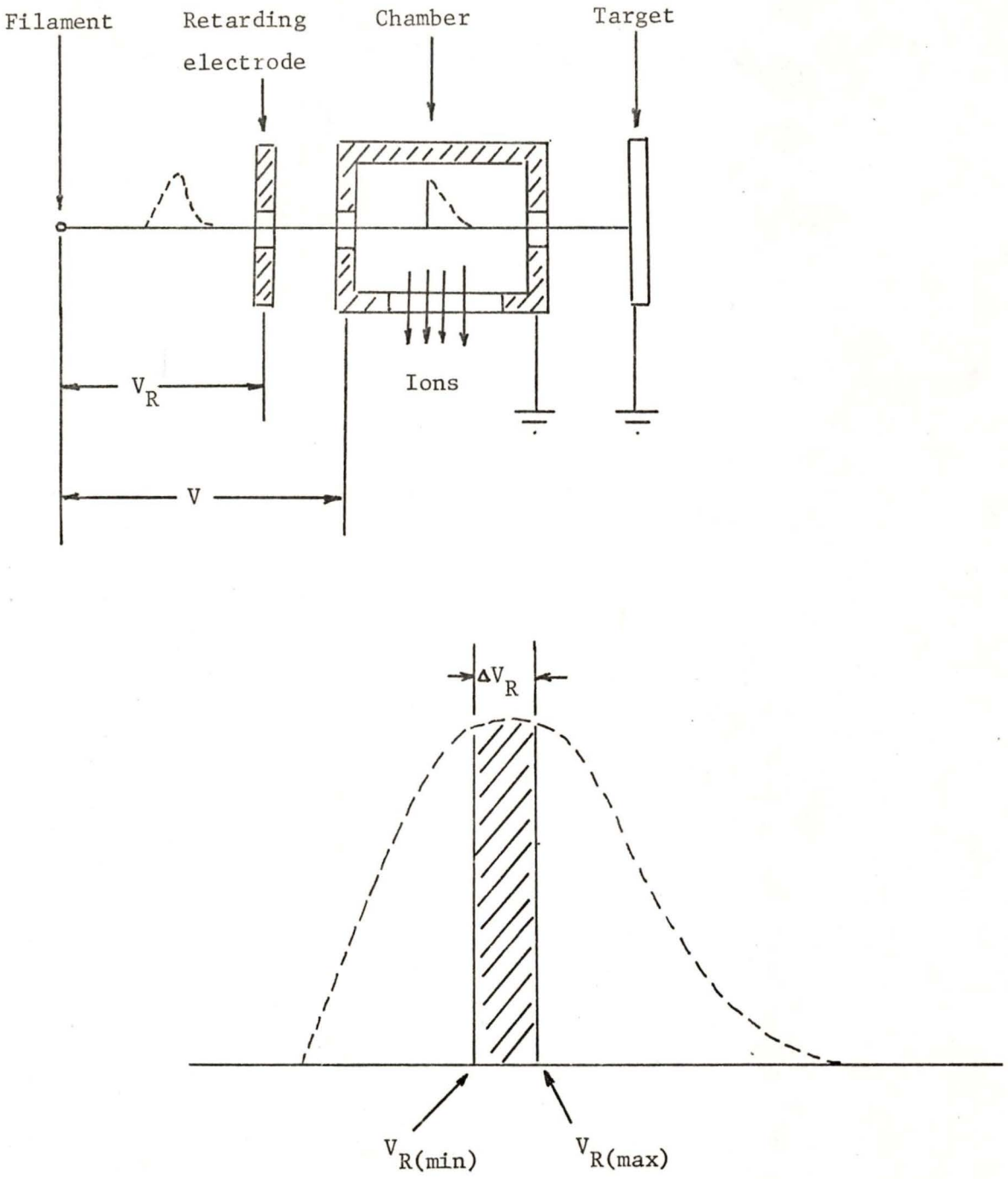

side of the electron energy spread is eliminated. The observed ion current is the result of the new electron energy spread (i.e. from $V_{R(min)}$ to higher energies in fig. 9). While keeping V constant, V_R can be increased by ΔV_R (say 0.1 eV). Another new electron energy spread is obtained and the ion current is the result of this electron energy spread. The difference in the two observed ion currents corresponds to the ion current which would be obtained with the electron energy spread of ΔV_R. Usually, ΔV_R is 0.1 eV and the effective spread on the energy of the electron beam may be reduced to approximately this value. It is then possible to observe the fine structure in the ionization efficiency curves.

(c) Analytical Techniques

Apart from experimental methods for producing monoenergetic electron beams, there are also analytical techniques which are designed to achieve essentially the same result but with considerably less modification to existing instrumentation. The two main ones are the Energy Distribution Difference method and the Fourier Transform method.

(1) The Energy Distribution Difference (EDD) Method

The EDD method developed by Winters et al (14) is the simplest analytical method. It is based on the assumptions that the electron energy spread may be represented by a Maxwellian distribution, with a very steep rise in the low energy side (fig. 10) and that the linear threshold law holds above a few volts of the threshold ionization (this may be represented by p(E), see fig. 11).

From equation (2.15), the Maxwellian distribution function is:

$$f(U) = \text{const} \times U \exp\left[-(W+U)/kT\right] \qquad (2.19)$$

The total energy of the electron is given by E.

Thus $$E = V + U \qquad (2.20)$$

Fig. 10. MAXWELLIAN DISTRIBUTION CURVE

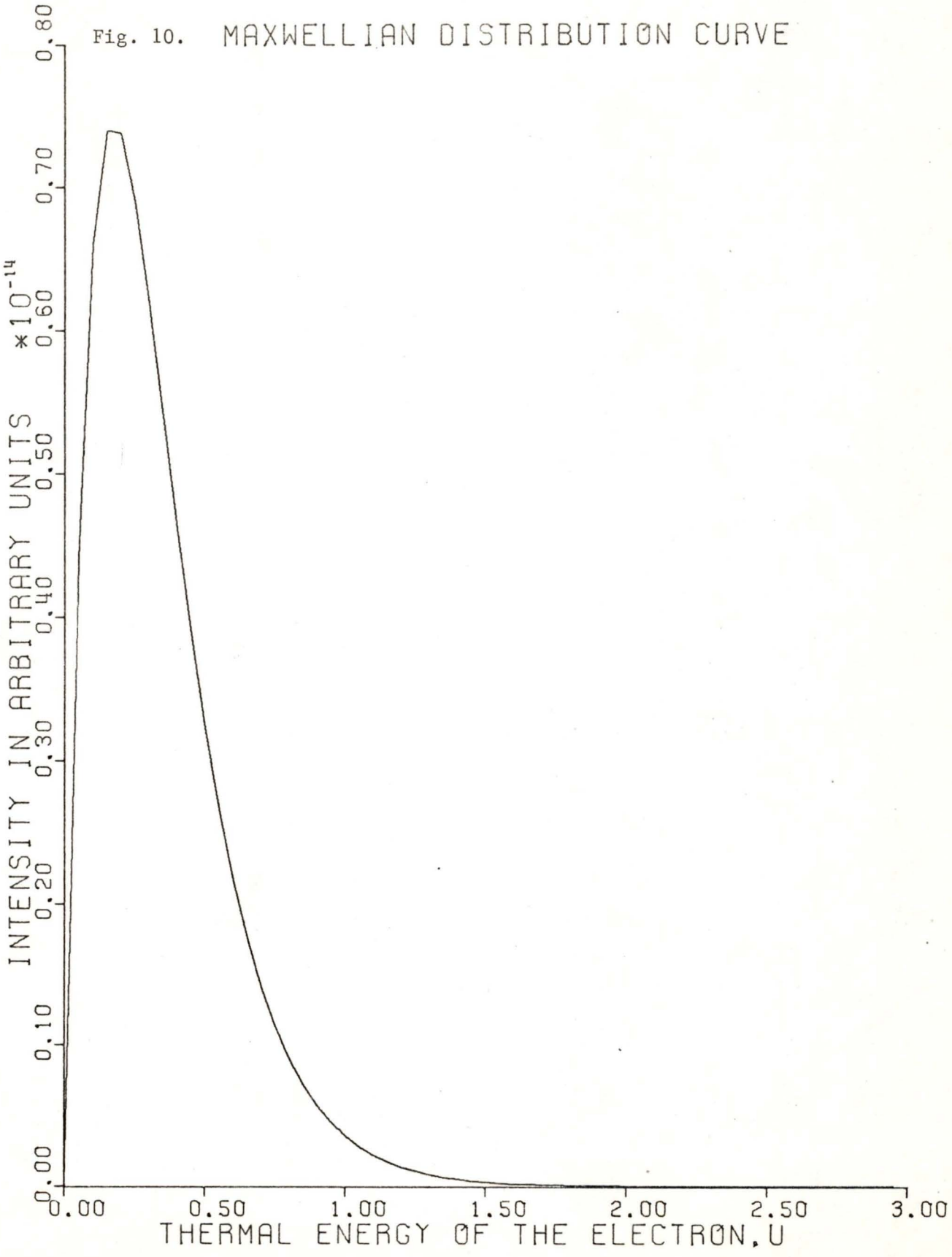

Fig. 11. Probability of ionization p(E).

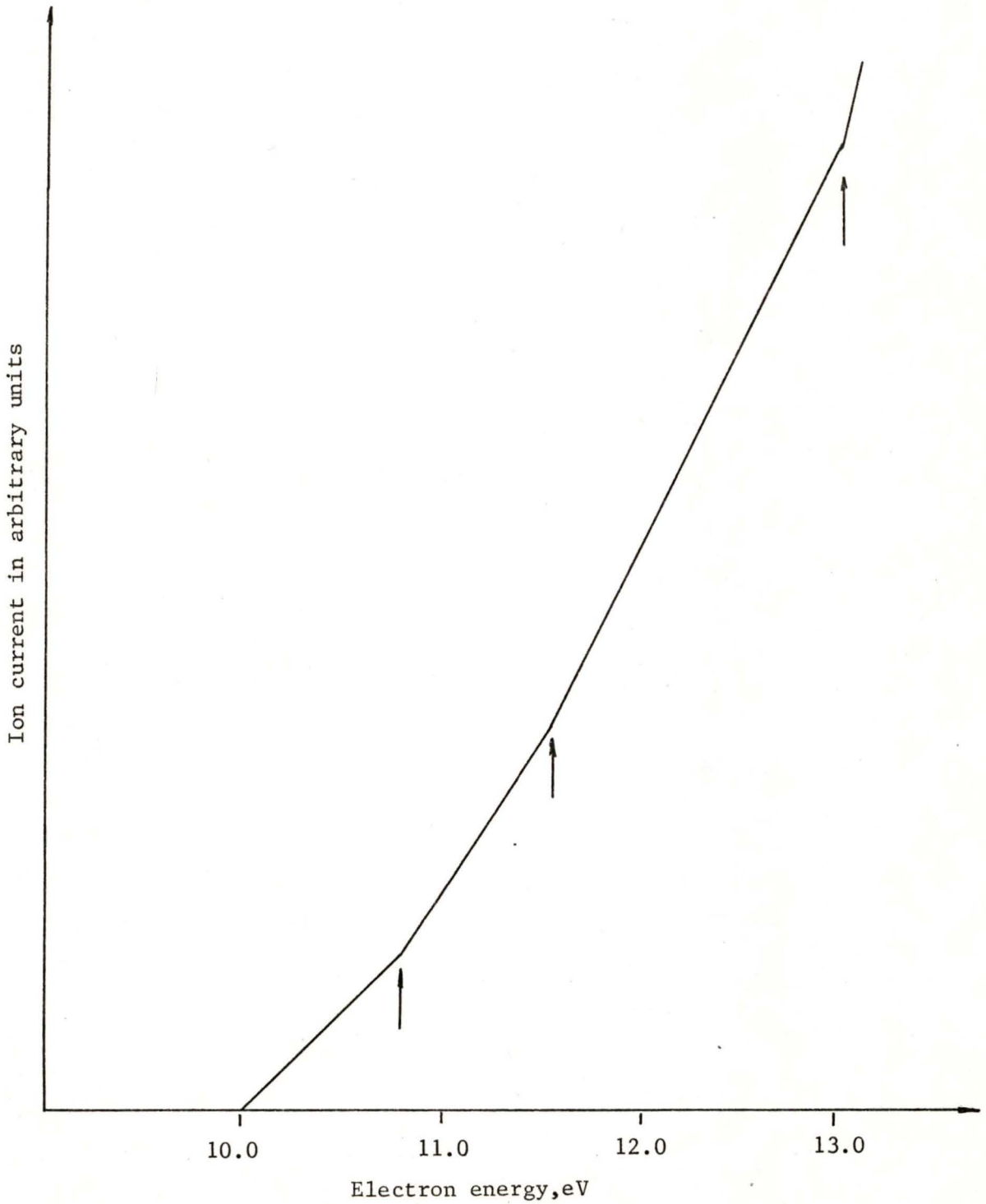

where V : the accelerating potential of the electron i.e. the potential difference between the filament and the ionization chamber

U : the thermal energy of the electrons

The ion current I(V) at the potential V is the convolution of f(U) and p(E) (fig. 12). The concept of convolution is outlined in the appendix.

$$I(V) = \text{const} \int_{V}^{\infty} f(E-V)p(E)dE \qquad (2.21)$$

where p(E) is the probability of ionization by an electron of total energy E.

As an approximation, a summation is used instead of integration.

$$I(V) = \text{const} \sum_{V}^{V+U_{max}} f(E-V)p(E)\,\Delta E \qquad (2.22)$$

U_{max} is taken to be the value above which f(U) is very small.

$$E = V + U$$

therefore $$U = E - V \qquad (2.23)$$

It can be seen from the above that the ion current I(V) at a particular potential V is the convolution of p(E) with the reverse electron energy spread f(-U) (see p. 39)

An approximate deconvolution, $\Delta I(V)$, can be obtained by use of the following difference formula:

$$\Delta I(V) = I(V) - B \times I(V + \Delta V) \qquad (2.24)$$

where B is a factor, always less than unity and ΔV is usually about 0.1 eV.

Equation(2.24) may be expanded as:

$$I(V) = \text{const} \sum_{V}^{V+U_{max}} f(U)p(E)\,\Delta E - \text{const} \times B \sum_{V+\Delta V}^{V+\Delta V+U_{max}} f(U-\Delta V)p(E)\Delta E$$

Fig. 12. Theoretical

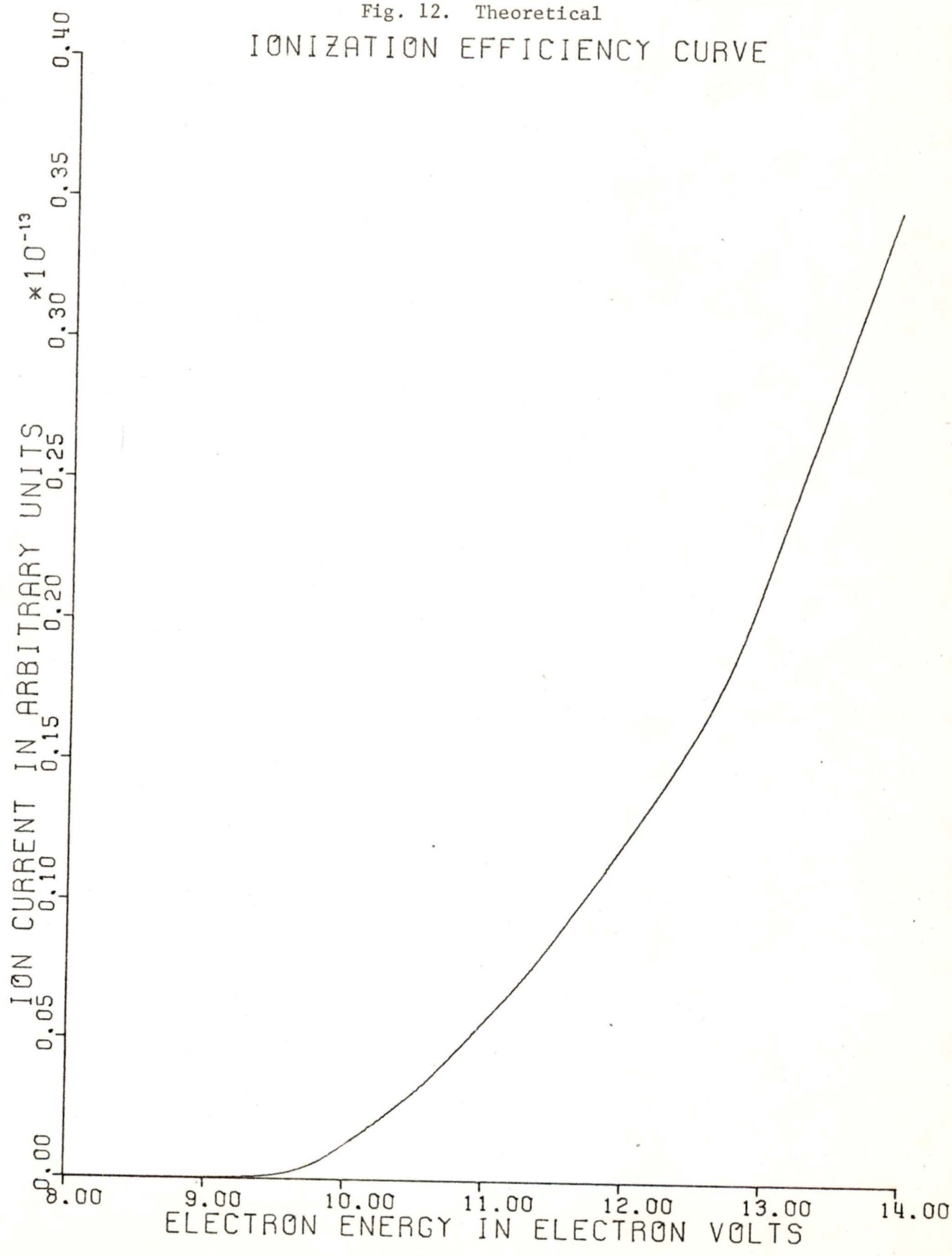

Fig. 13. Reduced electron energy spread by EDD method.

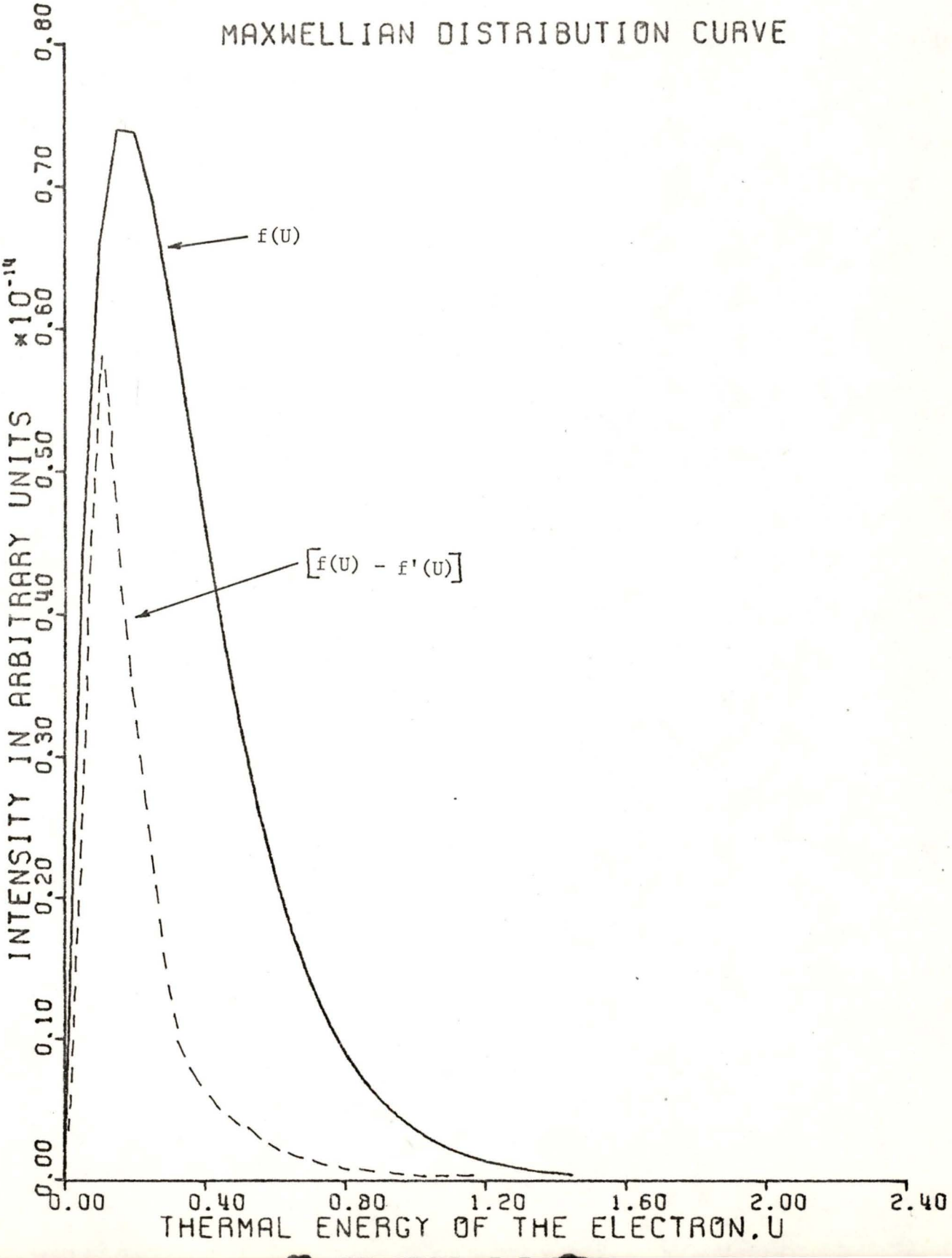

For the second term of this expression, the lower limit may be replaced by V since f(U-ΔV) is essentially zero for the range from V to V+ΔV and the upper limit replaced by $V+U_{max}$ by making a suitable choice of U_{max}.

Thus $$\Delta I(V) = \text{const} \sum_{V}^{V+U_{max}} \left[f(U) - f'(U) \right] p(E) \Delta E$$

where f'(U) = B x f(U-ΔV)

Mathematically, f'(U) is obtained by shifting f(U) by ΔV from the original distribution function and multiplying a factor B, i.e. f'(U) = B x f(U-ΔV). The value of B is chosen so that f'(U) is superimposed on the high energy side of the original distribution function f(U). As can be seen from fig. 13, this is equivalent to having a new distribution function, $\left[f(U) - f'(U) \right]$, which has a smaller energy spread.

Equation(2.24) can be used to determine the ion current at a particular potential without knowing the actual shape of the distribution function. The ion current thus obtained is equivalent to that which would be given by a reduced electron energy spread and the fine structure in the ionization efficiency curves can be observed more easily (fig. 14).

The EDD technique is actually a difference method and in this respect it has some analogies to the retarding potential difference method. The EDD method was used in the present work for determining ionization and appearance potentials and for observing fine structure in the ionization efficiency curves.

(2) The Fourier Transform (FT) Method

Morrison (15) used the Fourier Transform (FT) method to observe the fine structure in the ionization efficiency curves. The principles behind this method will be briefly outlined here.

From equation (2.21), the ion current I(V) at the potential V is given by:

$$I(V) = \text{const} \int_{V}^{\infty} f(E-V) p(E) dE \qquad (2.21)$$

Fig. 14. Deconvoluted

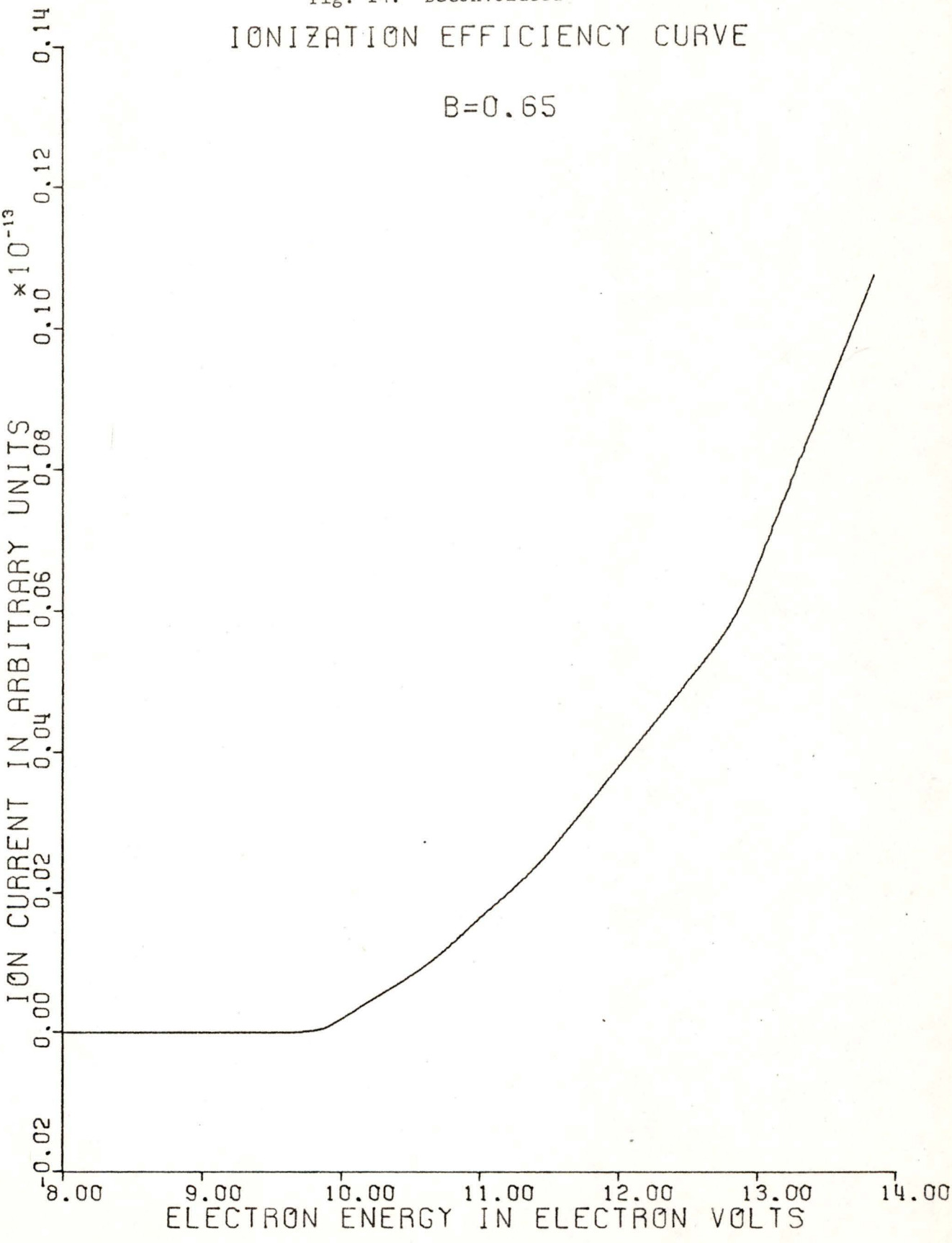

$$I(V) = \text{const} \int_{V}^{\infty} \bar{f}(V-E)p(E)dE$$

where $\bar{f}(U) = f(-U)$ (see appendix)

i.e. $$I(V) = \text{const}\ p(V)*\bar{f}(V) \qquad (2.25)$$

where * : convoluted with

Equation (2.25) can be represented by Fourier Transforms T (16).

$$T\left[I(V)\right] = T\left[p(V)\right] \cdot T\left[\bar{f}(V)\right] \qquad (2.26)$$

therefore $$T\left[p(V)\right] = T\left[I(V)\right] / T\left[\bar{f}(V)\right] \qquad (2.27)$$

$$p(V) = T^{-1}\left\{T\left[p(V)\right]\right\}$$

$$= T^{-1}\left\{T\left[I(V)\right] / T\left[\bar{f}(V)\right]\right\} \qquad (2.28)$$

If f(U) is known, Fourier Transforms can be obtained for I(V) and $\bar{f}(V)$. Therefore, from the above equations, p(V) can be determined. In this way, the probability of ionization p(V) (p(V)=p(E)) is the result of a monoenergetic electron beam since the effect of the electron energy spread has been eliminated. The major drawback with this method is that the experimental data must be very nearly noise free, and thus the method is extremely restricted in its applicability.

Chapter Three
Experimental Methods

3.1 Materials

(a) Cyclobutanone

Cyclobutanone was obtained from Aldrich Chemical Company, Inc., Milwaukee, Wis., 53233, U.S.A. (C-9600-1, Lot. No. 030607, Aldrich analyzed by I.R. and G.C.). The molecular weight is 70.09 and the boiling point is 100-102°C. The purity of a sample of the cyclobutanone was checked by gas chromatography (G.C.). The sample was analyzed on two separate columns (180 cm in length) using the Microtek MT 220 Gas Chromatograph. The columns used were 5% SE-30 (on Chromport) and 5% QF-1 (on 60/80 Varaport 30). In both cases, only one peak was detected. Thus, the purity of the cyclobutanone was estimated to be more than 99%. Further, an N.M.R. spectrum of the cyclobutanone was obtained by means of the Varian HA 60 NMR spectrometer (operated by Mrs. Christine Greenwood) with tetramethylsilane (TMS) as an internal standard. The NMR spectrum obtained was essentially the same as that given by Gutshe et al (17). The cyclobutanone was used for this work without further purification.

(b) Xenon

Xenon was obtained from Airco Industrial Gases, Division of Air Reduction Co. Inc. Riverton, N.J., U.S.A. The purity of Xenon (research grade) was estimated to be 99.99% (Supplier's data).

(c) Argon

Argon (Linde specialty gas) was obtained from Union Carbide Canada Ltd., Toronto. The purity was estimated to be more than 99.99% (Supplier's data).

3.2 The Mass Spectrometer

A schematic diagram of the Hitachi Perkin-Elmer RMU-7 double focusing mass spectrometer is shown in fig. 2, p 15. The temperature of the ionization

chamber was maintained at 250°C. A rebuilt filament of rhenium was used. The filament was rebuilt by Vaccumetrics Inc. (Mass Spectrometers and Accessories), 241 Crescent St., Waltham, Ma 02154, U.S.A. Since the boiling point of cyclobutanone is 100-102°C, the inlet system for volatile liquids was used. The background pressure was usually about 4×10^{-7} torr and the pressure in the analyser tube was usually about 3×10^{-6} torr when a sample was being run.

3.3 Mass Spectra at Various Electron Energies

The first part of this work was to obtain mass spectra of the cyclobutanone at various electron energies i.e. from the threshold ionization to 70 eV. A typical setting of the parameters of the mass spectrometer is shown in Table 3.

Table 3

A Typical Setting of the Parameters of the Mass Spectrometer

Slit width
Si=0.1 mm
S_α=1.0 mm
S_β=1.0 mm
Sc=0.1 mm

Note: the locations of Si, S_α, S_β, and Sc are shown in fig. 2, p 15.

Multiplier Voltage = 1.75 KV
Sensitivity = 100

Grid Voltage = -4 volts

Dial setting for
Repeller 1 = 1.5
Repeller 2 = 1.0
Lens Fine 1 = 5.5
Lens Fine 2 = 0.8
Lens Coarse = 7

Mass range = 300
Scanning speed setting = 9
Paper speed = 6 mm/sec.

Mass spectra of the cyclobutanone at various electron energies are shown in fig. 15. The voltage readings were taken from the Vidar 520 digital voltmeter, which was connected between the filament and the ionization chamber. These voltage readings are uncorrected.

It should be mentioned here that a metastable peak was observed at m/e=25.2. The metastable peak was first observed at about 2 eV above the threshold ionization of the molecule of cyclobutanone. The observation of a metastable peak at m/e=25.2 indicated that a metastable transition occurred from m/e=70 to m/e=42. However, at m/e=42 two fragment ions CH_2CO^+ and $C_3H_6^+$ are possible from the decomposition of the parent molecular ion, m/e=70. The two possible fragmentation pathways are as follows:-

Path A 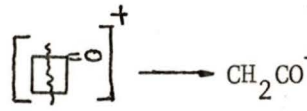 $\longrightarrow CH_2CO^+ + C_2H_4$ (3.1)

Path B 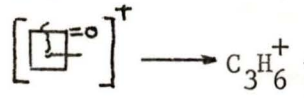 $\longrightarrow C_3H_6^+ + CO$ (3.2)

In order to observe any doublets in the peaks, particularly at m/e=42 and m/e=28, a new setting of the parameters of the mass spectrometer was selected (Table 4).

Table 4

Settings for Detecting Doublets

Slit width

Si=0.08 mm

S_α=1.00 mm

S_β=1.00 mm

Sc=0.05 mm

Multiplier Voltage=2.0 KV

Sensitivity=100

Chamber Voltage=70 eV

Scanning speed setting=6

Paper speed=1.5 mm/sec.

Other settings were the same as in table 3

Fig. 15. Mass spectra of cyclobutanone at various electron energies.

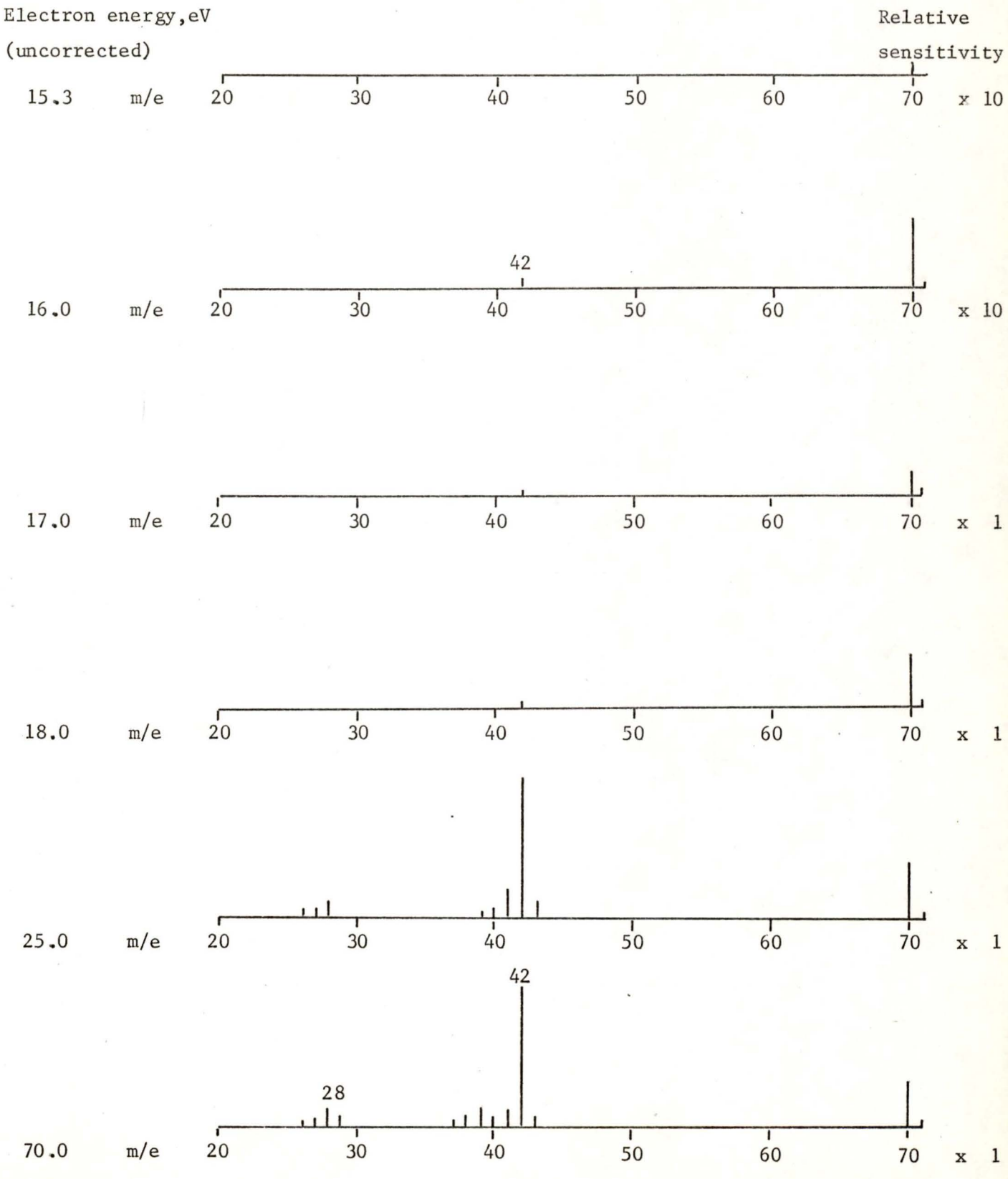

When examining the mass spectrum obtained by the new settings, doublets were observed at m/e=42,41,40 and only one peak was observed at m/e=39. Similarly, a doublet was observed at m/e=28 (actually, three peaks were observed at m/e=28 but one of them was N_2^+ from the air in the background). Further, by changing the scanning speed and paper speed, the three peaks could be well separated as shown in fig. 16. They are assigned to $C_2H_4^+$, N_2^+ and CO^+.

The doublet at m/e=42 was closely examined at various electron energies just above the threshold ionization. The results are shown in fig. 17.

Similarly, doublets at m/e=41 and m/e=40 were examined at various electron energies near to the threshold for their production and the results are shown in fig. 18 and fig. 19 respectively.

In all cases, the background was carefully checked and no trace of peaks could be detected at these masses under the operating sensitivities.

3.4 Accurate Mass Determinations of the Doublet at m/e=42

Experimental results (18) have suggested that most cyclobutanones undergo two major fragmentation pathways. One yields a ketene and an olefin (Path A) and the other yields carbon monoxide and a hydrocarbon fragment (Path B).

Path A 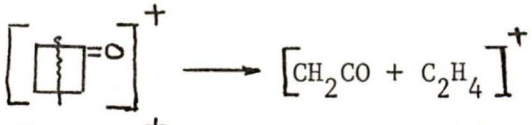 (3.3)

Path B 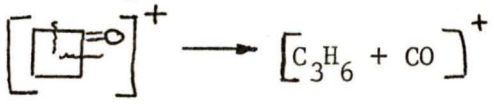 (3.4)

However, using high resolution mass spectrometry, Hofman (19) in 1964 showed that cyclobutanone gives only ketene and ethylene (Path A) at 70 eV. The doublet at m/e=42 found in the present work is in contrast to Hofman's findings and consequently it was decided to determine the accurate masses of the peaks in the doublet. This would confirm the identity of the peaks.

Fig. 16. Triplet spectrum at m/e=28.

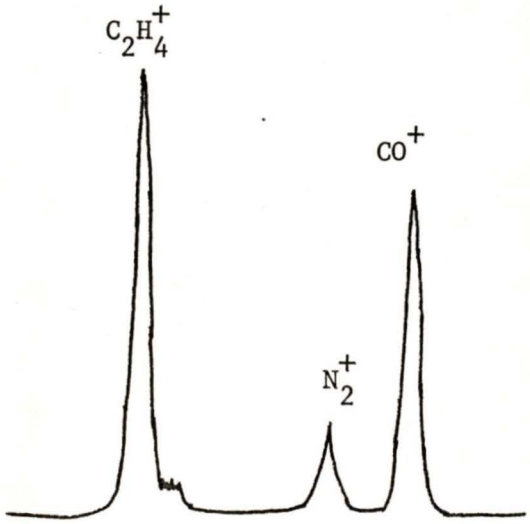

CO^+	m/e=27.994914
N_2^+	m/e=28.006148
$C_2H_4^+$	m/e=28.031300

Electron energy,eV (uncorrected) | Relative sensitivity

m/e=42

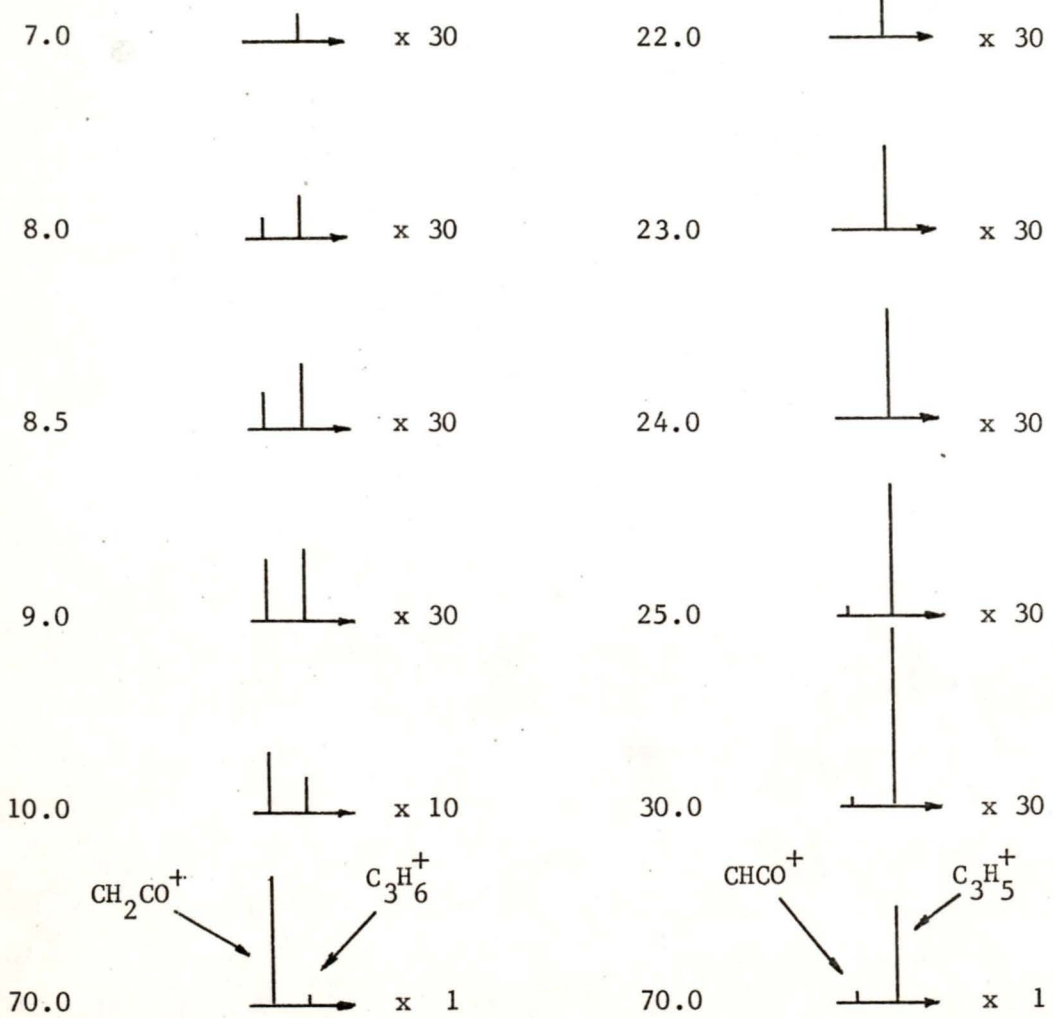

Fig. 17.

Electron energy,eV (uncorrected) | Relative sensitivity

m/e=41

Fig. 18.

CH_2CO^+ m/e=42.0106

$C_3H_6^+$ m/e=42.0470

Electron energy,eV (uncorrected) | Relative sensitivity

m/e=40

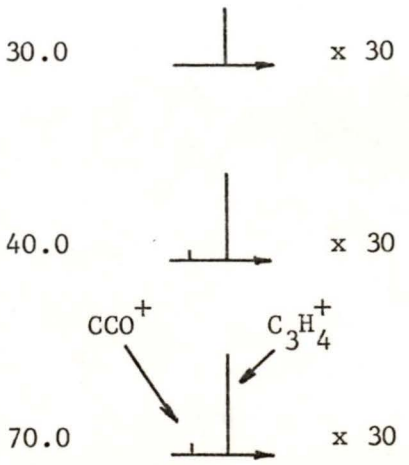

Fig. 19.

In order to carry out the accurate mass determinations, a Hitachi MK 14-B peak matcher was used in conjunction with the double focusing mass spectrometer. The standard used in this case was n-butane gas. The standard, n-butane, was introduced through the gas inlet system and the sample cyclobutanone through the volatile liquid inlet system. As two known peaks were required for the determinations, the two chosen were $C_3H_5^+$ (m/e=41.0391) and $C_3H_7^+$ (m/e=43.0548). In the standard, there was a small peak at m/e=42 (or 42.0470) i.e. $C_3H_6^+$. The determinations were carried out on mass range 300 of the mass spectrometer.

Using the Hitachi MK 14-B peak matcher, the two known peaks were first matched. The unknown peak was between the two known peaks m_o and m_1 where $m_o > m_1$. The unknown peak m was the more intense peak (at lower mass number) of the cyclobutanone doublet. Then, the unknown peak was matched exactly with the known peak m_o. Two determinations were carried out on different days. The readings Δm on the peak matcher were found to be 0.50633 and 0.50642.

Using the following equation:

$$m = \frac{m_o}{1 + \left[\frac{m_o}{m_1} - 1 \right] \Delta m} \qquad (3.5)$$

For the two determinations, the values of the unknown peak m were calculated to be 42.0101 and 42.0099. Within experimental errors and with no other possibilities, the unknown peak m corresponds to CH_2CO^+. The experimental values and the theoretically calculated value for CH_2CO^+ are shown in Table 5.

Table 5

Accurate Mass Determinations for One of the Doublet at m/e=42

Nuclidic mass used

H= 1.007825

O=15.994915

C=12.000000

		I	II
Δm		0.50633	0.50642
m found		42.0101	42.0099
CH_2CO^+	calculated	42.0106	42.0106
Difference		.0005	.0007

Therefore, the average value of m was found to be 42.0100 and compared with the theoretical calculated value of CH_2CO^+, the error is less than one millimass unit.

It was noticed at the same time that the other peak of the doublet (less intense one, at higher mass number) matched exactly with the small known peak of the standard i.e. $C_3H_6^+$, m/e=42.0470.

Therefore, the doublets at m/e=42 were found to be CH_2CO^+ and $C_3H_6^+$. This suggested that cyclobutanone does undergo two major fragmentation pathways as shown by equations (3.3) and (3.4).

3.5 Ionization Efficiency Curves

In order to obtain ionization efficiency curves of any ions, slight modifications were made to the mass spectrometer. First, a Vidar 520 digital voltmeter was connected between the filament and the ionization chamber so that the energy

acquired by the electrons emitted from the heated filament could be accurately monitored. Secondly, a stepping motor (manufactured by the A.W. Haydon Company, Waterbury, Conn., U.S.A.) was directly connected to the potentiometer which controls the energy of the electron beam. In this way, the energy of the electron beam could be scanned gradually with equal voltage intervals corresponding to equal time intervals.

(a) Procedures

A sample of cyclobutanone was introduced into the mass spectrometer through the volatile inlet system and, simultaneously, a calibrating inert gas, Xe, was introduced through the gas inlet system. Using the mass spectrometer i.e. by varying the magnetic field strength, a particular ion peak was selected. The slit widths were so chosen that at the given ion peak, a small change in the magnetic field strength produced essentially no change in the ion current. A typical peak shape is shown in fig. 20. When obtaining the ionization efficiency curve of a particular ion peak, the magnetic field strength was chosen to be approximately in the middle of the plateau (indicted by the arrow in fig. 20).

The slit width chosen were as follows:-

Si=0.1 mm

S_{α}=0.5 mm

S_{β}=0.5 mm

Sc=0.5 mm

Other settings were so adjusted as to give the best sensitivity and stability.

The ion current of the particular peak was detected by the electron multiplier. A Cary 401 Vibrating Reed Electrometer was connected to the electron multiplier and thus the ion current was amplified. The value of the ion current was digitized and stored in a NS 560 Signal Averaging Computer (SAC).

Great care had to be taken with the doublet at m/e=42, since the two ion peaks CH_2CO^+ and $C_3H_6^+$ were in part superimposed on each other (fig. 21).

Fig. 20. Peak shape of ion current versus magnetic field.

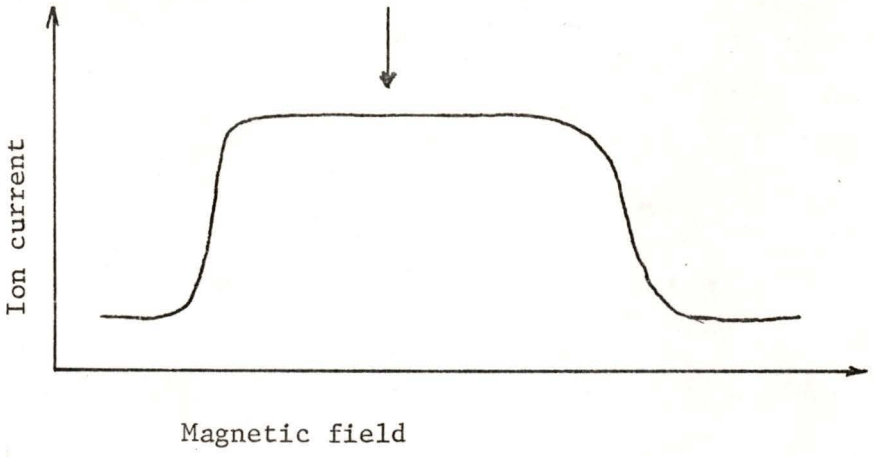

Fig. 21. Peak shape at m/e=42.

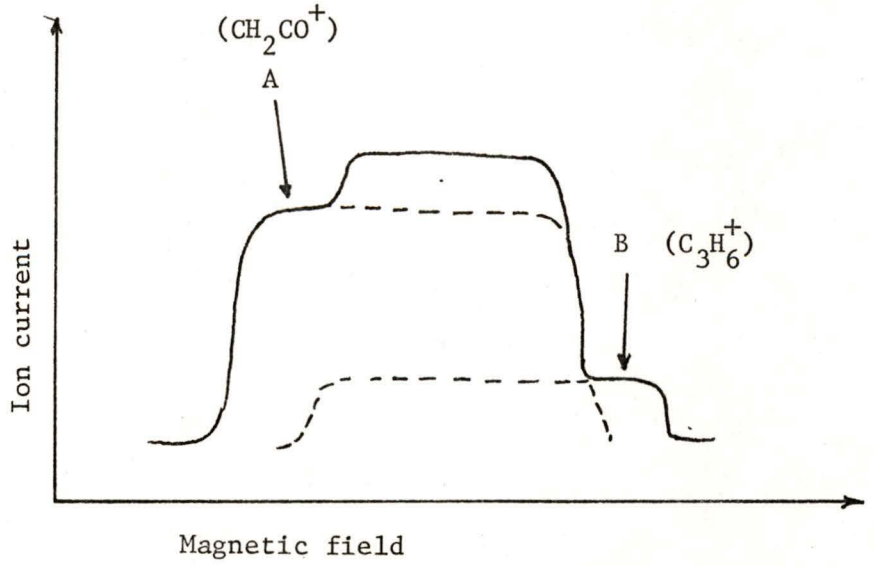

With the slit settings required to give a highly stable ion beam, it was not possible to separate these two ion peaks completely. The ionization efficiency curves were obtained by setting the magnetic field at position A on the peak for CH_2CO^+ and at position B on the peak for $C_3H_6^+$. It was obvious that the ion currents at these positions were not as stable as those given by cyclobutanone at m/e=70 and Xe^+ at m/e=132 as shown by the peak shape in fig. 20. Nevertheless, the ionization efficiency curves for CH_2CO^+ and $C_3H_6^+$ were different from one another and at the same time reproducible.

(b) Methods for Obtaining Ionization Efficiency Curves

Using the settings mentioned above, a particular ion peak was selected. Sitting at the position of the ion peak as shown in fig. 20 or fig. 21, the energy of the electron beam was set a few volts below the threshold ionization of the ion so that there was no ion current reading on the vibrating reed electrometer. The stepping motor was started and this increased the voltage gradually as observed on the Vidar 520 digital voltmeter. When the voltage reached a certain value, say 10.0V, a switch was pushed to trigger the NS 560 SAC, thus recording in digital form, the values of the ion current (in arbitrary units) in the memory addresses of the SAC. When the last address was reached (i.e. after 8 min. 31 sec. with a dwell time of 0.5 sec. per channel), the stepping motor was stopped and the final voltage recorded. There are 1023 memory addresses in the NS 560 SAC. Generally, the voltage interval for 8 min. 31 sec. was about 8 volts, thus each address interval was equivalent to approximately 0.008 volt interval.

The initial and final voltages were recorded and values for ion current were stored in the memory addresses of the NS 560 SAC. These values were converted to paper tape through the teletype.

Once the values of the ion current were stored on the paper tape; these data were treated as follows:

At the University of Victoria Computing Centre, the paper tape was converted into magnetic tape by means of Mohawk 6405 paper tape reader / Mohawk 6401 keyed data recorder. Using a program, Catran (written by A.L. Wilkinson of the Department

of Chemistry) together with the University of Victoria computer IBM 360/50, the data on the magnetic tape were converted and stored on IBM punch cards. In this way, the data could be used several times without tying up a magnetic tape.

In order to use the Calcomp Pen Plotters to produce the ionization efficiency curves, a program was specially written. In this program, the main input data are the initial and final voltage readings together with the values of the ion current available from the punch cards.

A 15-point 5th degree smoothing (20) subroutine was incorporated in the main program. Using least square methods, the smoothing subroutine takes 15 data points and fits them to a 5th degree equation and produces a new value. In this way, seven initial and seven final points are lost each time the smoothing subroutine is called. The smoothing subroutine can be called as many times as required. In this work, the smoothing processes were only repeated three times in every case, and this provided data of sufficient quality to be treated by the EDD method.

The smoothed values of the ion current were used in equation (3.6) to give new deconvoluted values of the ion current.

$$\Delta I(V) = I(V) - B \times I(V+\Delta V) \qquad (3.6)$$

In the program, the values of B and ΔV could be varied.

A plotting subroutine was also incorporated in the main program. Thus, all the plotting instructions were stored in tape file through the IBM 360/50 computer. The tape file was then removed from the computer and put onto the Calcomp Pen Plotters. In this way, plots of the ionization efficiency curves were obtained.

A flowchart diagram for obtaining ionization efficiency curves is shown in fig. 22. Unsmoothed, smoothed, and deconvoluted ionization efficiency curves of $Xe^{+}\{132\}$ plotted by the Calcomp Pen Plotters are shown in fig. 23,24, and 25.

Fig. 22. Flowchart diagram for obtaining ionization efficiency curve.

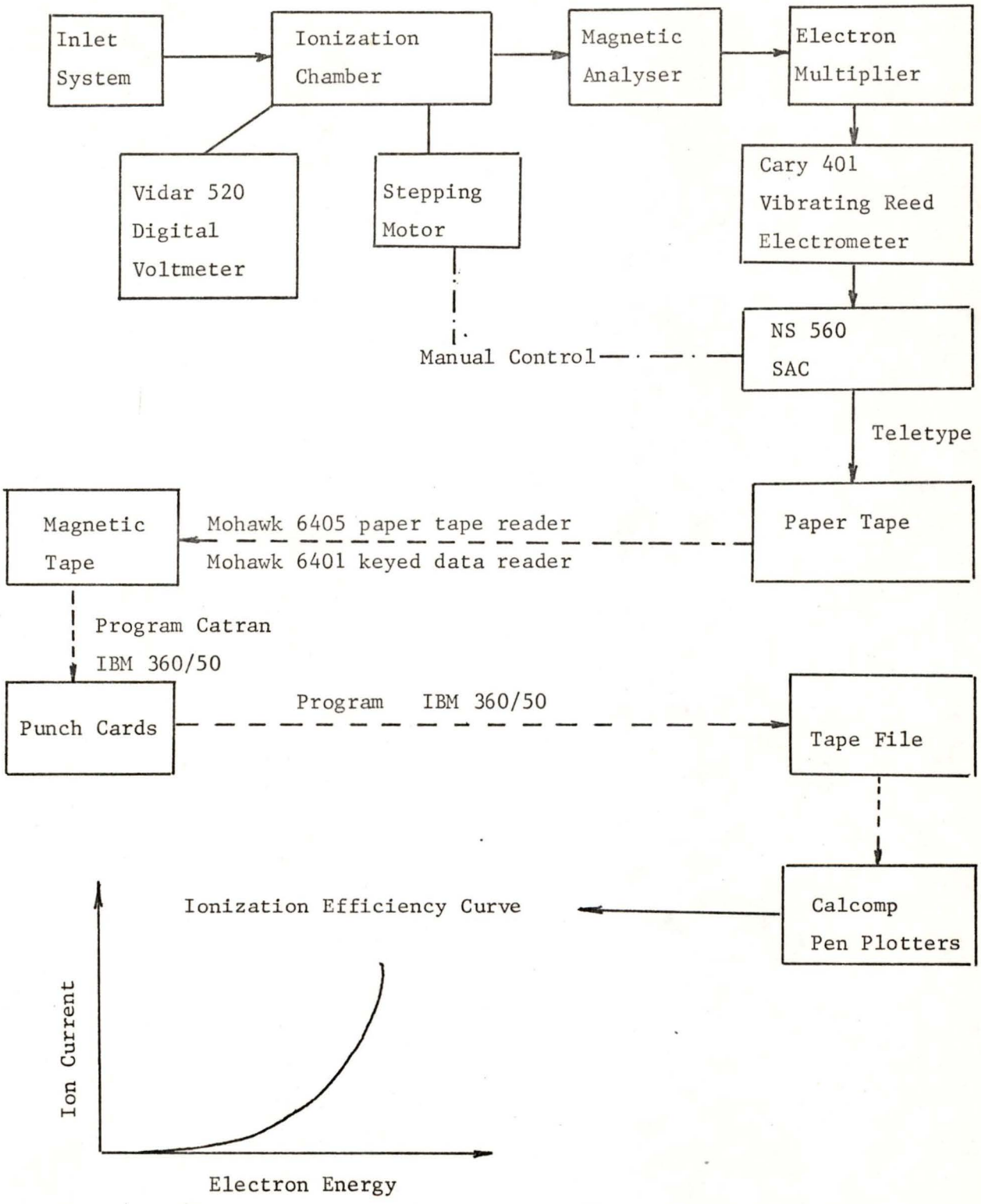

Fig. 23.

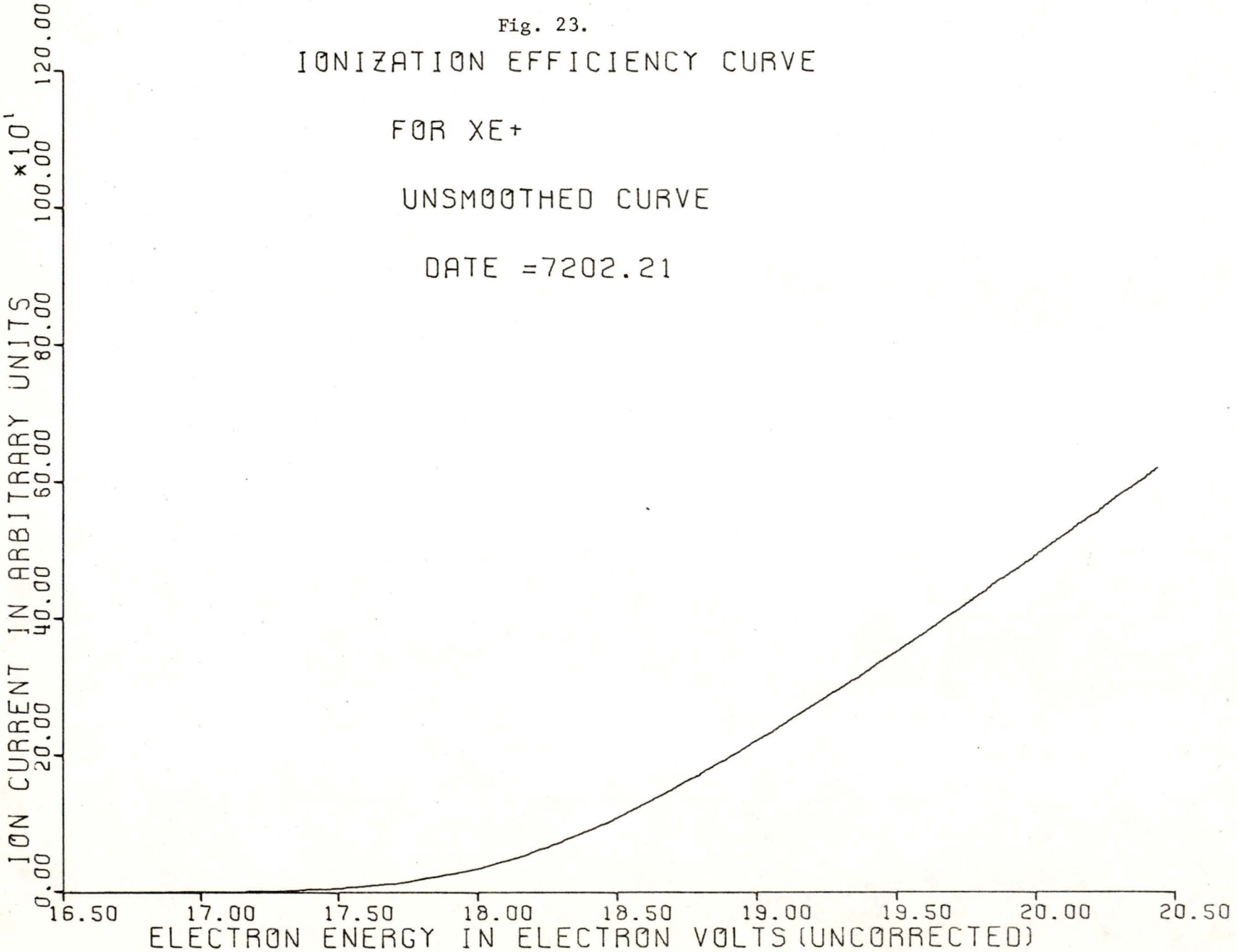
IONIZATION EFFICIENCY CURVE
FOR XE+
UNSMOOTHED CURVE
DATE =7202.21
ION CURRENT IN ARBITRARY UNITS
*10¹
0.00
20.00
40.00
60.00
80.00
100.00
120.00
16.50
17.00
17.50
18.00
18.50
19.00
19.50
20.00
20.50
ELECTRON ENERGY IN ELECTRON VOLTS (UNCORRECTED)

Fig. 24.

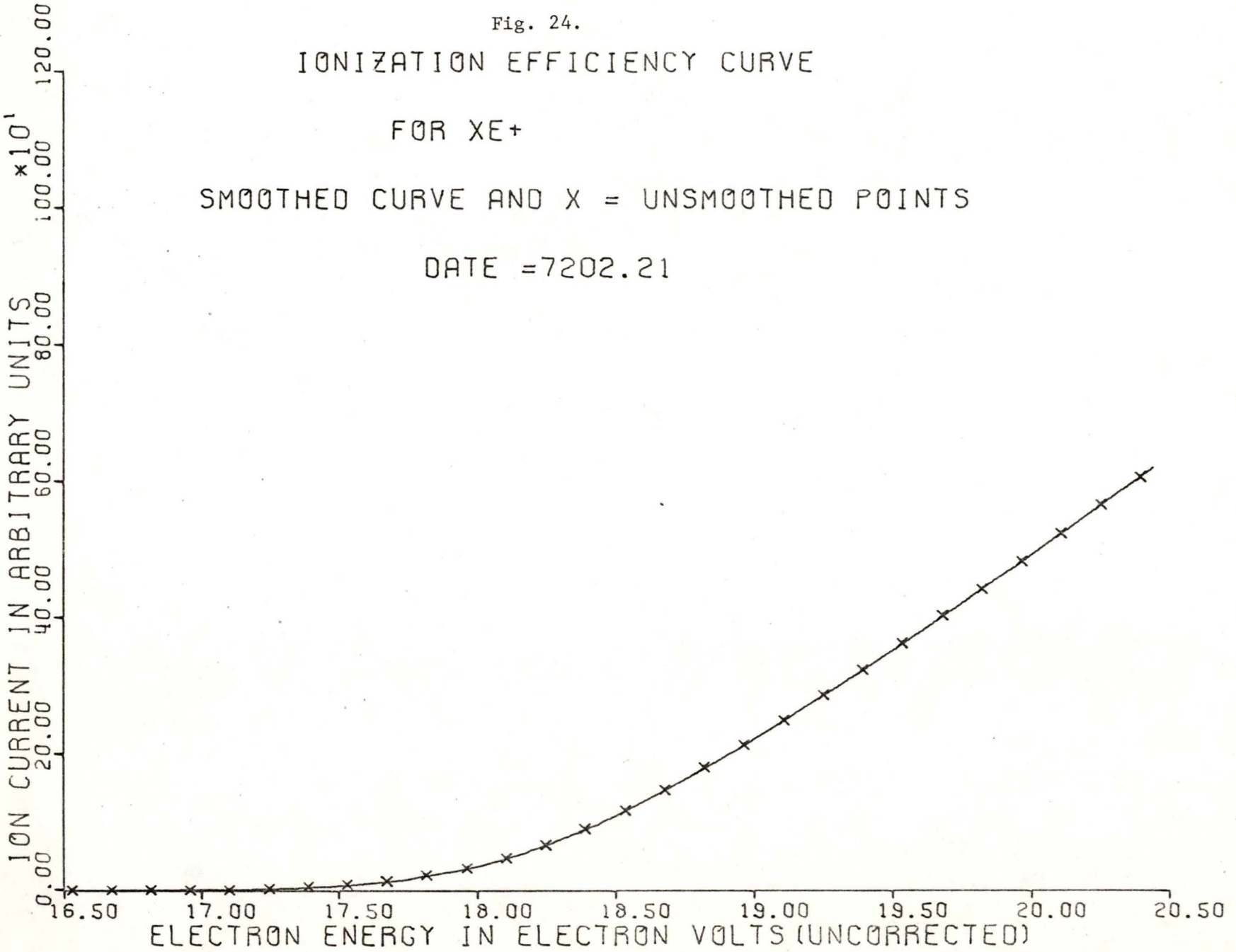
IONIZATION EFFICIENCY CURVE
FOR XE+
SMOOTHED CURVE AND X = UNSMOOTHED POINTS
DATE =7202.21
ION CURRENT IN ARBITRARY UNITS
*10¹
0.00
20.00
40.00
60.00
80.00
100.00
120.00
16.50
17.00
17.50
18.00
18.50
19.00
19.50
20.00
20.50
ELECTRON ENERGY IN ELECTRON VOLTS (UNCORRECTED)

Fig. 25.

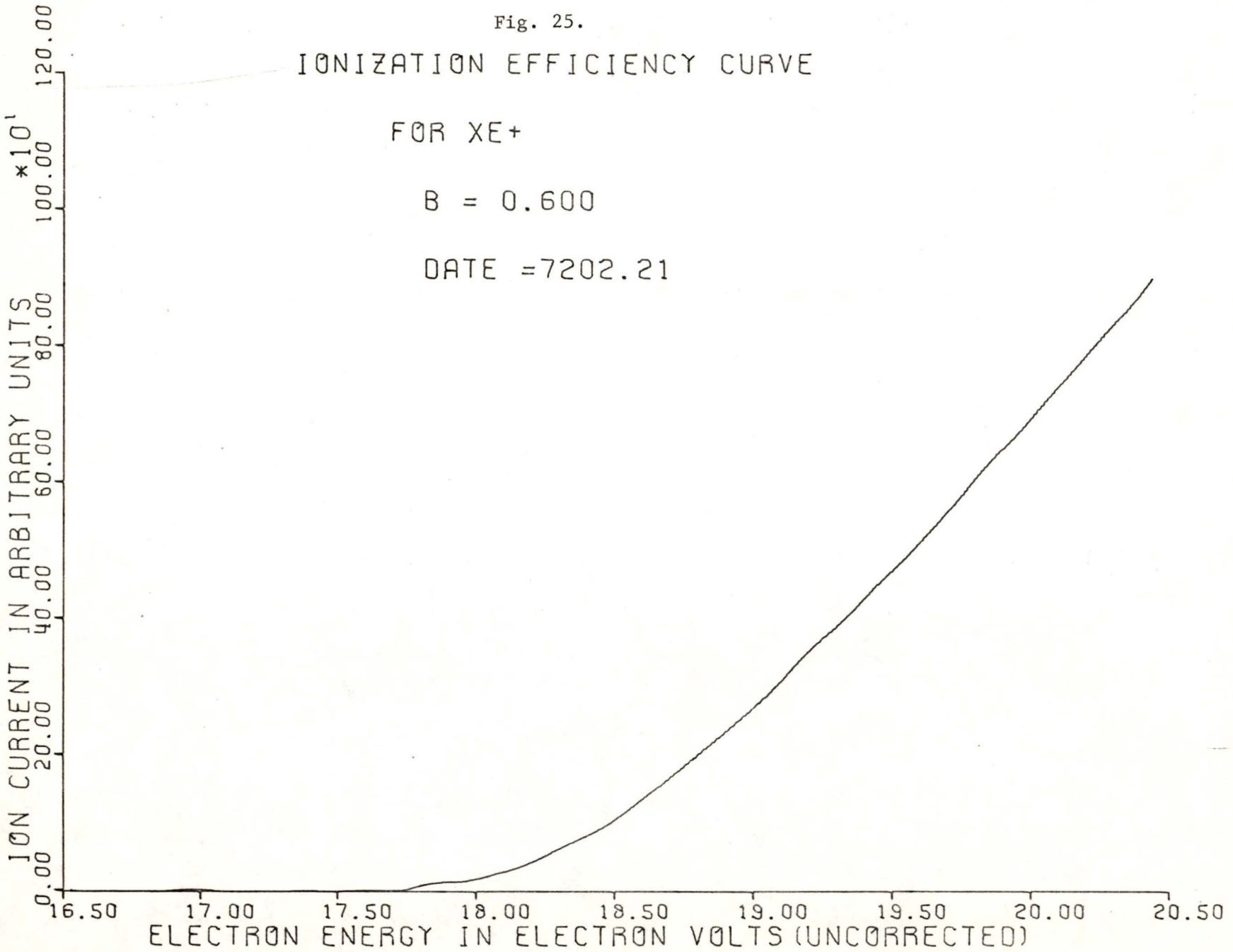
IONIZATION EFFICIENCY CURVE
FOR XE+
B = 0.600
DATE =7202.21
ION CURRENT IN ARBITRARY UNITS
*10¹
0.00
20.00
40.00
60.00
80.00
100.00
120.00
16.50
17.00
17.50
18.00
18.50
19.00
19.50
20.00
20.50
ELECTRON ENERGY IN ELECTRON VOLTS (UNCORRECTED)

Using the above prodedures, ionization efficiency curves were obtained for $Xe^{+}\{132\}$, cyclobutanone at m/e=70, the fragment ions CH_2CO^{+} and $C_3H_6^{+}$. All the ionization efficiency curves were repeated at least six times.

As a check for the whole system, ionization efficiency curves were obtained for Xe^{+} and Ar^{+} (as a mixture). The results of this check could be compared with the literature to show whether the system could be used to determine ionization potentials and to observe fine structure in the ionization efficiency curves.

Chapter Four
Results and Discussions

4.1 Check on Experimental Methods

As a check on the EDD method of deconvolution and on the experimental methods to be used in this study, a series of tests were undertaken. In these tests, a hypothetical ionization efficiency curve was constructed by the convolution of a suitable energy distribution function with an idealized curve consisting of a series of straight line segments. This curve was then deconvoluted using the EDD technique. In order to test the experimental methods employed, a detailed study of the ionization efficiency curves of argon and xenon was undertaken, in order to compare the curves obtained in the present work with cases which are well reported in the literature (14).

(a) Hypothetical and Deconvoluted Ionization Efficiency Curves

As mentioned in section 2.10(c), the ion current I(V) at a potential V is the convolution of the Maxwellian distribution function f(-U) with the probability of ionization p(E). Thus a hypothetical ionization efficiency curve can be constructed by using equation (2.22).

$$I(V) = \text{const} \sum_{V}^{V+U_{max}} f(E-V)p(E)\Delta E \qquad (2.22)$$

The Maxwellian distribution curve can be constructed by using equation (2.19).

$$f(U) = \text{const} \times U \exp\left[-(W+U)/kT\right] \qquad (2.19)$$

If a rhenium filament is used and the operating temperature is 2000°K, the half-width of the electron energy spread is about 0.5 eV (the thermionic work function of rhenium is 5.12 eV). In this way, a Maxwellian distribution curve was obtained and is shown in fig. 26. A hypothetical p(E) curve (fig. 27)

Fig. 26.

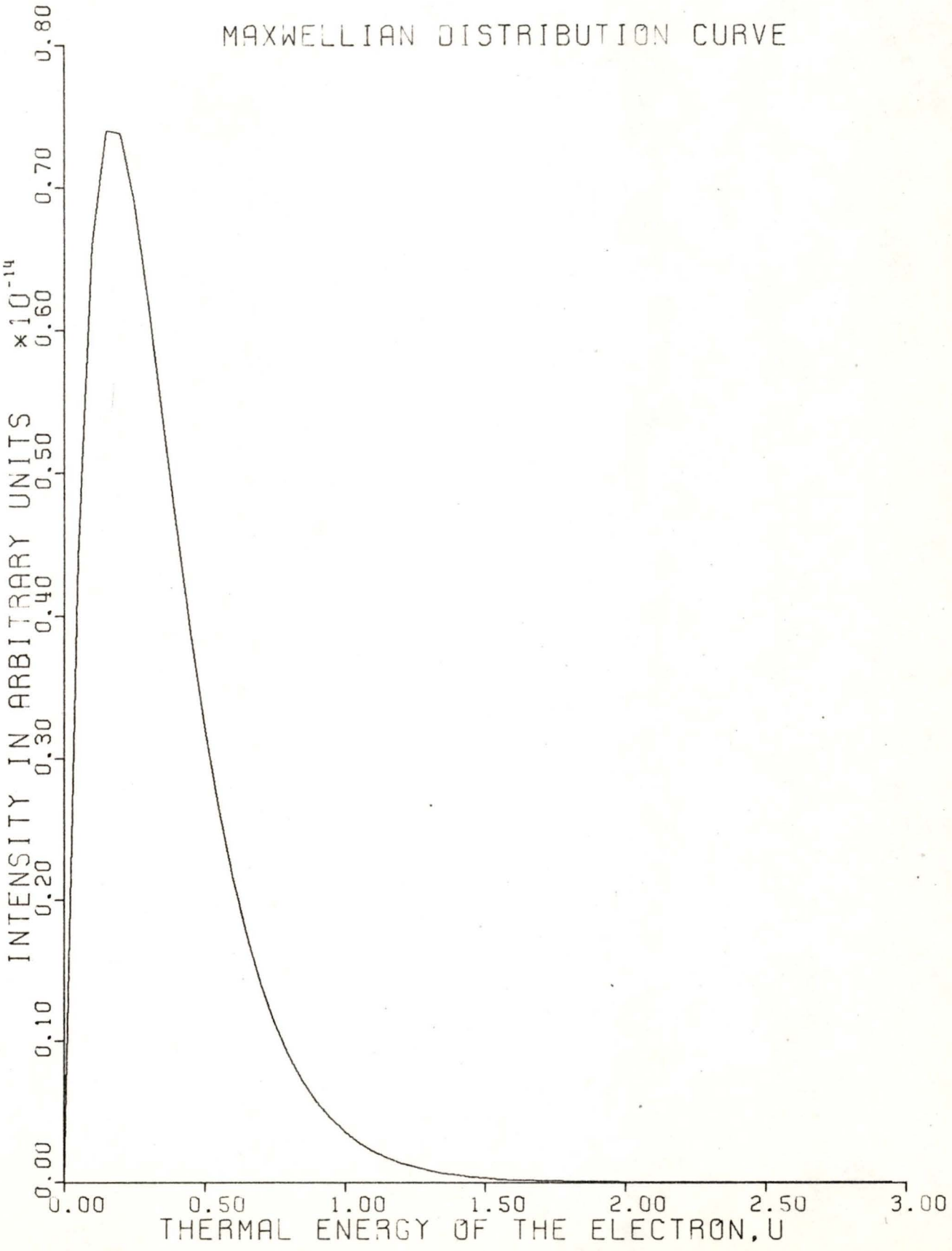
MAXWELLIAN DISTRIBUTION CURVE
INTENSITY IN ARBITRARY UNITS
×10⁻¹⁴
0.00
0.10
0.20
0.30
0.40
0.50
0.60
0.70
0.80
0.00
0.50
1.00
1.50
2.00
2.50
3.00
THERMAL ENERGY OF THE ELECTRON, U

Fig. 27. Hypothetical p(E) curve.

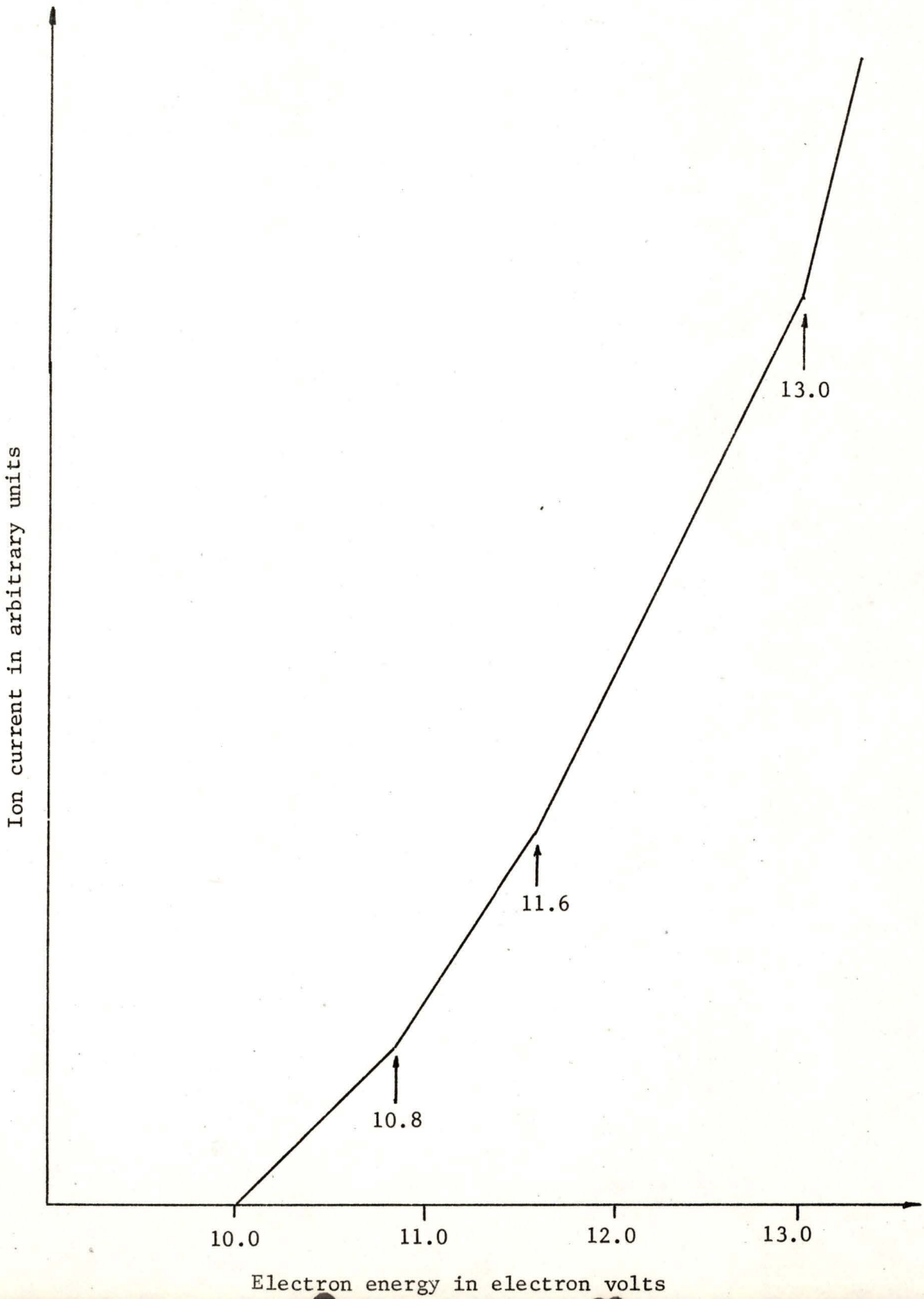

was selected with initial break at 10.0 eV and also breaks at 10.8, 11.6 and 13.0 eV. Thus, by using equation (2.22), a hypothetical ionization efficiency curve, containing an electron energy spread similar to that expected for the ion source of the Hitachi Perkin-Elmer RMU-7 double focusing mass spectrometer, was obtained (fig. 28).

In order to carry out the deconvolution process, the EDD method was used.

Thus $$\Delta I(V) = I(V) - B \times I(V + \Delta V) \qquad (2.24)$$

The value of ΔV selected was 0.1 eV. Using a computer program(similar to that discussed in section 3.5(b)), plots of deconvoluted ionization efficiency curves at various values of B were obtained. The best value of B selected was that which gave a deconvoluted curve with a zero slope, or slightly positive slope just prior to the initial break (fig. 29). In this way, the initial break was estimated to be 9.9 eV (actually this should be 10.0 eV; however due to the fact that $\Delta V = 0.1$ eV, the position of the break was shifted). Comparing the deconvoluted and the hypothetical curves, it was noted that the initial break on the deconvoluted curve was at least 0.5 eV higher than the initially observable ion current in the hypothetical curve. This is understandable because the hypothetical curve is the convolution of p(E) with f(-U) and the half-width of the electron energy spread is about 0.5 eV. This fact will be shown to be useful in considering the deconvolution of the experimental ionization efficiency curves. Breaks were also observed at 0.8, 1.6 and 3.0 eV above the observed initial break. It was noted at the same time that even with higher values of B for the deconvoluted curve, breaks were also observed as shown in fig. 30. The only differences were that just prior to the break the curve had a negative slope (or a smaller positive value than the preceeding segment) and the "straight line" segments were actually curved. This is the consequence of the EDD method which is really a difference method. As it will be seen later this property of the EDD method was also useful in dealing with the experimental ionization efficiency curves.

Fig. 28. Hypothetical

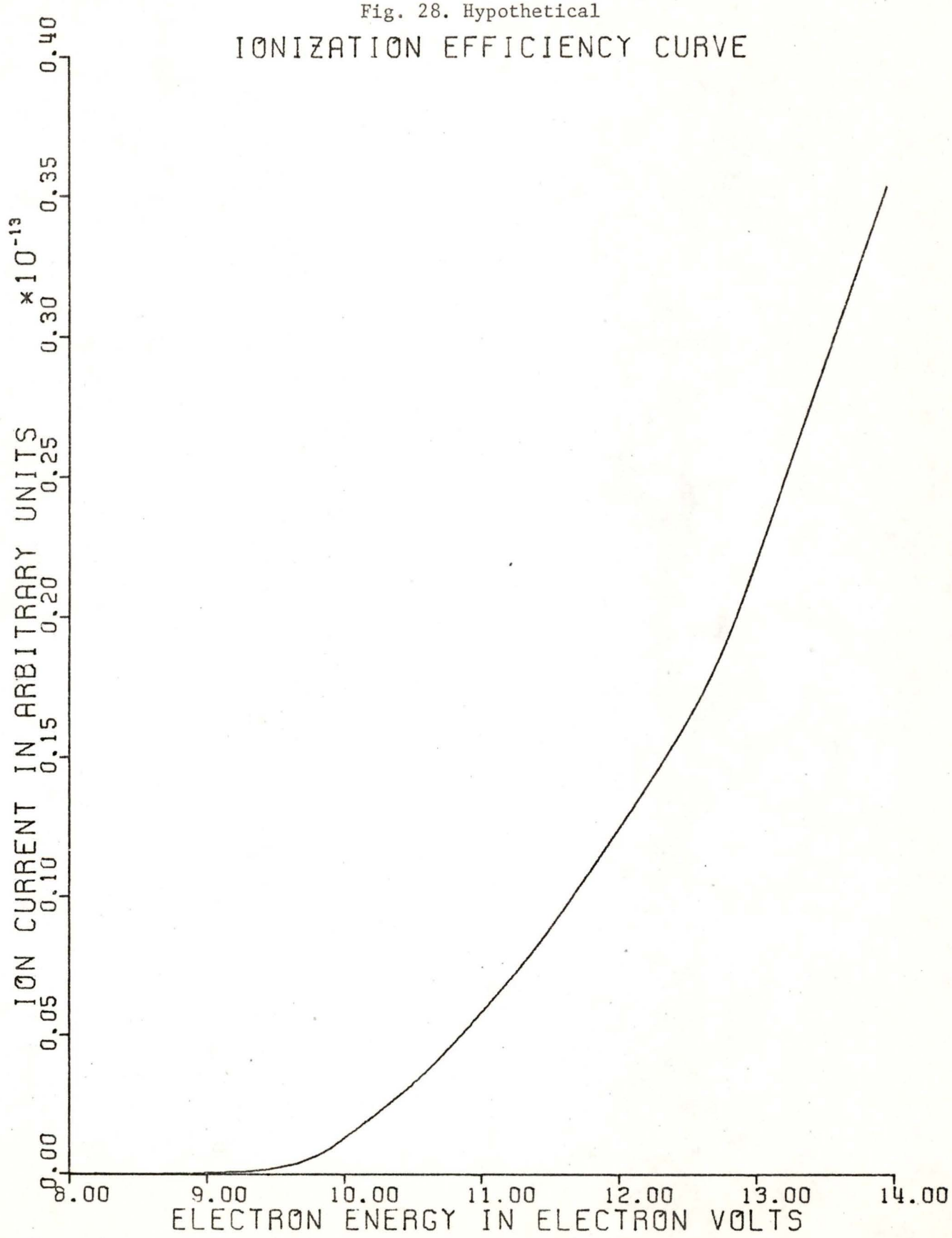

Fig. 29. Deconvoluted

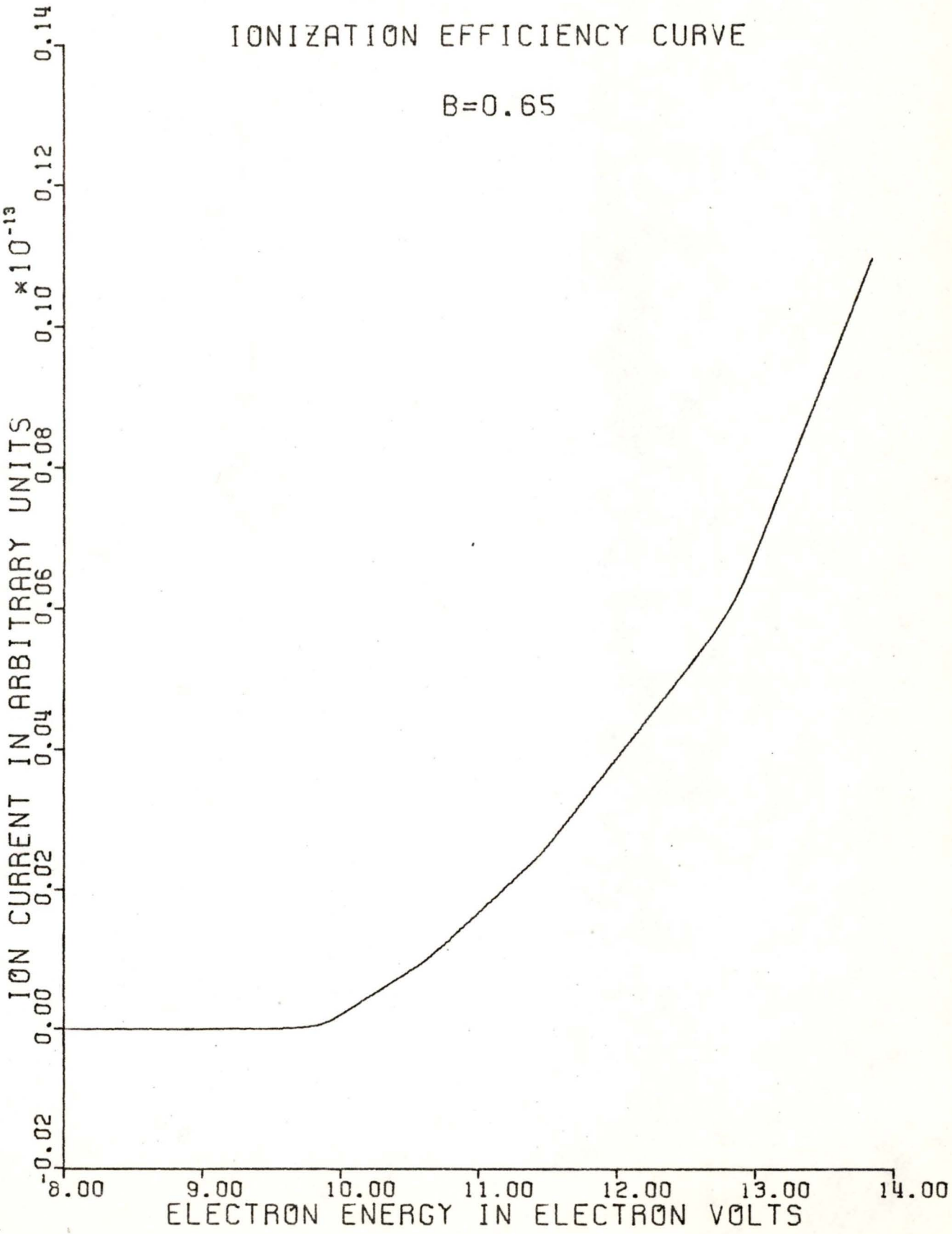

Fig. 30. Deconvoluted

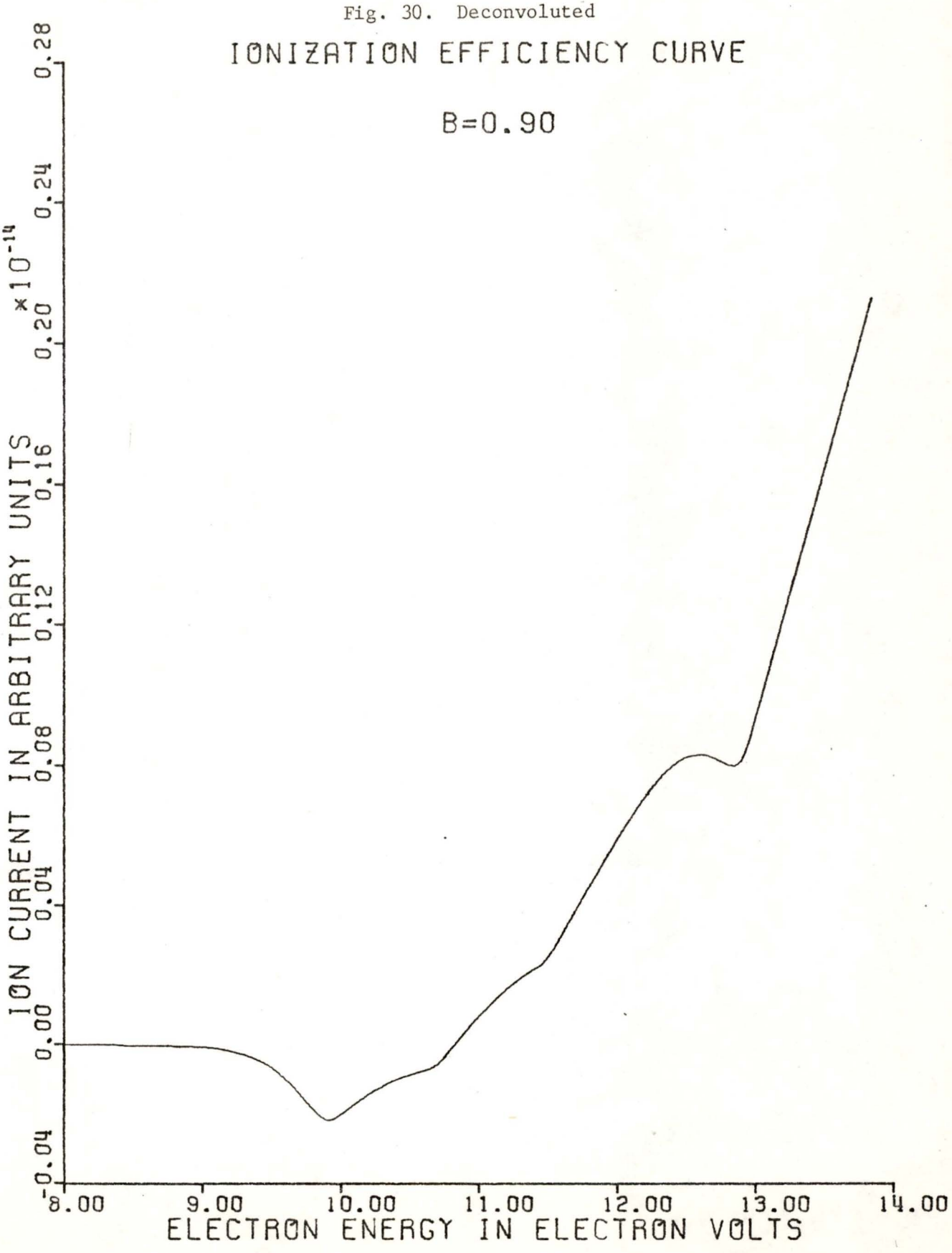

From the above hypothetical results, it is evident that the EDD technique can be used satisfactorily to observe breaks in the ionization efficiency curves.

(b) Ionization Potential of Argon

As a check for the mass spectrometric system, the ionization potential of argon was determined. Xenon was used as an internal calibrating gas for the electron energy scale. The use of an internal reference standard is to eliminate contact potential effects. The value of this potential is not known. Therefore, the unknown sample and the calibrating gas have to be present in the mass spectrometer at the same time. Assuming the contact potentials are the same in both cases, the ionization potential of the unknown can be determined. Usually, inert gases are used as calibrating gases because their ionization potentials are known very accurately from spectroscopic data. In this case, xenon was used as the calibrating gas and its ionization potential is 12.13 eV (14).

Adopting the procedures mentioned in the previous section i.e. the initial break of the deconvoluted curve was at least 0.5 eV higher than initially observable ion current in the original smoothed ionization efficiency curve, the values of the initial breaks of xenon and argon were estimated and their difference was found to be +3.60 eV. Thus the ionization potential of argon was found to be 15.73±0.1 eV. This value compares very favourably with the literature value of 15.75 eV (14).

(c) Ionization Efficiency Curves of Argon and Xenon

Breaks were observed in the deconvoluted ionization efficiency curve of argon. The technique of using deconvoluted curves of higher B value was used to pin-point breaks. However, due to noise and instability of the mass spectrometric system, the deconvoluted curve was not as good as that of the hypothetical deconvoluted curve. Nevertheless the results were encouraging. The results obtained by this work for argon and the literature values are shown in Table 6.

Table 6

Energy separation (eV) of the fine structure in the ionization efficiency curve for argon

State	Spectroscopic(21)	This work	EDD(14)	Velocity selector(22)
$^2P_{1/2}$	0.178	0.24	0.18	0.19
		0.56	0.42	0.58
		0.80		0.77
		1.04	1.01	0.97
		1.32	1.36	1.30

Using the same procedure as that for argon, breaks were observed in the deconvoluted ionization efficiency curve of xenon. The results obtained by this work for xenon and the literature values are shown in Table 7.

Table 7

Energy separation (eV) of the fine structure in the ionization efficiency curve for xenon

State	Spectroscopic(21)	This work	EDD(14)	Velocity selector(23)	RPD(24)
		0.28	0.33		0.35
		0.74		0.70	0.75
$^2P_{1/2}$	1.31	1.30	1.27	1.33	1.3
		1.88		2.05	1.9

It can be seen from the tables that agreement between the present study and the velocity selector (or RPD) work is remarkably good. Thus it was felt that further studies could be undertaken with some confidence.

4.2 The Cyclobutanone(CB) System

The experimental results will be discussed under the following headings:

(a) Ionization potential.

(b) Fragmentation processes and appearance potentials.

(c) "Bond dissociation" energies.

(d) Thermal and photochemical decompositions.

(e) Correlations of mass spectral fragmentation patterns with thermal and photochemical decompositions.

(f) Fine structure in the ionization efficiency curves.

(a) Ionization Potential

The ionization potential of cyclobutanone was determined in the same manner as that for argon. Using the EDD technique and xenon as the calibrating gas, the ionization potential of cyclobutanone was found to be 9.58±0.1 eV. This value is the average of six determinations. Table 8 shows the ionization potential of cyclobutanone and its literature values.

Table 8

Ionization Potential of Cyclobutanone

This work	Photoelectron Spectroscopy	Spectroscopic
9.58±0.1 eV	9.56 eV (25)	9.35 eV (27)
	9.61±0.02 eV (26)	

The ionization potential of cyclobutanone obtained by this work compares favourably with those values obtained by photoelectron spectroscopy. These values are the vertical ionization potential. In contrast, the spectroscopic value is the adiabatic ionization potential. That is why the value determined by this work is higher than the spectroscopic value (9.35 eV).

(b) Fragmentation Processes and Appearance Potentials

(1) From the experimental results (fig. 15, p 45; fig. 17, p 48), it is evident that cyclobutanone (CB) undergoes two major fragmentation pathways at 70 eV and also at low electron energies. The observation of metastable peak at m/e=25.2 at 70 eV and also at low electron energies suggests that the molecular ion decomposes in one step to yield an ion whose m/e=42. However, at m/e=42, two peaks were observed. By accurate mass determination using peak matching technique, these two peaks were identified as CH_2CO^+ and $C_3H_6^+$.

The calculated apparent masses of the metastable peak by these two possible metastable transitions can be obtained by using equation (2.2).

$$m_1^+ \longrightarrow m_2^+ + m_3$$

$$m^* = m_2^2/m_1 \qquad (2.2)$$

Thus

$$CB^+ \longrightarrow CH_2CO^+ + C_2H_4$$

$$m^* = (42.011)^2/\ 70.042 = 25.20$$

$$CB^+ \longrightarrow C_3H_6^+ + CO$$

$$m^* = (42.047)^2/70.042 = 25.24$$

Thus the observation of a metastable peak at m/e=25.2 indicates that the molecular ion decomposes into CH_2CO^+ (and C_2H_4) and/or $C_3H_6^+$ (and CO). At the same time, it was also observed that at approximately two volts above the threshold ionization of the molecule, cyclobutanone was found to decompose only into $C_3H_6^+$ and CH_2CO^+ and no other ions were observed (apart from the metastable peak at m/e=25.2).

The experimental results definitely indicate that cyclobutanone, like substituted cyclobutanones (18), undergoes two major fragmentation pathways to give either a ketene and an olefine (Path A) or carbon monoxide and a hydrocarbon fragment (Path B). This is in contrast to earlier studies (19).

Path A (C_2 path) $\quad CB^+ + e^- \longrightarrow CH_2CO^+ + C_2H_4 + 2e^- \quad (4.1)$

Path B (C_3 path) $\quad CB^+ + e^- \longrightarrow C_3H_6^+ + CO + 2e^- \quad (4.2)$

(2) The appearance potentials of the two ions at m/e=42 were determined in the same manner as that for the ionization potential of cyclobutanone.

The appearance potential of the CH_2CO^+ ion according to equation (4.1) was found to be 10.53±0.2 eV whereas that of the $C_3H_6^+$ ion according to equation(4.2) was found to be 9.85±0.2 eV. It can be seen from the above that the appearance potential of the $C_3H_6^+$ ion is only 0.27 eV above the threshold ionization of the molecule, cyclobutanone. This means only a very small amount of energy above the threshold ionization of the molecule is necessary for the fragmentation process to occur.

(3) At high electron energy e.g. 70 eV, a doublet was detected at m/e=28. These peaks correspond to $C_2H_4^+$ and CO^+. In comparing the intensities of ions formed by the two different pathways, it is interesting to note that at 70 eV, the ion intensity of the CH_2CO^+ is much greater than that of the $C_3H_6^+$. On the other hand, within one pathway, the ion intensity of the CH_2CO^+ is greater than that of the $C_2H_4^+$ and similarly, the ion intensity of the $C_3H_6^+$ is greater than that of the CO^+. It is hoped to attempt to offer some explanations for the above phenomena.

The appearance potential of the $C_3H_6^+$ ion was found to be 9.85 eV and that of the CH_2CO^+ ion was found to be 10.53 eV. Simply on the basis of the appearance potentials, one would expect the ion intensity of the $C_3H_6^+$ should be greater than that of the CH_2CO^+. At the threshold energy near to 10 eV (fig. 17, p 48), the ion intensity of the $C_3H_6^+$ ion was greater than that of the CH_2CO^+ ion.

However, at slightly higher electron energies, the ion intensity of the CH_2CO^+ ion was greater than that of the $C_3H_6^+$ ion. At even higher electron energies, (fig. 15, p 45), it can be seen that the $C_3H_6^+$ and the CH_2CO^+ were undergoing further fragmentation processes to yield the $C_3H_5^+$, $C_3H_4^+$, $C_3H_3^+$, $C_3H_2^+$ and $CHCO^+$, CCO^+ ions respectively. At three or four volts above the threshold for the ionization of the molecule, only the fragment ions $C_3H_6^+$ and CH_2CO^+ were observed; yet the ion intensity of the CH_2CO^+ is greater than that of the $C_3H_6^+$, showing a reversal of the true threshold behaviour. Therefore, it is obvious that the ion intensities of the $C_3H_6^+$ and the CH_2CO^+ can only be satisfactorily explained in other terms, such as the Quasi-Equilibrium Theory of Mass Spectra. This is because the relative ion intensities are probably governed by the respective unimolecular decomposition rate constants.

However, in order to calculate and intepret the ion intensities, values for parameters in rate expressions such as equation (2.13) are needed. Unfortunately, at the present time, these values are not available and so the calculated mass spectrum cannot be given here for comparison. Nevertheless, it is felt that the Quasi-Equilibrium Theory of Mass Spectra could provide a reasonable intepretation for these observations, and this is one area where further work should be carried out.

It is hoped that a qualitative explanation for these observations may be given by comparison with the thermal and photochemical decomposition processes in the neutral molecule (see section 4.2(e)).

The second point of interest is why the ion intensity of the CH_2CO^+ ion is greater than that of the $C_2H_4^+$ ion.

Examining the fragmentation process by pathway A (equation 4.1), a Born-Haber cycle can be written as follows:

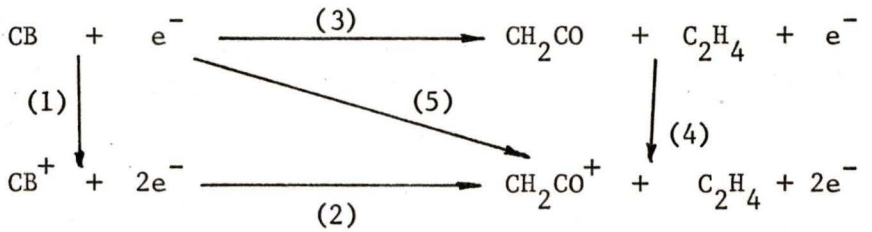

(4.3)

Kinetically, the scheme is envisaged as follows:
The first step is the formation of the molecular ion by the pathway(1) and then immediately afterwards fragmentation process occurs to yield CH_2CO^+ and C_2H_4 by the pathway(2). On the other hand, from energy consideration i.e. Born-Haber cycle, the energies required by the pathways(1) and (2), or (3) and (4), or (5) are equivalent.

Thus $$A.P.(CH_2CO^+) = D(CB) + I.P.(CH_2CO) + K.E. + E.E._{exc.} \qquad (4.4)$$

Note : CB = Cyclobutanone

where $A.P.(CH_2CO^+)$: Appearance potential of CH_2CO^+
$D(CB)$: Energy required to dissociate CB according to the pathway given ("Bond dissociation" energy)
$I.P.(CH_2CO)$: Ionization potential of CH_2CO
K.E. : Kinetic energies carried by CH_2CO^+ and C_2H_4
$E.E._{exc.}$: Any excitation energies of the products

Assuming that K.E. and $E.E._{exc.}$ are negligible, equation (4.4) can be written as:

$$A.P.(CH_2CO^+) = D(CB) + I.P.(CH_2CO) \qquad (4.5)$$

Similarly for the fragmentation process:

$$CB + e^- \longrightarrow CH_2CO + C_2H_4^+ + 2e^- \qquad (4.6)$$

Thus $$A.P.(C_2H_4^+) = D(CB) + I.P.(C_2H_4) \qquad (4.7)$$

The I.P. of CH_2CO is 9.6 eV (28) and that of C_2H_4 is 10.5 eV (26). Since D(CB) should be the same for both fragmentation processes, it is obvious that the A.P. of $C_2H_4^+$ should be greater than the A.P. of CH_2CO^+, i.e. more energy is required for the production of the $C_2H_4^+$ ion than the CH_2CO^+ ion.

Therefore, when the I.P. of C_2H_4 is greater than that of CH_2CO, the fragmentation of molecular ion to give CH_2CO^+ and C_2H_4 is more probable. This means that the ion intensity of CH_2CO^+ should be greater than that of $C_2H_4^+$. This predication has been shown by many experimental results. The generalisation based on experimental results is known as Stevenson's Rule (29).

Similarly for the fragmentation processes:

$$CB + e^- \longrightarrow C_3H_6^+ + CO + 2e^- \qquad (4.8)$$

and

$$CB + e^- \longrightarrow C_3H_6 + CO^+ + 2e^- \qquad (4.9)$$

The I.P. of CO is 14.01 eV (30) and that of $CH_3CH=CH_2$ is 9.74 eV (30) or cyclopropane is 10.09 eV (30). Since the I.P. of CO is greater than that of $CH_3CH=CH_2$ or cyclopropane, the formation of $C_3H_6^+$ is more probable than that of CO^+. Experimental results have also shown this to be the case.

From mass spectra only, there is no way of indicating what is the structure for $C_3H_6^+$. Thus $C_3H_6^+$ can either be $[\text{cyclopropane}]^+$ or $[CH_3CH=CH_2]^+$. However, thermochemical data can provide some insight into the structure of $C_3H_6^+$ ion.

For the fragmentation reaction

$$CB + e^- \longrightarrow C_3H_6^+ + CO + 2e^-$$

Ignoring K.E. and $E.E._{exc.}$

$$A.P.(C_3H_6^+) = \Delta H_{reaction} = \Delta H_f(C_3H_6^+) + \Delta H_f^o(CO) - \Delta H_f^o(CB) \qquad (4.10)$$

where ΔH_f is the heat of formation.

If $C_3H_6^+$ is $CH_3CH=CH_2^+$, using equation (4.10), $A.P.(CH_3CH=CH_2^+)$ can be calculated provided all the ΔH_f^o's are known.

Thus for $CH_3CH{=}CH_2^+$,

$\Delta H_f(CH_3CH{=}CH_2^+)$ = 229 kcal/mole (30)

$\Delta H_f^o(CO)$ = -26.4 kcal/mole (30)

$\Delta H_f^o(CB)$ = -20.5 kcal/mole (31)

Therefore $A.P.(CH_3CH{=}CH_2^+)$ = 223.1 kcal/mole

= 9.67 eV

Where 1 eV = 23.06 kcal/mole

Similarly for cyclopropane

$\Delta H_f(\triangle^+)$ = 245 kcal/mole (30)

Therefore $A.P.(\triangle^+)$ = 239.1 kcal/mole

= 10.36 eV

The $A.P.(C_3H_6^+)$ was found by this work to be 9.85 eV. From the above calculations, the structure of the $C_3H_6^+$ ion would more likely be of the form $CH_3CH{=}CH_2^+$. This result appears rather surprising since a hydrogen shift is required in the formation of this ion, but not for cyclopropyl ion.

It should be noted here that if the fragment ion undergoes further fragmentation processes, then Stevenson's Rule may not hold. In such cases, the Quasi-Equilibrium Theory should be used. However, near the threshold of ionization, Stevenson's Rule is definitely applicable as shown by the experimental results of this work.

(4) The fragmentation processes of cyclobutanone may be summarised as follows:

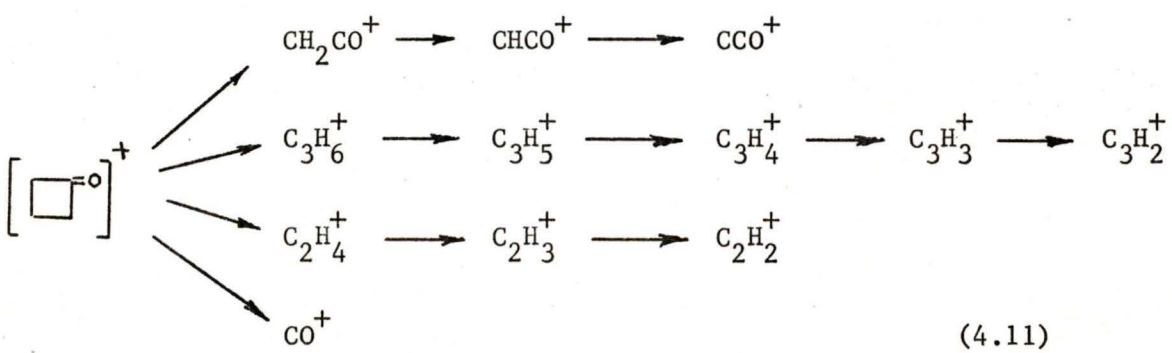

(4.11)

(c) "Bond Dissociation" Energies

From equation (4.4), it is useful to check the validity of the appearance potential data by calculating the "bond dissociation" energy and comparing it with the analogous energy for the process in the neutral state.

$$A.P.(CH_2CO^+) = D(\text{cyclobutanone}) + I.P.(CH_2CO) + K.E. + E.E._{exc.} \quad (4.4)$$

D(cyclobutanone) can be calculated provided other values are known. In this case, the "bond dissociation" energy is the energy necessary to break the two bonds of the cyclobutanone ring. As mentioned in section 4.2(b), for the reactions:

$$CB + e^- \rightarrow CH_2CO^+ + C_2H_4 + 2e^- \quad \text{I}$$

$$CB + e^- \rightarrow CH_2CO + C_2H_4^+ + 2e^- \quad \text{II}$$

If $I.P.(C_2H_4)$ is greater than $I.P.(CH_2CO)$, Stevenson's Rule says that the formation of CH_2CO^+ and C_2H_4 is more probable. However, if $C_2H_4^+$ ion is formed, the products, $C_2H_4^+$ and CH_2CO, would carry excess energy (45). This can be shown on an energy diagram as in fig. 31.

The energy diagram shows reaction II has a marked "energy barrier" while reaction I has little or none. Therefore, in equation (4.4), the K.E. and $E.E._{exc.}$ terms can be ignored.

Thus $$D(\text{cyclobutanone}) = A.P.(CH_2CO^+) - I.P.(CH_2CO) \quad (4.12)$$

$$D(\text{cyclobutanone}) = 10.53 \text{ eV} - 9.6 \text{ eV}$$
$$= 0.93 \text{ eV}$$
$$= 21.4 \text{ kcal/mole}$$

The calculated "bond dissociation" energy from the values of ionization and appearance potentials can be checked by thermochemical data.

Thus $$\text{cyclobutanone} \longrightarrow CH_2CO + C_2H_4 \quad (4.13)$$

Fig. 31. Energy diagram.

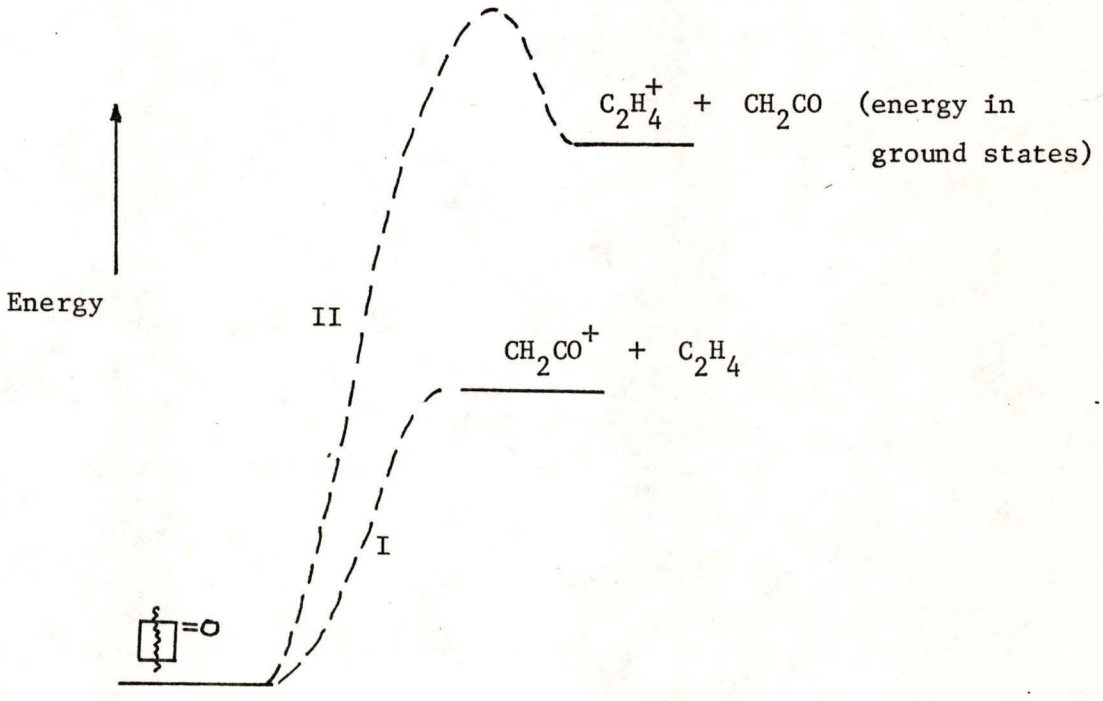

An illustration of Stevenson's rule

$$D(\text{[cyclic]}) = \Delta H_f^o(CH_2CO) + \Delta H_f^o(C_2H_4) - \Delta H_f^o(CB) \qquad (4.14)$$

$$D(\text{[cyclic]}) = 18.4 \text{ kcal/mole}$$

where $\Delta H_f^o(CH_2CO) = -14.6$ kcal/mole (31)
$\Delta H_f^o(C_2H_4) = 12.5$ kcal/mole (31)
$\Delta H_f^o(CB) = -20.5$ kcal/mole (31)

Similarly for the fragmentation reaction:

$$\text{[cyclic]} + e^- \longrightarrow C_3H_6^+ + CO + 2e^-$$

$$D(\text{[cyclic]}) = A.P.(C_3H_6^+) - I.P.(CH_3CH{=}CH_2) \qquad (4.15)$$
$$D(\text{[cyclic]}) = 9.85 \text{ eV} - 9.74 \text{ eV}$$
$$= 0.11 \text{ eV}$$
$$= 2.5 \text{ kcal/mole}$$

From thermochemical data:

$$D(\text{[cyclic]}) = \Delta H_f^o(CH_3CH{=}CH_2) + \Delta H_f^o(CO) - \Delta H_f^o(CB)$$
$$D(\text{[cyclic]}) = 4.9 \quad -26.4 \quad + \quad 20.5$$
$$= -1.0 \text{ kcal/mole}$$

where $\Delta H_f^o(CH_3CH{=}CH_2) = 4.9$ kcal/mole (30)
$\Delta H_f^o(CO) = -26.4$ kcal/mole (30)

Thus, in both cases, the "bond dissociation" energies calculated by means of appearance potential determinations and thermochemical data are approximately the same. There are many cases (32) in which bond dissociation energies are determined by electron impact studies. In certain cases, this is the only method available and it is certainly the easiest one. However, since the structure of the ion is not known, the value obtained by electron impact technique should be compared, if possible, with that obtained by other techniques.

(d) Thermal and Photochemical Decompositions

Fragmentation processes in the mass spectrometer are similar to ordinary chemical unimolecular decomposition reactions. It is therefore of interest to compare the fragmentation patterns with the pyrolysis and photolysis of cyclobutanone. It is hoped that these comparisons will provide some insight into the chemical properties of the compound.

(1) Recent studies (33) of the thermal decomposition of cyclobutanone at 350°C indicated that the major products (> 99%) were ethylene and ketene with about 0.5% of cyclopropane and CO (and also less than 0.005% propylene).

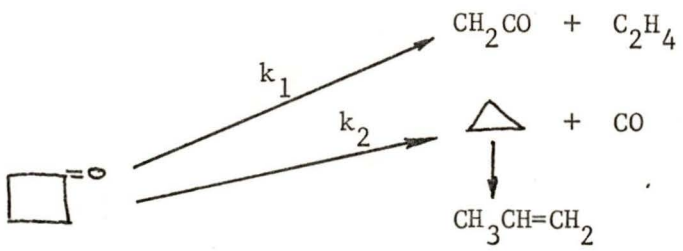

(4.17)

The rate constants were given:

$$k_1 = 3.6 \times 10^{14} \exp(-52000/RT) \qquad (4.18)$$

$$k_2 = 2.34 \times 10^{14} \exp(-58000/RT) \qquad (4.19)$$

The small amount of propylene detected is probably due to the isomerization of cyclopropane.

(2) There have been many studies (34) of the photochemical decomposition of cyclobutanone in the gas phase. The direct photolysis and triplet photosensitised (Benzene ($^3B_{1u}$) (35) and Mercury ($^3P_1$) (36)) photolysis of cyclobutanone have been studied. It has been proposed (37) that cyclobutanone yields ketene and ethylene via the (n,π^*) singlet state and cyclopropane, propylene and CO via the (n,π^*) triplet state. However, the thermal decomposition studies made by Blades (33) suggested that, because of the fact that pyrolysis involves

only the ground singlet state, the photochemical mechanism should be modified as follows so as to include the possibility of the excited singlet state also yielding the cyclopropane products.

$$CB(S_o) \xrightarrow[313\ nm]{h\nu} (S_1^*) \longrightarrow S_o^* \longrightarrow C_2H_4 + CH_2CO \quad (C_2\ path)$$

$$\hookrightarrow \text{cyclo-}C_3H_6^* + CO \quad (C_3\ path) \qquad (4.20)$$

$$(S_1^*) \longrightarrow T_1^* \longrightarrow \text{cyclo-}C_3H_6^* + CO \quad (C_3\ path)$$

In view of Blades' suggestion, further studies were carried out by Hemminger and Lee (38). A revised mechanism was proposed for the photolysis of cyclobutanone. The main points are as follows:

(i) The C_3 products may come from three sources i.e.
$S_1^* \rightsquigarrow T_1 \rightsquigarrow C_3$ products; $S_1^* \rightsquigarrow C_3$ products; $S_o^* \rightsquigarrow C_3$ products.

(ii) The C_2 products may come from two sources i.e.
$S_1^* \rightsquigarrow C_2$ products; $S_o^* \rightsquigarrow C_2$ products.

The proposed photochemical transformation mechanism of cyclobutanone is shown in fig. 32.

Recently, photochemical predissociation of cyclobutanone was studied in some detail by Hemminger et al (39). The results are best shown in fig. 33. At long exciting wavelengths ($>$319 nm) i.e. low energies, the C_3 products predominated over C_2 products, and although the fluorescence quantum yield was small, the fluorescence was measurable. Near to 319 nm there was a sudden change in the ratio of the products, the C_2 products becoming more abundant than the C_3 products, and the fluorescence quantum yield dropping to near zero. The authors suggested that a predissociation process was responsible for this behaviour. The process which yields C_2 products provides a new pathway for de-excitation of the excited singlet state and thus the fluorescence quantum yield falls. It was suggested that the onset of predissociation was about 3 kcal/mole vibrational excitation above the first singlet (n,π^*) state.

Fig. 32.

Proposed photochemical transformation mechanism of cyclobutanone.

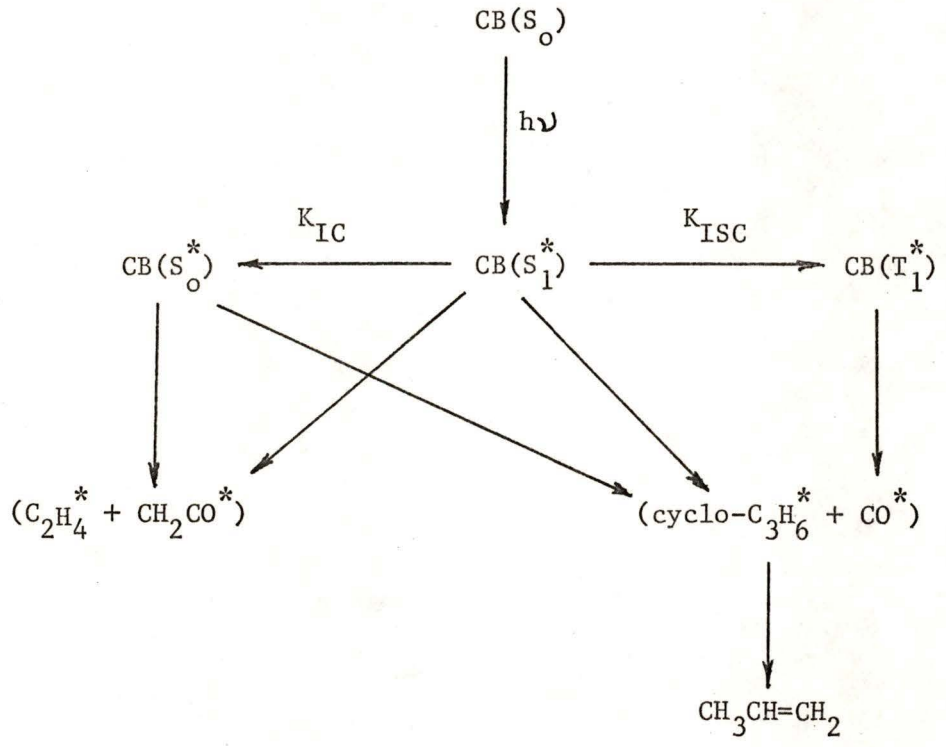

Fig. 33.

The ratio of the (C_3/C_2) products at low total pressure versus exciting wavelength.

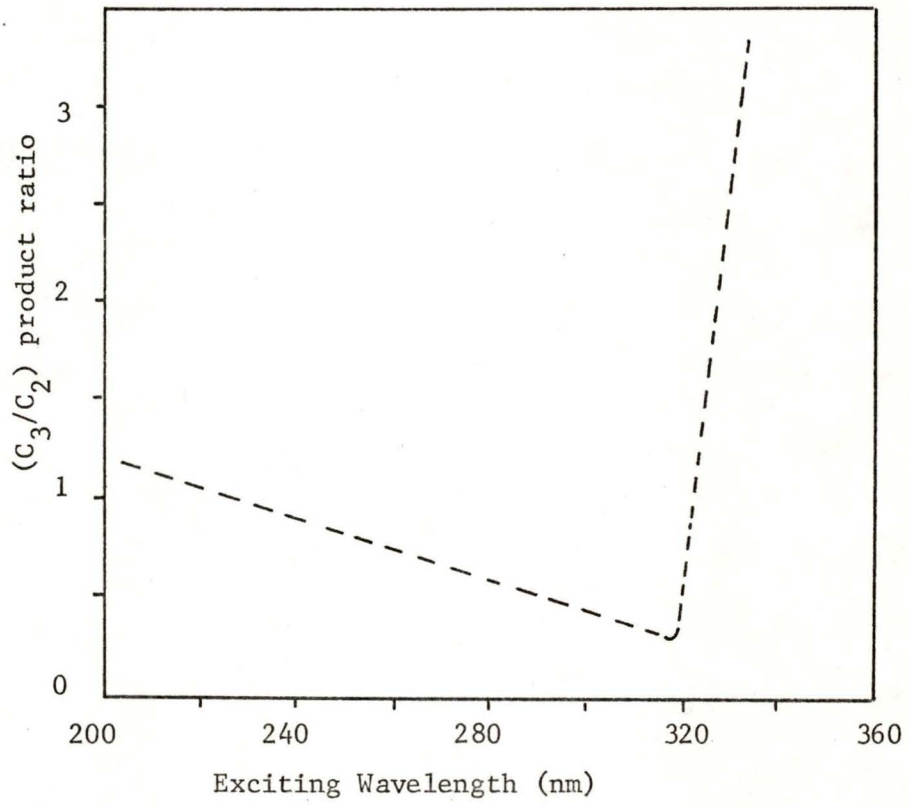

Further it was suggested that there was a considerable degree of ring strain for CB(S_1) and the "predissociation behaviour" may be a result of the rupture of C_1-C_2 bond. This suggested that a biradical, $\dot{C}H_2CH_2CH_2\dot{C}=O$, was formed as a first step, this biradical further decomposing to give ethylene and ketene.

(e) Correlations of Mass Spectral Fragmentation Patterns with the Thermal and Photochemical Decompositions

(1) The first ionization potential of cyclobutanone is assigned to the removal of one electron from one of the oxygen n levels (26). In photolysis of cyclobutanone, the first step is the promotion of one electron from one of the oxygen n levels to π^* ($^1A_2$ state) excited singlet state. Hence one might expect that the properties of the ionic species would be intermediate between those of the ground state neutral species and its first excited state (since the electron is completely removed in the ionic species and is not in an antibonding orbital).

(2) Recent work on the photolysis of cyclobutanone has shown that near its absorption threshold, decomposition occurs via two different pathways to yield C_3 and C_2 products but the ratio of C_3/C_2 products is greater than unity (see fig. 33, p 82). However, at a slightly higher energies a new decomposition process sets in (predissociation) leading to the formation of C_2 products. The value of the ratio of C_3/C_2 products was 0.4 or less at about 313 nm. This behaviour is very similar to that observed in the present studies i.e. initially $C_3H_6^+$ ion predominated but at a slightly higher energies CH_2CO^+ ion predominated.

The observations are in agreement with the suggestion that the ionic species behaves similarly to that of the excited neutral. However, the ionic species is somewhat more stable since in photolysis the excited neutral decomposes near its threshold whereas 0.27 eV (6.2 kcal/mole) excess energy is required for the production of $C_3H_6^+$ ion and 0.95 eV (22 kcal/mole) excess energy is required for the production of CH_2CO^+ ion. Shortly after the formation of CH_2CO^+ ion, C_2 products become more important than C_3 products as is the case for the excited neutral species but again the energy difference between the formation of the CH_2CO^+ ion and the energy where C_2 products predominate , is greater than that for the excited neutral species.

(3) Mechanism:

In the past, the thermal decomposition of cyclobutanone has been treated in terms of a biradical mechanism (31), the relatively low activation energy having been accounted for in terms of resonance stabilization of the acetonyl radical. However, more recent measurements (40) of the stabilization energy of the radical have been shown it to be essentially zero and thus the biradical mechanism must be rejected in favour of a concerted process, for which the Woodward-Hoffmann rules (41) predict the appropriate products. Similar arguments for the concerted mechanism have been made in photolysis (42).

In the present case of the mass spectrometric fragmentation, again either a biradical or a concerted mechanism may be considered for either of the two main fragmentation pathways. In both cases, in a biradical mechanism, the first step would be the fission of one of the C-C bonds of the cyclobutanone ring yielding an intermediate biradical. From the thermochemical estimates presented below, the estimated threshold energy required for the production of the products would be considerably higher than those observed. Therefore, the most reasonable mechanism for the formation of the products would be a concerted process, which is again consistent with the postulates for the thermal and photochemical transformation of the neutral cyclobutanone molecule.

For the biradical mechanism, the first step is the formation of the biradical.

Thus CB

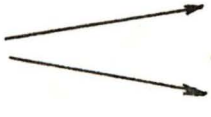

$\dot{C}H_2COCH_2\dot{C}H_2$ (4.21)

$\dot{C}H_2CH_2CH_2\dot{C}O$ (4.22)

The heat of formation of the above biradicals can be estimated (30). Since ΔH_f^o(CB) is -20.5 kcal/mole, the $D_{(C-C)}$ of either process can be calculated. Thus, for equation (4.21) $D_{(C-C)}$ was estimated to be 51.9 kcal/mole whereas for equation (4.22) $D_{(C-C)}$ was estimated to be 44.5 kcal/mole.

In the ionic case, the analagous steps are:

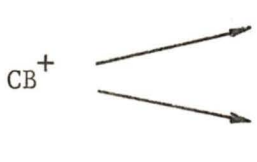

(4.23)

(4.24)

For the production of $C_3H_6^+$ ion, the energy required in addition to the I.P. of CB is only 0.27 eV (6.2 kcal/mole). If biradical mechanism is applicable, this requires a bond dissociation energy of about 6 kcal/mole or less. In the neutral species, the bond dissociation energy was estimated to be 44.5 or 51.9 kcal/mole. Therefore, it would seem to be improbable that the removal of an essentially non-bonding electron would affect such a drastic change in the bond dissociation energy and a concerted mechanism must be considered to be more likely than a biradical mechanism.

For the production of CH_2CO^+ ion, however, a further 0.68 eV (15.7 kcal/mole) of energy is required. If a biradical mechanism is operative, then the bond dissociation energy would be as high as about 22 kcal/mole. This makes the argument against the biradical mechanism in this case much less compelling, especially since Lee (43) has suggested that for the $^1A_2$ excited state of the neutral species (one electron in an antibonding orbital), the bond dissociation energy could be as low as 3.8 kcal/mole. Consequently, either a biradical or a concerted or both mechanisms might be possible in the case of the production of CH_2CO^+ ion. The addition of this biradical pathway offers a possible qualitative explanation for the rapid increase in the production of CH_2CO^+ ion (relative to $C_3H_6^+$ ion) as the energy is increased. This again is analogous to the suggestion by Lee (39) that the biradical process is responsible for the rapid increase in the C_2 products relative to C_3 products in the photolysis of the neutral species.

(f) Fine Structure in the Ionization Efficiency Curves

Using the same procedure as that for xenon, ionization efficiency curves were obtained for cyclobutanone at m/e=70, and the ions $C_3H_6^+$ and CH_2CO^+ (m/e=42). Breaks were observed in all the deconvoluted curves of these three ions. The results were not readily reproducible from one run to the next. However, within experimental error in a given run, whenever there was a break in the deconvoluted curve of cyclobutanone, breaks were also observed in the deconvoluted curves of $C_3H_6^+$ and CH_2CO^+ ions at the same voltage. These observations are shown in Table 9.

Table 9

Energy(eV) of the breaks in the ionization efficiency curves of $(\text{cyclobutanone})^+$, $C_3H_6^+$ and CH_2CO^+ ions

$(\text{cyclobutanone})^+$	$C_3H_6^+$	CH_2CO^+
9.58		
9.83	9.85	
10.03	(10.05)	
(10.23)	(10.25)	
(10.52)	10.55	10.53
10.76	10.85	10.83
	11.10	(11.08)
		11.53
		11.83

Since the second ionization potential of cyclobutanone is 11.4 eV (26) or 11.7 eV (27), the breaks in the ionization efficiency curve of cyclobutanone could be assigned to autoionizing states. This is the result of promoting an electron from an inner orbital to a higher orbital, the energy of which is above the first ionization potential of the molecule. Thus, the molecule is in an excited state. The excited molecule may undergo radiationless transition to yield the ground state of an ion with the ejection of an electron. The excess energy present may be lost as kinetic energy carried away by the ejected electron,

or may be retained as vibrational excitation of the ion. This vibrational energy may well lead to rapid fragmentation of the ion so produced.

4.3 Conclusions

This work clearly showed that cyclobutanone(CB) undergoes two major fragmentation pathways in the mass spectrometer.

$$CB + e^- \rightarrow \begin{cases} [C_3H_6 + CO]^+ + 2e^- \\ [CH_2CO + C_2H_4]^+ + 2e^- \end{cases}$$

With only slight modifications to a commercial mass spectrometer and applying the EDD technique, the ionization potential of cyclobutanone was found to be 9.58±0.1 eV and the appearance potentials of $C_3H_6^+$ and CH_2CO^+ were found to be 9.85±0.2 eV and 10.53±0.2 eV respectively. The EDD technique was found to be able to determine the ionization potential of a chemical compound. However, the maximum error was within ±0.1 eV of the mean value. The main sources of experimental errors were noise problems and instability of the commercial mass spectrometer. It was found that it was more difficult to obtain good reproducibility of the values of the appearance potentials of $C_3H_6^+$ and CH_2CO^+. This was due to the fact that the two ions peaks, $C_3H_6^+$ and CH_2CO^+, were superimposed on each other. Nevertheless, within ±0.2 eV, the results were reproducible.

A good correlation exists between the fragmentation pathways and the pyrolytic and photolytic decompositions of the cyclobutanone. A consideration of the energetics of the mass spectral fragmentation has shown that the molecular ion behaves very similarly to the first excited electronic state of the neutral species. The results suggest that it is most probable that the molecular ion fragments via a concerted process, but the possibility of a biradical pathway cannot be completely excluded.

In spite of the apparent similarities between the mass spectral fragmentation and the pyrolytic or photolytic processes, one must view such similarities with caution. This is because two different kinds of species are involved i.e.

ions and excited neutral molecules. It is unfortunate that very little is known about the structure of ions and further studies directed towards the elucidation of the structure of ions in the mass spectrometer are needed.

Breaks were observed in all the ionization efficiency curves. However, reproducibility was poor. This was consistent with the findings by Giesser and Meisels (44). They attributed to the fact that in conventional electron gun, apart from filament temperature, other factors also contribute to electron energy spread. However, within each run, the results were encouraging. The observation of breaks in the parent molecular ion as well as in the fragment ions, $C_3H_6^+$ and CH_2CO^+, at the same electron energies suggested that autoionizing states could contribute to the fragmentation processes and further work is required to investigate this possibility, although considerably better reproducibility will be required than was possible in the present studies.

The results obtained by this work could possibly contribute to the understanding of the fragmentation mechanism in the mass spectrometer. Further work should be done in this field because this kind of study is not only interesting but also it should throw some light into our understanding about chemical processes in general, not only those in a mass spectrometer. In this respect, a detailed study should be carried out on some aspects of the Quasi-Equilibrium Theory of Mass Spectra as applied to the fragmentation processes at the threshold.

References

1. W.M. Hickam, R.E. Fox and T. Kjeldaas,Jr. Phys. Rev. 96,63(1954)
2. R.W. Kiser Introduction to Mass Spectrometry and Its Applications (1965)
3. H.M. Rosenstock, M.B. Wallenstein, A.L. Wahrhatig and Henry Eyring Proc. Natl. Acad. Sci. (U.S.) 38,667(1952)
4. H.M. Rosenstock and M. Krauss Quasi-Equilibrium Theory of Mass Spectra in Mass Spectrometry of Organic Ions edited by F.W. McLafferty (1963)
   M. Vestal, A.L. Wahrhaftig and W.H. Johnston J. Chem. Phys. 37,1276(1962)
5. J.E. Collin Physical Meaning of Photon and Electron Impact Ionization Processes in Mass Spectrometry edited by R.I. Reed (1965)
6. A.J.C. Nicholson J. Chem. Phys. 95,954(1963)
7. W.M. Hickam Phys. Rev. 95,703(1954)
8. R.E. Fox, W.M. Hickam and J. Kjeldaas,Jr. Phys. Rev. 89,555(1953)
9. R.E. Fox and W.M. Hickam J. Chem. Phys. 22,2059(1954)
10. C.A. McDowell and J.W. Warren Discussion Faraday Soc. 10,53(1951)
11. P. Marmet and L. Kerwin Can. J. Phys. 38,787(1960)
12. C.E. Brion, D.C. Frost and C.A. McDowell J. Chem. Phys. 44,1034(1966)
13. R.E. Fox, W.M. Hickam, D.J. Grove and T. Kjeldaas Phys. Rev. 84,859(1951)
14. R.E. Winters, J.H. Collins and W.L. Courchene J. Chem. Phys. 45,1931(1966)
15. J.D. Morrison J. Chem. Phys. 39,200(1963)
16. A.R. Stokes Proc. Phys. Soc.(London) 61,382(1948)
17. C.D. Gutshe and T.D. Smith J.A.C.S. 82,4067(1960)
18. D.S. Weiss, R.B. Gagosian and N.J. Turro Org. Mass Spectrm. 3,145(1970)
19. H.J. Hofman Tetrahedron Letters 2329(1964)
20. A. Savitzky and M.J.E. Golay Analyt. Chem. 36,1627(1964)
21. C.E. Moore "Atomic Energy Levels" Natl. Bur. Std. Circ. No. 467(1949)
22. L. Kerwin, P. Marmet and E.M. Clarke Advan. Mass Spectrometry 2,522(1959)
23. S.N. Foner and B.H. Nall Phys. Rev. 122,512(1961)
24. C.E. Melton and W.H. Hamill J. Chem. Phys. 41,546(1964)

25. M.B. Robin (Bell Laboratories, Murray Hill, New Jersey) private communication to R. Whitlock of the University of Victoria dated June 23, 1971.
26. D. Chadwick, D.C. Frost and L. Weiler Tetrahedron Letters 4543(1971)
27. R. Whitlock and A.B.F. Duncan J. Chem. Phys. 55,218(1971)
28. F.H. Field and J.L. Franklin Electron Impact Phenomena (1957)
29. D. P. Stevenson Disc. Faraday Soc. 10,35(1951)
30. J.L. Franklin, J.G. Dillard, H.M. Rosenstock, J.T. Herron, K. Draxl, and F.H. Field Ionization Potentials, Appearance Potentials, and Heats of Formation of Gaseous Positive Ions NSRDS-NBS 26 (1969)
31. S.W. Benson and H.E. O'Neal Kinetic Data on Gas Phase Unimolecular Reactions NSRDS-NBS 21 (1970)
32. V.I. Vedeneyev, L.V. Gurvich, V.N. Kondrat'yev, V.A. Medvedev and Ye L. Frankevich Bond Energies, Ionization Potentials and Electron Affinities (1966)
33. A.T. Blades Can. J. Chem. 47,615(1969)
34. E.K.C. Lee Role of Singlet and Triplet States in Photochemistry of Gaseous Molecules with π-Bonds in Excited State Chemistry edited by J.N. Pitts,Jr (1970)
35. H.O. Denschlag and E.K.C. Lee J.A.C.S. 90,3628(1968)
36. D.C. Montague and F.S. Rowland J.A.C.S. 91,7230(1969)
37. H.O. Denschlag and E.K.C. Lee J.A.C.S. 89,4795(1967)
38. J.C. Hemminger and E.K.C. Lee J. Chem. Phys. 56,5284(1972)
39. J.C. Hemminger, C.F. Rusbult, and E.K.C. Lee J.A.C.S. 93,1867(1971)
40. K.D. King, D.M. Golden and S.W. Benson J.A.C.S. 92,5541(1970)
41. R.B. Woodward and R. Hoffmann The conservation of orbital symmetry (1970)
42. H.A.J. Carless and E.K.C. Lee J.A.C.S. 92,6683(1970)
43. J.C. Hemminger and E.K.C. Lee J. Chem. Phys. 54,1405(1971)
44. B.G. Giesser and G.G. Meisels J. Chem. Phys. 55,2269(1971)
45. P.F. Knewstubb Mass Spectrometry and Ion-Molecule Reactions (1969)

Appendix
Convolution

The measured ionization efficiency curve is the variation of the probability of ionization with the electron energy blurred by the thermal energy spread of the electron beam. This may be represented by the formula:

$$I(V) = \int_{V}^{\infty} p(E)f(E-V)dE$$

As shown in section 2.10(c), this is very similar to the convolution integral which is mathematically defined as:

$$h(x) = \int_{-\infty}^{\infty} m(w)g(x-w)dw$$

or $$h(x) = m(x)*g(x)$$

Note the difference in the arguments of the functions f and g in the two integrals; this requires the reversal of the function f when comparing the integrals.

It is mathematically convenient to treat the ionization efficiency curve as a convolution integral, since the convolution theorem, defined below, is valid and for convolution the functions involved are commutative.

The Convolution Theorem

If $T[m(x)]$ and $T[g(x)]$ are the Fourier Transforms of $m(x)$ and $g(x)$ respectively, then

$$T[h(x)] = T[m(x)*g(x)] = T[m(x)] \cdot T[g(x)]$$

or in words, the Fourier Transform of the convolution of two functions is equal to the product of their Fourier Transforms.

It should be mentioned that another common situation where the convolution integral is useful is in the treatment of spectral line broadening, where the observed spectral line may be considered as the convolution of the natural

spectral line with the Doppler broadening.

For numerical evaluation of the convolution integral, it is convenient to represent the function m(x) by a sequence of values separated by a small regular interval:

$$m(x) = \{ m_o, m_1, m_2, - - -, m_p \}$$

similarly $$g(x) = \{ g_o, g_1, g_2, - - -, g_q \}$$

where the interval for g(x) is the same as that for m(x).
It can be readily shown (see footnote) that the convolution integral may be written as:

$$h(x) = \{ m_o g_o,\ m_1 g_o + m_o g_1,\ m_2 g_o + m_1 g_1 + m_o g_2,\ - - - \}$$

For the observed ion current, the integral may be approximately represented by the formula:

$$I(V) = \text{const} \sum_{V}^{V+U_{max}} f(E-V)p(E)\Delta E$$

where U : thermal energy of the electrons
E = U + V

The convolution at a particular potential V_1 (corresponding to one term in the above sequence for h(x)) can be obtained as follows:

$$I(V_1) = (f_1 p_1 + f_2 p_2 + f_3 p_3 + f_4 p_4 + f_5 p_5 + f_6 p_6 + - - -)\Delta E$$

where ΔE can have any arbitrary small value e.g. 0.1 eV.

Footnote : R. Bracewell "The Fourier Transform and Its Applications"
McGraw-Hill Co. New York (1965)

Similarly, at a higher potential V_3 ($V_3 > V_1$), $I(V_3)$ can be obtained:

$$I(V_3) = (f_1p_3 + f_2p_4 + f_3p_5 + f_4p_6 + f_5p_7 + f_6p_8 + - - -)\Delta E$$

This procedure is illustrated in fig. A1.

In this way the ion current I(V) at all the potentials V can be obtained. A computer program can be written for the above process. A plot of the results known as the ionization efficiency curve is shown in fig. A2.

Fig. A1. Convolution by the summation formula.

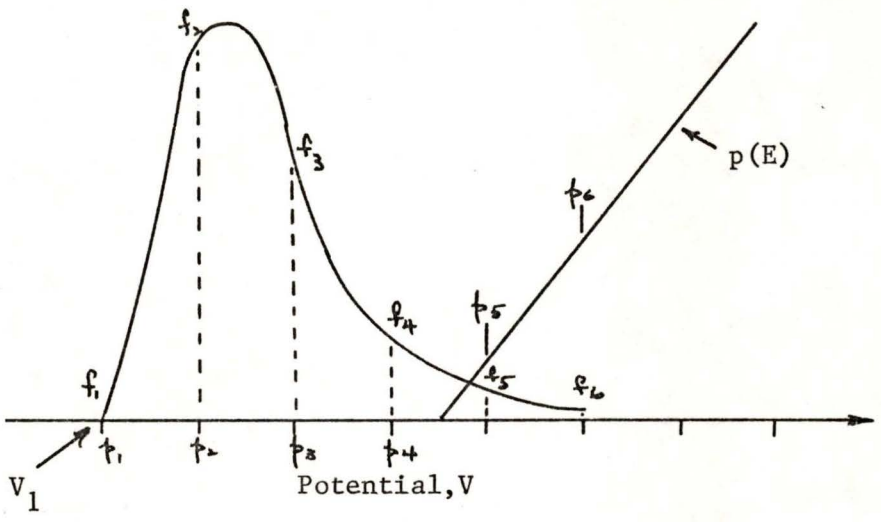

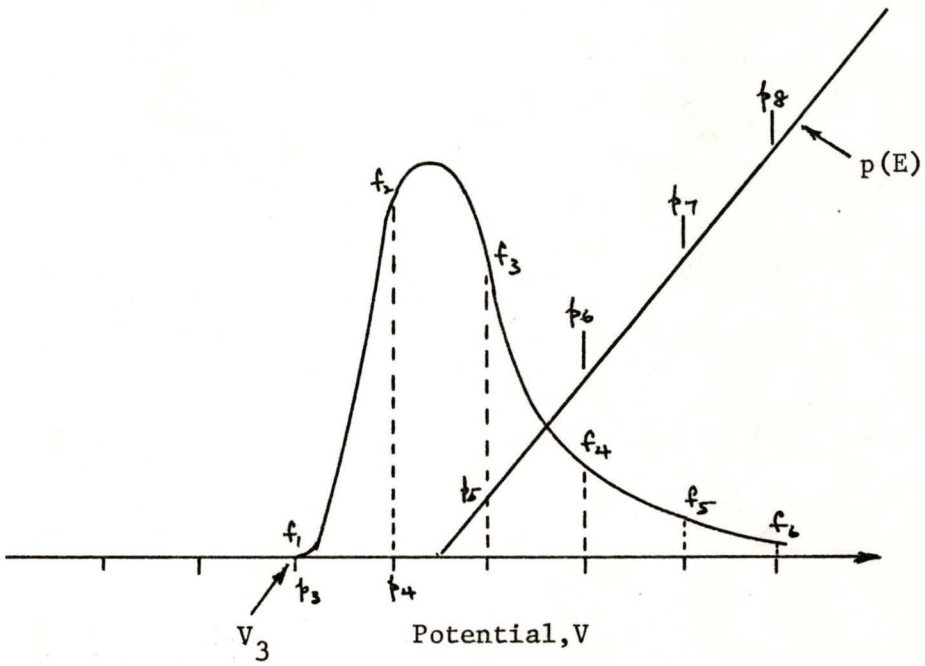

Fig. A2. Ionization efficiency curve.

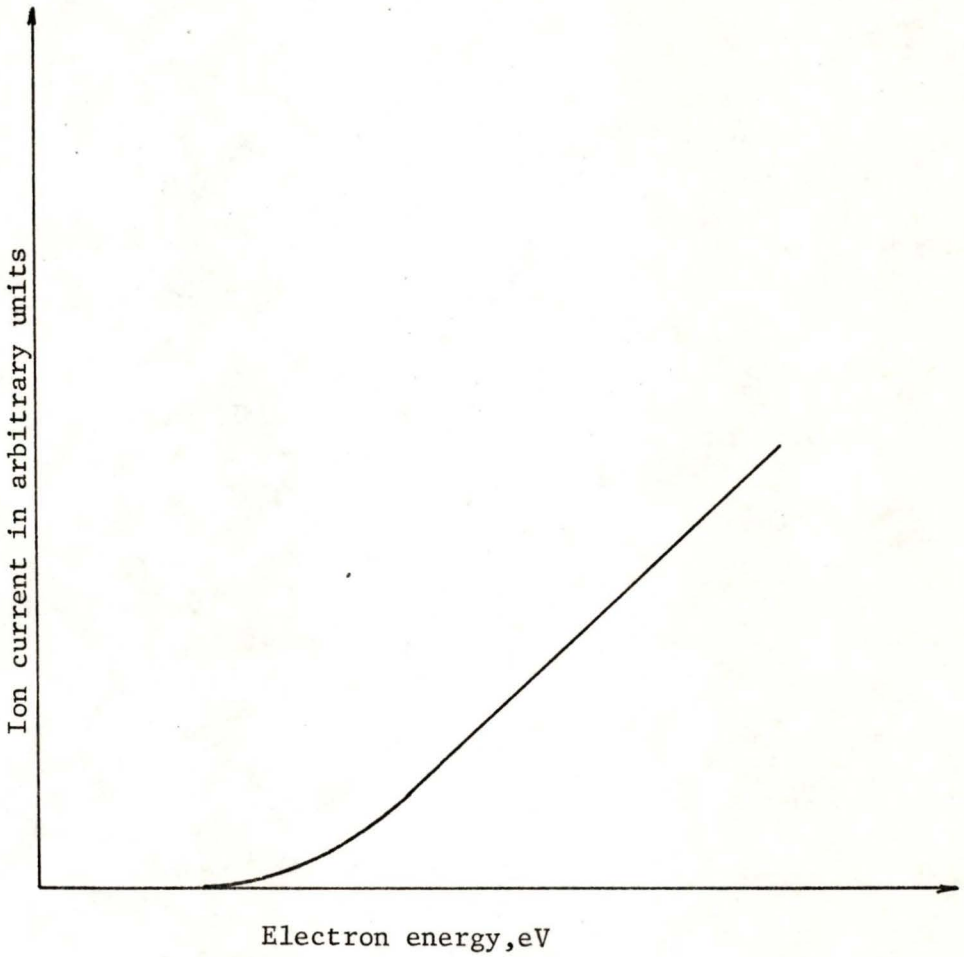

VITA

Surname: PUA Given Names: CLAUDIO KONG NAM

Place of Birth: PHILIPPINES Date of Birth: JUNE 6, 1939

Educational Institutions Attended, with Dates of Entering and Leaving:

THE AUSTRALIAN NATIONAL UNIVERSITY	1965 to 1966
THE UNIVERSITY OF ADELAIDE	1968 to 1968

Degrees, Diplomas, Etc., Awarded, with Dates and Names of Institutions:

B.Sc.	1967	THE AUSTRALIAN NATIONAL UNIVERSITY
B.Sc.(Hon.)	1969	THE UNIVERSITY OF ADELAIDE

THE UNIVERSITY OF VICTORIA LIBRARY

MANUSCRIPT THESIS

AUTHORITY TO DISTRIBUTE

AUTHOR: This thesis may be lent or microfilm copies made available:

(a) Without restriction [redacted]

(b) With the restriction that, for a period of five years (until _____) the written approval of the following is required:

(1) The Chairman, School of Graduate Studies _____

(2) The Author _____

(3) both the Chairman, School of Graduate Studies, and the Author _____

BORROWERS: The borrower undertakes, by signing below, to give proper credit for any use made of the thesis, and to obtain the consent of the author if it is proposed to make extensive quotations, or to reproduce the thesis in whole or in part.

Signature of Borrower Address Date